REPETITIVE LOADING MODEL TESTS OF PRESTRESSED RIGID PAVEMENT ON A LOW STRENGTH SUBGRADE

TECHNICAL REPORT NO. 4-28

MAY 1964

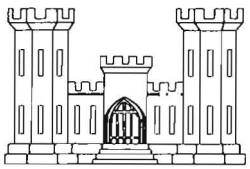

U. S. ARMY ENGINEER DIVISION, OHIO RIVER

CORPS OF ENGINEERS

OHIO RIVER DIVISION LABORATORIES

CINCINNATI, OHIO

Ohio River Division Laboratories, CE, U. S. Army, Mariemont, Ohio. REPETITIVE LOADING MODEL TESTS OF PRESTRESSED RIGID PAVEMENT ON A LOW-STRENGTH SUBGRADE, by P. F. Carlton and Ruth M. Behrmann. May 1964, 70 pp - illus - formulas - figures - tables (Technical Report No. 4-28).

Unclassified Report

This report presents the results of a laboratory model study to observe the behavior of prestressed concrete slabs supported on a low-strength subgrade and tested to complete failure by repetitive loading. The purpose of the study was to develop relationships between magnitude of load, number of load applications, and pavement physical properties. Included in this report is a description of the design of the model, physical properties of the materials comprising the model, test procedures and instrumentation used with the model. The test results are presented with an analysis and discussion.

UNCLASSIFIED
1. Prestressed Concrete
2. Airfield Pavements
3. Model Studies

I. Carlton, P. F.
II. Behrmann, Ruth M.
III. Ohio River Division Laboratories Technical Report No. 4-28

Ohio River Division Laboratories, CE, U. S. Army, Mariemont, Ohio. REPETITIVE LOADING MODEL TESTS OF PRESTRESSED RIGID PAVEMENT ON A LOW-STRENGTH SUBGRADE, by P. F. Carlton and Ruth M. Behrmann. May 1964, 70 pp - illus - formulas - figures - tables (Technical Report No. 4-28).

Unclassified Report

This report presents the results of a laboratory model study to observe the behavior of prestressed concrete slabs supported on a low-strength subgrade and tested to complete failure by repetitive loading. The purpose of the study was to develop relationships between magnitude of load, number of load applications, and pavement physical properties. Included in this report is a description of the design of the model, physical properties of the materials comprising the model, test procedures and instrumentation used with the model. The test results are presented with an analysis and discussion.

UNCLASSIFIED
1. Prestressed Concrete
2. Airfield Pavements
3. Model Studies

I. Carlton, P. F.
II. Behrmann, Ruth M.
III. Ohio River Division Laboratories Technical Report No. 4-28

Ohio River Division Laboratories, CE, U. S. Army, Mariemont, Ohio. REPETITIVE LOADING MODEL TESTS OF PRESTRESSED RIGID PAVEMENT ON A LOW-STRENGTH SUBGRADE, by P. F. Carlton and Ruth M. Behrmann. May 1964, 70 pp - illus - formulas - figures - tables (Technical Report No. 4-28).

Unclassified Report

This report presents the results of a laboratory model study to observe the behavior of prestressed concrete slabs supported on a low-strength subgrade and tested to complete failure by repetitive loading. The purpose of the study was to develop relationships between magnitude of load, number of load applications, and pavement physical properties. Included in this report is a description of the design of the model, physical properties of the materials comprising the model, test procedures and instrumentation used with the model. The test results are presented with an analysis and discussion.

UNCLASSIFIED
1. Prestressed Concrete
2. Airfield Pavements
3. Model Studies

I. Carlton, P. F.
II. Behrmann, Ruth M.
III. Ohio River Division Laboratories Technical Report No. 4-28

Ohio River Division Laboratories, CE, U. S. Army, Mariemont, Ohio. REPETITIVE LOADING MODEL TESTS OF PRESTRESSED RIGID PAVEMENT ON A LOW-STRENGTH SUBGRADE, by P. F. Carlton and Ruth M. Behrmann. May 1964, 70 pp - illus - formulas - figures - tables (Technical Report No. 4-28).

Unclassified Report

This report presents the results of a laboratory model study to observe the behavior of prestressed concrete slabs supported on a low-strength subgrade and tested to complete failure by repetitive loading. The purpose of the study was to develop relationships between magnitude of load, number of load applications, and pavement physical properties. Included in this report is a description of the design of the model, physical properties of the materials comprising the model, test procedures and instrumentation used with the model. The test results are presented with an analysis and discussion.

UNCLASSIFIED
1. Prestressed Concrete
2. Airfield Pavements
3. Model Studies

I. Carlton, P. F.
II. Behrmann, Ruth M.
III. Ohio River Division Laboratories Technical Report No. 4-28

Ohio River Division Laboratories, CE, U. S. Army, Mariemont, Ohio. REPETITIVE LOADING MODEL TESTS OF PRESTRESSED RIGID PAVEMENT ON A LOW-STRENGTH SUBGRADE, by P. F. Carlton and Ruth M. Behrmann. May 1964, 70 pp - illus - formulas - figures - tables (Technical Report No. 4-28).

Unclassified Report

This report presents the results of a laboratory model study to observe the behavior of prestressed concrete slabs supported on a low-strength subgrade and tested to complete failure by repetitive loading. The purpose of the study was to develop relationships between magnitude of load, number of load applications, and pavement physical properties. Included in this report is a description of the design of the model, physical properties of the materials comprising the model, test procedures and instrumentation used with the model. The test results are presented with an analysis and discussion.

UNCLASSIFIED
1. Prestressed Concrete
2. Airfield Pavements
3. Model Studies

I. Carlton, P. F.
II. Behrmann, Ruth M.
III. Ohio River Division Laboratories Technical Report No. 4-28

Ohio River Division Laboratories, CE, U. S. Army, Mariemont, Ohio. REPETITIVE LOADING MODEL TESTS OF PRESTRESSED RIGID PAVEMENT ON A LOW-STRENGTH SUBGRADE, by P. F. Carlton and Ruth M. Behrmann. May 1964, 70 pp - illus - formulas - figures - tables (Technical Report No. 4-28).

Unclassified Report

This report presents the results of a laboratory model study to observe the behavior of prestressed concrete slabs supported on a low-strength subgrade and tested to complete failure by repetitive loading. The purpose of the study was to develop relationships between magnitude of load, number of load applications, and pavement physical properties. Included in this report is a description of the design of the model, physical properties of the materials comprising the model, test procedures and instrumentation used with the model. The test results are presented with an analysis and discussion.

UNCLASSIFIED
1. Prestressed Concrete
2. Airfield Pavements
3. Model Studies

I. Carlton, P. F.
II. Behrmann, Ruth M.
III. Ohio River Division Laboratories Technical Report No. 4-28

Ohio River Division Laboratories, CE, U. S. Army, Mariemont, Ohio. REPETITIVE LOADING MODEL TESTS OF PRESTRESSED RIGID PAVEMENT ON A LOW-STRENGTH SUBGRADE, by P. F. Carlton and Ruth M. Behrmann. May 1964, 70 pp - illus - formulas - figures - tables (Technical Report No. 4-28).

Unclassified Report

This report presents the results of a laboratory model study to observe the behavior of prestressed concrete slabs supported on a low-strength subgrade and tested to complete failure by repetitive loading. The purpose of the study was to develop relationships between magnitude of load, number of load applications, and pavement physical properties. Included in this report is a description of the design of the model, physical properties of the materials comprising the model, test procedures and instrumentation used with the model. The test results are presented with an analysis and discussion.

UNCLASSIFIED
1. Prestressed Concrete
2. Airfield Pavements
3. Model Studies

I. Carlton, P. F.
II. Behrmann, Ruth M.
III. Ohio River Division Laboratories Technical Report No. 4-28

Ohio River Division Laboratories, CE, U. S. Army, Mariemont, Ohio. REPETITIVE LOADING MODEL TESTS OF PRESTRESSED RIGID PAVEMENT ON A LOW-STRENGTH SUBGRADE, by P. F. Carlton and Ruth M. Behrmann. May 1964, 70 pp - illus - formulas - figures - tables (Technical Report No. 4-28).

Unclassified Report

This report presents the results of a laboratory model study to observe the behavior of prestressed concrete slabs supported on a low-strength subgrade and tested to complete failure by repetitive loading. The purpose of the study was to develop relationships between magnitude of load, number of load applications, and pavement physical properties. Included in this report is a description of the design of the model, physical properties of the materials comprising the model, test procedures and instrumentation used with the model. The test results are presented with an analysis and discussion.

UNCLASSIFIED
1. Prestressed Concrete
2. Airfield Pavements
3. Model Studies

I. Carlton, P. F.
II. Behrmann, Ruth M.
III. Ohio River Division Laboratories Technical Report No. 4-28

REPETITIVE LOADING MODEL TESTS OF PRESTRESSED RIGID PAVEMENT ON A LOW STRENGTH SUBGRADE

TECHNICAL REPORT NO. 4-28

MAY 1964

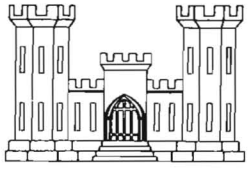

U. S. ARMY ENGINEER DIVISION, OHIO RIVER

CORPS OF ENGINEERS

OHIO RIVER DIVISION LABORATORIES

CINCINNATI, OHIO

PREFACE

This report describes the initial phase of a continuing study employing the use of a small-scale laboratory model to investigate the behavior of prestressed rigid pavements subjected to repetitive loadings under varying conditions.

The studies reported herein were made by the Research Branch of the Ohio River Division Laboratories as a part of the investigational program, "Engineering Investigations for Rigid Pavements," sponsored by the United States Air Force. This program is directed and coordinated by the Civil Engineering Branch, Engineering Division for Military Construction, Office of the Chief of Engineers.

Authority for this report and the model studies described is contained in Paragraph 3 of Instructions and Outline for, "Study of Basic Theory for Rigid Pavement Design Using Models," F. Y. 1961, as issued by the Office of the Chief of Engineers.

Members of the Board of Consultants for the investigational program were particularly helpful in providing guidance for this study, and in interpreting and analyzing the data obtained. Members of the Board serving as consultants for prestressed pavements include:

Mr. Eric C. Molke	Professor N. M. Newmark
Professor Gerald Pickett	Professor C. P. Siess

This report was prepared by Paul F. Carlton, Chief, Research Branch, and Ruth M. Behrmann, Research Mathematician; under the supervision of Ronald L. Hutchinson, Chief, Rigid Pavement Laboratory, and under the direction of Frank M. Mellinger, Director, Ohio River Division Laboratories.

CONTENTS

CONTENTS (Cont'd)

SUMMARY

This study was made to develop information relative to the performance of prestressed pavements supported on a low-strength subgrade and subjected to repetitive moving loads. Such information is required to refine and expand existing design and evaluation procedures for prestressed rigid pavements for military airfields. Specifically, the study was designed to develop relationships between the magnitude of the applied load, the number of load applications, and the physical properties of the pavement and subgrade.

The pavements used in the model were slabs of portland cement concrete 1 inch thick, 6 feet wide and 15 feet long. The slabs were prestressed to 250 pounds per square inch by the pre-tensioning method using single strands of high-strength steel wire placed at mid-depth in the slab and at 4-inch intervals both longitudinally and transversely. Support for the pavement was provided by a prepared subgrade 4 feet deep and composed of a relatively low-strength clay. The test loads were applied by a rolling single wheel with a solid rubber tire trafficking an area 2 feet wide by 10 feet long in the interior portion of the slab. The loading apparatus was designed so that, as the wheel traveled the length of the area to be trafficked, it also traversed transversely over the width of the traffic area.

Included in this report is a detailed description of the design, construction, instrumentation and testing of the model as well as information concerning the physical properties of the materials comprising the model. The test results are presented with an analysis and discussion.

Tests were performed on a total of seven slabs, six being subjected to repetitive loadings to failure and one being subjected to static loadings to failure. The one slab was loaded statically to obtain information which could be used to correlate the performance of the repetitive loading model

with results from previous small-scale model tests employing static loadings only. The principal observation made was the number of coverages of the single wheel loading required to produce failure in the slab. In addition, load-strain and load-deflection data were obtained to provide a more complete description of the pavement behavior.

Based on the results of the tests described herein, it is shown that:

a. The repetitive loading model provided a reliable simulation of the behavior of full-scale prestressed pavements subjected to moving loads.

b. Good agreement between the model and the theoretical analyses of Westergaard was obtained for static loadings within the range of elastic behavior of the slab.

c. Dynamic rolling wheel loads produced lower stresses and deflections in prestressed pavements than did static loads of the same magnitude.

d. No abrupt increase in the maximum deflection of prestressed rigid pavements accompanied the development of the initial tensile cracks in the bottom surface of the slab.

e. Once the initial structural distress became visible in the top surface of a prestressed slab, the progression of this distress to a condition of complete failure was extremely rapid under continued application of the wheel load.

f. For prestressed rigid pavements subjected to repetitive traffic loadings, the magnitude of the wheel load may be related to the number of load applications by the use of an appropriate design factor applied to the static failure load.

g. The model is sufficiently versatile to be used for investigating the effects of other variables as they relate to the behavior of prestressed rigid pavements.

REPETITIVE LOADING MODEL TESTS OF PRESTRESSED RIGID PAVEMENT ON A LOW-STRENGTH SUBGRADE

SECTION I: DEVELOPMENT OF THE MODEL

Purpose of the Study

1. To date the design of prestressed rigid pavement has been based almost entirely on theoretical considerations. Only data obtained from a few full-scale test pavements (1, 2, 3, 4)*, laboratory studies using small-scale models (5, 6), and observations made relative to the performance of a limited number of full-scale operational airfield pavements in Europe and in the United States (7, 8, 9, 10) have been available to use as a basis for extending and refining the theoretical design procedures.

2. At the time the tests described herein were initiated, practically all information pertaining to the behavior of prestressed airfield pavements was based on static loadings. The theoretical approaches to the problem of design were limited to the assumption of a single static application of the load. In addition, much of the information obtained under controlled conditions had been on the basis of static loadings. Since no relationship had been established whereby the performance of a prestressed pavement under static loading could be related to the performance of a prestressed pavement under repetitive loading, it was felt that an attempt should be made to bridge this gap.

3. The purpose of this study was to observe the behavior, under laboratory-controlled test conditions, of model prestressed pavements subjected to repetitive loadings of various magnitudes; and to incorporate the information obtained from the model into existing design and evaluation procedures for prestressed rigid pavements for military airfields.

---

* Numbers in parentheses refer to references.

Scope of the Study

4. The scope of this study included: (1) the development of a small-scale prestressed concrete pavement model, the behavior of which would simulate adequately that of full-scale prestressed airfield pavements under operational loadings; (2) the design and construction of a loading apparatus capable of applying repetitive loadings to the model slabs in the desired manner; (3) the conducting of tests on a series of seven model slabs; and (4) the analysis and presentation of the test results so that they could be viewed as a basis for possible adjustments to existing procedures for the design and evaluation of full-scale prestressed rigid pavements.

5. Basically, the testing consisted of observing the behavior of a series of six model prestressed concrete slabs for the following conditions: (1) all slabs were supported continuously by a specially prepared low-strength clay subgrade, and (2) all slabs were subjected to a rolling single-wheel load applied over a definite area in the slab interior. The magnitude of the wheel loads was such that the behavior of the slabs was essentially inelastic. Sufficient loadings were applied to produce ultimate failures in all slabs. The behavior of each slab was evaluated through limited strain and deflection measurements, by the development and progression of cracking in the surface of the traffic area, by the physical properties of the slab and subgrade, by the magnitude of the applied loading, and by the number of load repetitions sustained by the slab prior to complete failure.

6. At the conclusion of dynamic tests on the six slabs, static loading tests were performed on a seventh prestressed model slab. The static loading tests were conducted in order to provide a means for correlating the results of the dynamic loading tests with results of other small-scale model tests of prestressed pavements in which only static loadings were used.

7. Included in this report is complete information regarding: (1) the design of the model and loading apparatus, (2) techniques used in constructing the model slabs, (3) instrumentation used on the slabs and in the

subgrade, (4) procedures followed in testing the slabs and the subgrade, and (5) methods used in analyzing the test data obtained.

General Description of the Model

8. Full-scale prestressed concrete pavements were simulated in the model by 1-inch thick portland cement concrete slabs prestressed to 250 pounds per square inch both longitudinally and transversely. All slabs were 6 feet wide by 15 feet long. High-strength, cold-drawn, stress-relieved wires 0.1055 inch in diameter, spaced 4 inches center to center, and positioned at mid-depth in the slabs were used as the stressing tendons. All of the slabs tested in this study were prestressed by the pre-tensioning method; that is, the wires were tensioned prior to placing the concrete. After the concrete had attained the minimum strength required, the wires were released from the anchorages and the prestress was effected by a transfer of stress through the bond between the wires and the concrete.

9. The subgrade support provided for the slabs was a relatively low-strength clay soil placed at a uniform moisture content and density in an enclosure 8 feet wide by 17 feet long by 4 feet deep. The moving load for these tests was applied by means of a 15.5-inch diameter single wheel having a solid rubber tire. The contact area of the tire ranged from slightly less than 7 square inches to slightly more than 9 square inches, depending on the magnitude of the applied load. The load wheel was mounted in an electrically-operated moving assembly so designed that the extent of both the longitudinal and transverse motion could be controlled. Thus the traffic could be confined to a definite area of the model slab. In these tests, the traffic was confined to an area 2 feet wide by 10 feet long in the interior portion of each slab. (A general view of the model is shown in Figure 22.)

Physical Properties of the Model Materials

10. Mix Design for the Concrete. Preliminary tests were made to develop a mix design suitable for use in constructing the model slabs. High early strength cement (Type III) was selected to provide a minimum waiting period for the slabs to attain the minimum strengths required for prestressing and for testing. The fine aggregate was a natural sand with 8 percent blending sand added. The coarse aggregate was a crushed limestone ranging in size from 100 percent passing the 3/8-inch screen to 100 percent retained on a No. 4 sieve. Using a cement factor of 6.50 and a water-cement ratio of 0.56, the average mix proportions were 1 : 2.85 : 1.55. Average values obtained from the batches for each test slab indicated a 4.5-inch slump and 8.1 percent entrained air.

11. Flexural Strength of the Concrete. Two methods were used to determine the flexural strength of the concrete in the model slabs: (1) tests on control beams made at the time of the casting of each slab, and (2) tests on beams sawed from undisturbed portions of each slab after completion of the traffic tests.

a. Control Beams. The control beams cast at the time each slab was constructed were made from samples of the batch for the slab, and were 1 inch by 2 inches in cross-section and 12 inches long. These beams were tested in flexure with third-point loading on a span of 9 inches. One beam in each group was broken at an age of 7 days. The remaining beams were broken periodically during the testing and upon complete failure of the slab. The results of the flexural strength tests on the control beams were used to construct a curve of flexural strength versus age, similar to the example shown in Figure 1, for each slab. These curves indicated that the flexural strength of each slab approached a constant value as the age of the slab increased. A summary of the flexural strengths, as indicated by the constant value for flexural strength attained by each slab, is given in Table 1.

b. "After-Traffic" Beams. Following completion of the loading tests for each slab, beams for flexural strength tests were sawed from portions of the slab outside the test area. These beams were approximately 3.8 inches wide and 30 inches long, and were sawed so as to contain a single prestressing wire at the longitudinal centerline of the beam. Thus each beam was prestressed longitudinally during the flexural strength tests, and the indicated failure stress represented a summation of the flexural strength and prestress. These beams were tested in flexure with third-point loading on a span of 13.5 inches. Owing to the eccentricity resulting from not being able to position the longitudinal prestressing wires exactly at mid-depth in the slab, two tests as follows, were made on each beam: (1) the beam was tested on one end in the "normal" or as-cast position, and (2) the beam was turned over and tested on the opposite end in the "reverse" or upside down position. By averaging the cracking stress obtained from the two tests, it was possible to eliminate any error introduced by the eccentricity of the prestressing wire. The actual flexural strength then was obtained by subtracting the computed prestress from the average cracking stress. A summary of the results obtained from the "after-traffic" beam tests is given in Table 2. The set-up used in making these tests is shown in Figure 2.

12. Modulus of Elasticity of the Concrete. A limited number of tests were performed to determine the modulus of elasticity, E, of the concrete used in the test slabs. Specimens for these tests were taken from the control beams used for the flexural strength tests. Each test specimen was instrumented with two Type AX-5, SR-4 strain gage rosettes, one mounted on each 2-inch wide surface so that the gages would indicate longitudinal and transverse strains. The beams then were placed in a special jig having each end pin-connected in two directions to prevent eccentricity during the loading. An axial tensile load was applied to the specimens as shown in Figure 3, and strain measurements were made for various increments of this loading. Typical stress-strain relationships obtained from these tests are shown in Figure 4. The average value of E as determined from all tests was 4.5×10^6 pounds per square inch.

13. Poisson's Ratio of the Concrete. Tests to determine the Poisson's ratio, μ, for the concrete were made in conjunction with those to determine the modulus of elasticity. The same procedure as described in the preceding paragraph was followed. The Type AX-5, SR-4 strain gage rosettes provided both the longitudinal and transverse strains required for computing μ. Typical load-strain data obtained from these tests are shown in Figure 5. The average value of μ as determined from all tests was 0.20.

14. Tensile Strength of the Prestressing Wire. The wire selected for the prestressing tendons in the model slabs was No. 12 gauge (0.1055-inch diameter), cold-drawn, stress-relieved steel wire furnished with a bright finish. Tests showed this wire to have an average ultimate tensile strength of 270,500 pounds per square inch, a value which agreed within 3 percent of that specified by the manufacturer.

15. Bond Between the Prestressing Wires and the Concrete. In order for the wire to be suitable for use as the prestressing tendons, it was necessary to obtain sufficient bond between the wire and the concrete to develop the desired magnitude of prestress. Tests were made to determine the bond strength developed for different ages of concrete, different lengths of wire embedment and different methods of surface treatment for the wire. Test specimens were prepared using single strands of wire embedded in 1 inch by 1 inch concrete beams of various lengths. Specimens were tested at ages varying from 7 to 14 days. Embedment lengths for the wire varied from 6 to 18 inches. Two types of surface treatment were used on the wire: (1) cleaning with acetone, and (2) etching with dilute hydrochloric acid followed by rinsing with clear water. Results of the pull-out tests are given in Table 3. These data indicate clearly that the acid etching of the wire surface produced a marked increase in bond strength. In the model slabs, it was necessary that the prestressing wires develop a pull-out load of not less than 1103 pounds (the anchoring load on each wire) over an embedment length of not more than 24 inches (the minimum distance from the edge of the

slab to the edge of the traffic area). As can be seen from Table 3, the degree of bond required was readily attained using the acid etching procedure. On the basis of these tests, it was decided to use the acid etching procedure and take advantage of the increased bond strength which this method produced.

16. Subgrade. The clay soil used as the subgrade in the model was obtained from the Sharonville, Ohio test site for full-scale accelerated traffic tests of airfield pavements. The material was a borderline CL-CH clay having a Liquid Limit of 49.7 percent and a Plasticity Index of 27.7. Based on the AASHO compaction test as modified by the Corps of Engineers, the optimum moisture content for the clay was 14 percent and the maximum dry density was 118 pounds per cubic foot. In order to provide the desired low-strength subgrade, the clay was placed in the model at a moisture content of 28.9 percent and at a dry density of 91.5 pounds per cubic foot. This density was 98 percent of the Modified AASHO Density for the placement moisture content. Although every effort was made to minimize moisture loss from the subgrade, subsequent testing indicated that five months after placement of the subgrade the moisture content had decreased to 26.4 percent and the dry density had increased to 97.5 pounds per cubic foot. At the conclusion of the test series, 21 months after placement of the subgrade, the moisture content had decreased to 25.3 percnet and the dry density had increased to 99.5 pounds per cubic foot. These tests also indicated that the changes in moisture content and density were relatively uniform throughout the depth of the subgrade.

17. Modulus of Subgrade Reaction. The modulus of subgrade reaction, k, was determined by two methods: (1) the plate bearing test using a 30-inch diameter plate, and (2) the volumetric displacement test using static loadings.

a. Plate Bearing Tests. These tests were made at three points along the longitudinal centerline of the subgrade: at the center and 5 feet on either side of the center. Due to the gradual loss of moisture from the

clay, the plate bearing tests were repeated periodically in order to determine the change in k as a result of this loss. In all, four different series of plate bearing tests were made. A plot of subgrade modulus versus time, as well as the time the plate bearing tests were made relative to the testing of the model slabs is shown in Figure 6. Values of the modulus of subgrade reaction used in the final analysis of each prestressed slab also are shown in Figure 6.

b. Volumetric Displacement Tests. In these tests, static loads were applied to the model slabs by means of a 3-inch square contact area positioned at a quarter-point along the longitudinal centerline of the traffic area. Dial gages, reading directly to 0.0001 inch, were spaced at 4-inch intervals in two lines extending longitudinally and transversely from the loaded area to the slab edges to indicate the deflection of the slab. The deflection at the center of the contact area was indicated by an electrical transducer-type deflection gage. Load was applied in increments of approximately 300 pounds and complete deflection data were obtained for each load increment. The subgrade modulus was computed on the basis of the total volumetric displacement measured at the surface of the slab. Results from these tests were quite erratic and were discarded in favor of the data obtained from the plate bearing tests.

Theoretical Considerations

18. Elastic Behavior. By giving special attention to the simulation of certain basic assumptions inherent in the theorectical analyses of Westergaard (15) and Pickett (16), a means of analyzing the behavior of the model in the elastic range was made available as well as a means of correlating the behavior of full-scale pavements with that of the model. In the case of the model used in this study, the portland cement concrete comprising the slab was essentially homogeneous, isotropic, and elastic as required by the theory.

Since the average of the length and width of the tire contact area was greater than the thickness of the slab, no correction of the ordinary theory of bending of plates was required. The subgrade was uniform in character and was in contact with the slab at all points. It was believed that the prepared subgrade simulated the "dense liquid" concept proposed by Westergaard, in that the reactive pressure acting at the interface between the slab and subgrade could be expressed as the deflection times a constant, k, the modulus of subgrade reaction.

19. Much of the analysis of the data from this model, as well as the correlation with other models and prototype prestressed pavements, was based on comparisons involving ℓ, the radius of relative stiffness.* Since the prestressing wires were located at mid-depth in the slabs, the stiffness of the slabs was not altered by the presence of the wires for conditions of loading within the range of elastic behavior. For these tests, the radius of relative stiffness for the slabs ranged between 8.57 and 8.98 inches. Based on an average value for ℓ, the horizontal dimensions of the slabs were 8.2 ℓ by 20.5 ℓ. These dimensions were large enough to permit the model slabs to be considered effectively infinite in extent, as assumed by the theory. No loads were applied closer than 2.7 ℓ to any edge. For loading conditions producing cracking of the slabs, the theoretical analyses of Westergaard and Pickett were not applicable.

$$* \ell = \left[\frac{E h^3}{12 (1-\mu^2) k} \right]^{1/4}$$

where:

E = modulus of elasticity of the concrete,

h = thickness of the slab,

μ = Poisson's ratio of the concrete,

k = modulus of subgrade reaction.

20. Inelastic Behavior. After tensile cracking occurred in the bottom surface of the slab, the load-stress relationships were no longer linear. For this phase of behavior, the analysis of the model was based on the premise that the tensile cracks in the bottom surface of the slab acted as plastic hinges under passage of the load. The redistribution of moments in the slab for this phase of inelastic action resulted in a rapid increase in the negative radial moment. When the negative radial moment reached a value equal to the resisting moment of the slab, secondary tensile cracking occurred in the top surface. Non-dimensional load-moment relationships for the inelastic behavior of prestressed rigid pavements have been developed from model studies described in Reference No. 6 and from full-scale accelerated traffic tests of prototype prestressed pavements described in Reference No. 3. These empirical relationships were used for the analysis of the inelastic behavior of the model slabs tested in this study.

21. Load Repetition. The theoretical approaches to the understanding of the behavior of prestressed pavement (7, 17) indicate the loading required to produce cracking from negative radial moment for the case of a single static application of this loading. These theories, however, make no provision for determining the reduction in loading necessary in order that a specified number of load applications may be sustained prior to either development of the negative moment cracking or development of complete failure in the slab. Neither do the theoretical analyses consider the case where the nature of the slab is changed from the idealized cracking in the bottom surface assumed in the theory to the random crack patterns developed in the bottom surface as a result of moving wheel loads. It is possible that interrelationships of design factors required to provide for the effect of repetitive moving wheel loads may be so complex as to defy theoretical analysis, and that predictions as to the life of prestressed rigid pavements may be forced to depend on analyses based on tests and observations similar to those covered by this study.

SECTION II: CONSTRUCTION OF THE MODEL

Subgrade

22. Enclosure for the Subgrade. The prepared subgrade for the model tests was confined to a space 8 feet wide by 17 feet long and 4 feet deep. One end and two sides of the enclosure were formed by concrete retaining walls constructed directly on a concrete floor slab which formed the lower boundary for the subgrade. The concrete end wall was vertical and uniformly 6 inches thick. The longitudinal retaining walls had a vertical inner face, with thickness tapering from 30 inches at the base to 12 inches at the top. Vertical slots were formed in the inner face of the side walls near the open end to accommodate 6-inch by 6-inch timbers stacked horizontally to effect the closure. Use of removable timbers at one end was to facilitate placement and removal of the subgrade material. A general view of the subgrade enclosure is shown in Figure 7. The floor and the concrete walls within the enclosure were treated with a water-proofing compound and the timbers were lined on the inside with polyethylene to reduce loss of moisture from the subgrade. Anchorages were constructed in the longitudinal retaining walls to provide a reaction for plate bearing tests on the subgrade and static loading tests on the model slabs.

23. Placement of the Subgrade. The soil comprising the subgrade was described previously in Paragraph 16. This material was mixed thoroughly using a mechanical tiller to assure uniform composition and moisture content. The soil was placed in the model in 4-inch thick lifts, each lift being compacted with pneumatic tampers as shown in Figure 8. Leveling of the top surface of the subgrade was accomplished using a specially devised planer operated as shown in Figure 9. After the subgrade had been leveled, it was covered with a single sheet of polyethylene to prevent loss of moisture from the soil. Figure 10 shows the completed subgrade.

Test Slabs

24. Casting Bed and Stressing Frame. The prestressed model slabs used in these tests were constructed in a combination casting bed and stressing frame, and later were placed on the subgrade for the actual testing. Since the slabs were pre-tensioned, the casting bed had to be not only strong enough to retain its shape under the weight of the concrete, but also strong enough to provide the reaction for the total load applied to the prestressing wires during construction of the slab. The casting bed was built over a framework of steel I-beams and reinforcing steel as shown in Figure 11. The outer frame was 6 1/2 feet wide by 15 1/2 feet long, and was leveled by means of adjustable jacks which provided support at six points. Four plate casters attached to the under side of the outer frame permitted the casting bed to be moved as required.

25. The framework for the casting bed was filled with concrete to within 3/8 inch of the surface. A sand-cement mortar then was used to finish filling the interior until it was flush with the top surface of the outer frame. The surface of the casting bed was finished to a smoothness tolerance of plus or minus 0.001 foot. The side forms were 3-inch channels bolted to the outer frame every 4 inches. The inside flange of each channel was milled to a height of 1 inch to serve in establishing the slab thickness. Holes, 7/64 inch in diameter, to accommodate the stressing wires were drilled through the flanges of the channels every 4 inches and centered at a height of 0.5 inch above the surface of the casting bed. The completed casting bed and stressing frame is shown in Figure 12.

26. Stressing Wires. Immediately prior to casting each test slab, a sheet of polyethylene was stretched over the surface of the casting bed to prevent the slabs from bonding to the casting bed. The channels used as side forms were then bolted in place and served to keep the polyethylene taut and wrinkle-free. Longitudinal and transverse stressing wires were cut to length, dipped in dilute hydrochloric acid and then rinsed in clear water.

As described previously in Paragraph 15, the acid treatment served to etch the surface of the wire and improve the bond with the concrete. The procedure used in treating the stressing wires is shown in Figure 13. The wires then were strung through the holes in the side forms and the anchoring devices attached to each end. In the first slab cast, the transverse wires were positioned below the longitudinal wires. In the next three slabs, the transverse wires were positioned above the longitudinal wires. In the last three slabs constructed, the individual transverse wires were positioned alternately above and below the longitudinal wires. These various arrangements of the stressing wires were tried in an effort to reduce the warping which occurred after the slabs were released from the stressing frame. Each of the last two methods used resulted in less warping than with all transverse wires positioned above the longitudinal wires.

27. Due to the short length and width of the model slabs, it was necessary to use an anchorage system in which there would be no prestress loss due to slippage of the wire in the anchor when the initial tensioning force was released. This was accomplished by applying the tensioning force at the inside face of the strand chuck rather than applying the pull on the wire behind the strand chuck as is the normal construction practice. Essentially, the anchorage assemblies were similar in design to those used in the small-scale static loading prestressed model studies (5) and are shown in Figure 14. Each assembly was composed of a commercially available strand chuck, a 5/8-inch cap screw having a 1/8-inch diameter hole drilled along the longitudinal centerline, a 5/8-inch lock nut, and a 1 1/2-inch long galvanized pipe sleeve. Insofar as tensioning the wires was concerned, it would have been necessary only to have the complete anchorage assembly on one end of each wire. In order to release the wires and remove the strand chucks, however, it was necessary that a complete assembly be placed on both ends of each wire. The arrangement used to apply the desired tension to the wires is shown in Figure 15. Figure 16 shows the stressing wires in place and tensioned just prior to placement of the concrete.

28. Magnitude of Prestress. Previous model studies (6) as well as experience obtained from the construction of full-scale prestressed pavements in Europe had indicated that the most practical range for prestressing appeared to be in the order of from 200 to 300 pounds per square inch. Accordingly, the design value for the prestress to be applied to the series of slabs tested in this study was 250 pounds per square inch. Since subgrade restraint forces would be negligible in the model, the longitudinal and transverse prestress were made equal. For a wire spacing of 4 inches and a slab thickness of 1 inch, the force required to produce 250 pounds per square inch of prestress was 1000 pounds per wire. Due to certain losses in prestress which would occur during construction of the slabs, it was necessary that the anchoring load on each stressing wire be somewhat greater than 1000 pounds in order to compensate for these losses. A summary of the computations made to establish the sum of these losses is given below. These computations were based on application of the prestress at a slab age of 7 days at which time the modulus of elasticity of the concrete was assumed to be 3.5×10^6 pounds per square inch.

a. Elastic Shortening.

$$f_s = \frac{E_s}{E_c} \times \sigma_p = \frac{28 \times 10^6}{3.5 \times 10^6} \times 250 = 2000 \text{ psi}$$

where f_s = stress loss in the wire,

E_s = modulus of elasticity of the wire,

E_c = modulus of elasticity of the concrete (7-day),

σ_p = prestress.

b. Creep. Other studies have indicated that creep in concrete during the life of the structure may range from 3×10^{-7} to 6×10^{-7} inch per inch for each pound per square inch of prestress. Since it was anticipated

that the slabs generally would be tested to failure within a period of two months, a value of 2×10^{-7} inch per inch was assumed for the model.

$$f_s = \epsilon_d \times E_s \times \sigma_p = 2 \times 10^{-7} \times 28 \times 10^6 \times 250 = 1400 \text{ psi}$$

where ϵ_d = creep strain.

c. Shrinkage. For the model, the coefficient of length change due to shrinkage was assumed to be 0.0003 inch per inch.

$$f_s = \epsilon_s \times E_s = 3 \times 10^{-4} \times 28 \times 10^6 = 8400 \text{ psi}$$

where ϵ_s = length change due to shrinkage.

d. Relaxation. Since the anchorage stress was less than 50 percent of the utlimate strength of the wire, the stress loss due to relaxation in the wire was assumed to be negligible. From the above, the total stress loss in the wire was 11,800 pounds per square inch which was equivalent to a force of 103 pounds per wire. Thus, a total load of 1103 pounds was applied to each stressing wire during the tensioning operation. This produced a stress of 126,170 pounds per square inch in the wire, or approximately 47 percent of the ultimate strength.

29. Concrete Placement. The slabs were constructed of portland cement concrete using the mix design described in Paragraph 10. The concrete was placed in two lifts, and each lift was consolidated with a plate-type vibrator as shown in Figure 17. A piece of aluminum angle was used to strike off the surface of the concrete as shown in Figure 18. Usually, three passes of the strike-off were required to produce the desired degree of accuracy in slab thickness. Three to four hours after completion of the strike-off operation, a final finish was applied to the surface using a steel trowel.

30. Curing. After the final finishing of the surface, each slab was covered with a layer of wet burlap curing blankets as shown in Figure 19. Although the burlap had a plastic coating on the exposed side, it was covered with a sheet of polyethylene as additional protection against loss of moisture. The concrete was allowed to cure in this manner for a period of 7 days.

31. Application of Prestress. At the end of the curing period, the prestress was applied to the slabs by loosening the lock nuts in each anchorage assembly. This permitted removal of the strand chucks and the remaining components of the anchorage assemblies. After the side forms had been removed, the stressing wires were clipped as close to the edge of the slab as possible with bolt cutters. Figure 20 shows a completed test slab ready to be placed on the subgrade.

32. Positioning on the Subgrade. The completed slabs were transferred from the casting bed to the subgrade by means of a special bridle attached to a chain hoist as shown in Figure 21. The bridle provided a 6-point pick-up and resulted in maximum pick-up stresses of approximately one-half the combined flexural strength and prestress. The slabs were placed directly on the polyethylene sheet covering the subgrade. After final positioning of the slab to meet instrumentation requirements, steel blocks were placed on the slab around the edges to insure that the slab remained in contact with the subgrade. A general view of the model with a slab in place ready for testing is shown in Figure 22.

Load Rig

33. Load Wheel. The load wheel used to apply the simulated traffic loadings to the test slabs was 15.5 inches in diameter and was equipped with a solid rubber tire. The edges of the tire were planed down from an original width of 4 inches to a width of 2.68 inches. This reduced the contact area of the tire so that the dimensional relationships between the tire and the slab in the model were similar to those found in the prototype. The contact area for the tire was not constant but varied with the magnitude

of the wheel load. The relationships between wheel load and the length and width of the tire contact area are shown in Figure 23. The relationship between wheel load and tire contact area is shown in Figure 24. A view of the load wheel is shown in Figure 25.

34. Load Box. The test load was applied to the load wheel by means of a load box attached to the wheel axle. The load box was designed so that steel plates could be used as the ballast to provide the desired loading. The load box was maintained in an upright position during traffic operations by means of four roller bearings attached to an outer stabilizing frame. These roller bearings operated in vertical guides provided at the center of each side of the load box. Use of the roller bearings permitted virtually unrestrained vertical movement of the box during the repetitive loadings. A view of the load box and load wheel removed from the stabilizing frame is shown in Figure 26. The dead weight of the load wheel and load box was 430 pounds. A view of the load box in place within the stabilizing frame and partially loaded with steel plates is shown in Figure 27.

35. Stabilizing Frame. In addition to maintaining the load box in an upright position during trafficking, the stabilizing frame provided the longitudinal and transverse motion required to move the load wheel through a pre-arranged pattern of traffic. The four corners of the stabilizing frame were mounted on flanged wheels which traveled on steel rails attached to the top surface of the longitudinal concrete retaining walls enclosing the subgrade. The load rig was so constructed that while the stabilizing frame was being driven back and forth longitudinally, the load box moved transversely within the stabilizing frame. An over-all view of the load rig used for applying the repetitive loadings to the model slabs is shown in Figure 28.

36. All movements of the load rig were controlled electrically. The longitudinal motion was powered by a 3-horsepower motor mounted on one corner of the stabilizing frame. Since the deceleration of the load rig was accomplished by reversing the current in this motor, special over-size windings were used to reduce the heat build-up in the motor. The transverse motion was powered by a smaller 1/2-horsepower motor also mounted on the

stabilizing frame. Both the longitudinal travel of the stabilizing frame and the transverse motion of the load box were controlled by limit switches. These switches served to reverse the flow of current to the drive motors, thus reversing the directions of movement of the load rig. The positioning of the limit switches could be adjusted readily to provide changes in the dimensions of the traffic area, as desired. The transverse limit switches are shown in Figure 27 and the longitudinal limit switches can be seen on the right side of the model in Figure 22.

37. Pass - Coverage Relationship. Designating the travel of the load wheel from one end of the traffic area to the other as one pass, the load rig moved at a speed producing 10 passes per minute for a 10-foot long run. Thus the average speed of the rig was 1.67 feet per second or 1.14 miles per hour. Since Corps of Engineers pavement design criteria that relate to traffic operations are based on the number of coverages of the design loading that must be sustained during the life of the pavement, it was necessary that a relationship be established between the passes of the load rig over the test slabs and coverages. A coverage is defined as a sufficient number of vehicle operations or passes to produce statistically one application of the design loading over the entire traffic area. Where there is uniform lateral distribution of the traffic, as was the case in the model, the number of passes required to produce one coverage may be obtained by dividing the width of the traffic area by the total width of the tire contact areas for all wheels carrying the design load. For the model, however, there was one additional factor which had to be considered. Because the load box tracked transversely constantly, the resultant traffic pattern was not truly rectangular and an area on each longitudinal side of the traffic area received fewer load applications than the interior portion of the traffic area. Each of these areas along the edge had a width equal to one half of the width of the contact area. In the areas along the edge, the number of coverages increased from zero at the edge to the full number applied at the interior at a distance of one half of the width of the contact area from the edge.

In determining the number of passes required per coverage for the interior portion of the traffic area, the following equation, which compensates for the areas along the edge, was used:

$$N = \frac{W-b}{b} \quad \ldots\ldots\ldots\ldots\ldots\ldots \quad (1)$$

where

N = passes required per coverage,

W = width of traffic area, inches,

b = width of tire contact area, inches.

For typical test conditions where W = 24 inches and b = 2.75 inches, the number of passes required to produce one coverage was 7.73.

SECTION III: INSTRUMENTATION

Separation Gages

38. Before placing the test slabs on the subgrade, three contact-type gages were installed on the bottom surface of the slabs to indicate when the pavement and subgrade were in contact during the traffic testing. These pavement-subgrade separation gages were located along the longitudinal centerline of the traffic area at the center and at the approximate quarter-points of the slab. Each gage consisted of a 1/2-inch diameter coil of uninsulated wire cemented to the slab at the gage location, and a 1-inch square metal plate embedded in the surface of the subgrade immediately beneath the wire coil. When the slab and subgrade were in contact, the plate and coil also were in contact. By incorporating each gage in an electrical circuit, having the coil and plate in contact closed the circuit and energized an indicator light. Thus the gages did not measure the magnitude of separation, but merely indicated whether or not the slab and subgrade were separated. A view of the wire coil attached to the slab is shown in Figure 29.

Deflection Gages

39. Dial Gages. Where deflections due to static loadings were obtained on the top surface of a slab, dial gages reading directly to 0.0001 inch were used. The construction of the model was such that it precluded using dial gages to obtain deflection measurements at points within the contact area of the device used to apply the loading to the test slab.

40. Differential-Transformer-Type Gages. During placement of the clay subgrade, three specially-built differential-transformer-type gages were installed to measure the vertical displacement of the model slabs during the testing operations. The gages were attached to the concrete floor which served as a reference elevation. Reference rods extending from the gages to

the test slabs were attached to the slabs by threading the upper end of the reference rods into brass fittings cemented into the slab. A view of one of the brass fittings in place in the slab is shown in Figure 29. The lower end of the reference rod served as the movable core in the transducer. Any vertical movement of the test slab was reflected in a similar movement of the core which, in turn, altered the output from the gage. Based on the individual calibration of each gage, deflections were measured to an accuracy of plus or minus 0.0005 inch. Friction between the reference rods and the subgrade was eliminated by enclosing the reference rods in an outer copper tube. During placement of the subgrade, soil adjacent to the reference rods was hand tamped to prevent damage to the rods and to maintain their vertical alignment. The rods were located along the longitudinal centerline of the traffic area, one at the center and one 45 inches on either side of the center. The three reference rods for the deflection gages can be seen in Figure 8 which shows the subgrade partially in place. By connecting the differential-transformer-type gages to a strip-chart recorder, permanent records of slab deflections were obtained for both static and dynamic loadings. By using these gages, deflections for points within the contact area of the applied loading could be obtained.

Strain Gages

41. Various arrangements of Type AX-5, SR-4 strain gage rosettes were used to measure strains in the top surface of the test slabs. Each rosette contained two 7/16-inch long gages oriented at 90° to each other. The maximum range of sensitivity for these gages, as given by the manufacturer, was 2 percent elongation or 0.02 inches per inch strain. Where the rosettes were used in connection with static loading tests, no additional covering for the gages was required. Where the slabs were loaded dynamically and the load wheel passed directly over the gages, each rosette was protected from damage by a covering consisting of a layer of 1/4-inch thick foam rubber held in place by a 3- by 4-inch piece of brass shim stock taped to the surface

of the slab. The gages were bonded to the surface of the slabs using conventional strain gage cement. All gages were allowed to air-dry at room temperature for a minimum period of 48 hours prior to testing. One arrangement of the rosettes showing the gages cemented to the slab surface prior to placement of the protective covering is shown in Figure 30. (These same gages with the protective covering in place may be seen in Figure 55.)

Pressure Gages

42. During the static loading tests made on Slab DM-7, an attempt was made to measure subgrade reactive pressures by placing three small pressure transducers on the bottom side of this slab prior to testing. These gages were approximately 3/4 inch in diameter by 1/16 inch in thickness, and were attached to the slab by means of a strip of pressure sensitive tape as shown in Figure 31. Construction of these gages was similar to that of a condenser so that a change in the pressure applied to the gages resulted in a measurable change in the capacitance of the gages. All gages were located along the longitudinal centerline of the slab, one approximately at the center and each of the quarter-points.

Data Recording Equipment

43. Provision was made whereby the output of the differential-transformer-type deflection gages, the SR-4 strain gages and the subgrade reactive pressure gages could be recorded on a 10-bank panel of Esterline-Angus strip-chart recorders. These recorders were equipped with plug-in amplifying circuits, designed and built at ORDL, which permitted easy switching of various combinations of gages as required by the testing. A view of the instrument panel containing the 10 recorders and associated amplifying circuits is shown in Figure 32.

44. For those tests where strain measurements were obtained for static loadings, it was not possible to use the strip-chart recorders due to the drift which occurred in the amplifying circuits. For these measurements, the

strain gages were connected to two multiple selector switches, each of which was connected to a transistorized, direct-reading, Baldwin-Lima-Hamilton SR-4 strain indicator, Type N.

SECTION IV: ANALYTICAL METHODS

45. Where possible, the experimental data obtained from the model tests were compared with corresponding values computed in accordance with applicable theoretical analyses. The various procedures followed in reducing the experimental and theoretical values to forms suitable for direct comparison are described in the following paragraphs.

Stresses

46. Experimental. All strain measurements obtained were for the case of interior loading. By orienting the strain gage rosettes so that the gages measured strains along the axes of symmetry of the applied loading, the strains thus obtained were converted to unit stresses by means of the following equations:

$$\sigma_x = \frac{E\,(\epsilon_x + \mu\,\epsilon_y)}{1 - \mu^2} \quad \ldots\ldots\ldots\ldots\ldots \quad (2)$$

$$\sigma_y = \frac{E\,(\epsilon_y + \mu\,\epsilon_x)}{1 - \mu^2} \quad \ldots\ldots\ldots\ldots\ldots \quad (3)$$

where

σ_x, σ_y = major and minor principal unit stresses,

ϵ_x, ϵ_y = major and minor principal unit strains,

E = modulus of elasticity of concrete,

μ = Poisson's ratio of concrete.

The above equations assume that the strains were obtained for conditions of elastic behavior of the concrete and that the strain in the vertical direction was negligible.

47. Theoretical. Assuming the shape of the tire contact area to be elliptical, the Westergaard analysis as given in Reference No. 15 was used to compute the theoretical stresses at the center of the loaded area. The applicability of this analysis is restricted to conditions of elastic behavior in both the slab and the subgrade.

$$\begin{matrix}\sigma_x \\ \sigma_y\end{matrix} = \frac{3P}{8\pi h^2}\left[(1+\mu)\log\frac{E h^3}{k\left(\frac{a+b}{2}\right)^4} \pm 2(1-\mu)\left(\frac{a-b}{a+b}\right)\right] \quad \ldots . \quad (4)$$

where

P = wheel load,

h = slab thickness,

μ = Poisson's ratio of concrete,

E = modulus of elasticity of concrete,

k = modulus of subgrade reaction,

a, b = semi-axes of elliptical contact area $\frac{x^2}{a^2} + \frac{y^2}{b^2} = 1$,

x, y = horizontal rectangular coordinates.

The influence charts prepared by Pickett (16) were used to determine the stresses at points other than at the center of the loaded area. These charts also were used to determine stresses at the center of the loaded area when the shape of the contact area was more rectangular than elliptical.

Deflections

48. Experimental. Since the deflections determined experimentally were indicated directly by both the dial gages and the strip-chart recorders, no conversions were necessary in order to put these data in a form suitable for comparison with the theory. All deflection measurements were obtained for the condition of interior loading.

49. Theoretical. Assuming the shape of the tire contact area to be elliptical, the Westergaard analysis as given in Reference No. 15 was used to compute the theoretical deflections at the center of the loaded area. The applicability of this analysis is restricted to conditions of elastic behavior in both the slab and the subgrade.

$$z_i = \frac{P}{8k\,\ell^2}\left[1 - \frac{a^2+b^2}{16\pi\,\ell^2}\log\frac{Eh^3}{k\left(\frac{a+b}{2}\right)^4} - \frac{a^2+4ab+b^2}{16\pi\,\ell^2}\right] \quad \ldots \quad (5)$$

where

z_i = maximum deflection,

P = wheel load,

k = modulus of subgrade reaction,

ℓ = radius of relative stiffness,

E = modulus of elasticity of concrete,

h = slab thickness,

a, b = semi-axes of elliptical contact area.

Repetitive Loadings

50. As a result of the changes in modulus of subgrade reaction, concrete flexural strength and slab thickness that occurred from one test slab to another, it was necessary to evaluate the over-all effect which these changes had on the load-carrying capacity of each test slab. For this evaluation, relationships developed from previous static-loading model studies (6) were used to compute the failure load under static loading conditions for each individual test slab. The ratio of the static load producing failure to the repetitive load producing failure was designated as the design factor for repetitive loading. These design factors, as determined for each slab, then were correlated with the number of coverages producing failure.

SECTION V: TEST RESULTS

Strain Measurements

51. Slab DM-1. For strain measurements in the top surface of Slab DM-1, six of the Type AX-5 rosettes were mounted in a line along the transverse centerline of the slab. One rosette was positioned 6 inches from the centerline of the traffic area, one on the edge of the traffic areas, and the remaining rosettes at distances of 3, 6, 9, and 12 inches outside the traffic area. All rosettes were oriented to measure longitudinal and transverse strains. Strain measurements were obtained for both static and dynamic loadings.

52. Static loadings were applied initially to Slab DM-1 using the loading rig with the load wheel centered over the rosette nearest the center of the slab. Strain measurements for all gages were obtained at loads of 430 pounds (the weight of the empty load box and load wheel) and at 610 pounds. In an attempt to determine the load producing initial cracking in the bottom surface of the slab, the loading was increased from 610 pounds to 770 pounds in increments of 10 pounds, from 770 pounds to 1070 pounds in increments of 25 pounds, and from 1070 pounds to 1205 pounds in increments of 45 pounds. For the load increments between 610 pounds and 1205 pounds, only strains from the rosette under the load wheel were obtained. At the 1205-pound loading, strains again were measured for all gages. A plot of strain versus static load for the rosette directly under the load wheel is shown in Figure 33. Since the tire contact area was nearly square in shape, the strains for the two gages should have been in rather close agreement. There was no readily apparent reason for the significant difference observed. It is of interest, however, that the theoretical load-strain curve coincides closely with the average strain indicated by the two gages. Examination of the curves of measured strain did not give a clear indication as to the

termination of purely elastic behavior in the slab. The discontinuity in measured strains which occurred at a load of 905 pounds developed during a 1-hour delay in the testing. Radial stresses determined from the measured strains for static loadings are shown in Figure 34. The theoretical strains and stresses indicated in Figures 33 and 34 were computed from Pickett's influence charts and are applicable to conditions of elastic behavior only.

53. Following completion of the static loading tests, repetitive loadings were initiated using a wheel load of 1240 pounds. At the completion of 2400 coverages of this loading, a complete set of strain measurements was obtained for the case of dynamic loading in which the load wheel was rolled directly over the rosette closest to the center of the slab. A plot of the radial stresses as determined from the measured strains for this dynamic loading of 1240 pounds is shown in Figure 35 for comparison with the experimental curve of radial stress obtained prior to any dynamic loading for a static loading of 1205 pounds.

54. Slab DM-4. For strain measurements in the top surface of Slab DM-4, five of the Type AX-5 rosettes were mounted on a longitudinal line offset two inches from the longitudinal centerline of the slab and in an area midway between two of the deflection gages. All rosettes were spaced 5 inches apart and were oriented to measure longitudinal and transverse strains. Strain measurements were obtained for both static and dynamic loadings.

55. Static loadings were applied initially to Slab DM-4 using the loading rig with the load wheel positioned alternately over each of the 5 rosettes. Strain measurements from all gages were obtained for each load position and for loads of 430, 792, 1342, and 1800 pounds. These strains then were converted to radial and tangential stresses. Considerable variation in magnitude of stress was indicated by the five rosettes when compared on the basis of similar conditions of loading. Curves of radial and tangential stresses computed from the measured strains from one to the rosettes are shown in Figure 36. These data represent what was considered to be the best obtained from any of the rosettes for Slab DM-4.

56. Following completion of the static loading tests, repetitive loadings were initiated using a wheel load of 1800 pounds. At the completion of 2400 coverages of this loading, strain measurements for both static and dynamic loadings were obtained from one rosette which appeared to be still functioning properly. Using the repetitive loading test load of 1800 pounds, strains were measured for the load wheel positioned at various distances offset longitudinally and transversely from the rosette. When converted to radial and tangential stresses, however, these strain data gave highly unrealistic values and have not been included in this report. Since the slab failed almost immediately after resumption of the repetitive loadings, it was concluded that cracking in the slab had progressed to a degree where it was not possible to obtain reliable strain measurements.

57. Slab DM-5. For strain measurements in the top surface of Slab DM-5, five Type AX-5 rosettes were used in an arrangement identical to that described previously for Slab DM-4. Static loadings were applied in conjunction with dynamic loadings in an initial series of tests conducted prior to initiation of the repetitive loadings. In these initial tests, strain measurements were obtained from one strain gage rosette only and with the load wheel centered over that rosette. Test loads included 430, 749, 995, 1247, 1494, and 1745 pounds. For each loading, both static and dynamic strain measurements were obtained before increasing the load to the next higher level. Longitudinal and transverse stresses computed from the measured strains for static and dynamic loadings are shown with comparable theoretical stresses in Figure 37. The theoretical stresses indicated in Figure 37 were based on elastic behavior of the slab and subgrade for the entire range of loadings used. The change in size of the tire contact area relative to the change in wheel load also was taken into consideration in computing the theoretical stresses.

58. Following completion of the initial static and dynamic tests, repetitive loadings were initiated on Slab DM-5 using a wheel load of 1750 pounds. Dynamic strain measurements were made periodically throughout the test life of the slab. Two of the five strain gage rosettes remained

operative during the entire test. A summary of maximum longitudinal and transverse stresses, as computed from the measured strains from these two rosettes, is given in Table 4 for various coverage levels. While there was relatively good agreement between the two rosettes which provided the data given in Table 4, there was an appreciable difference in the maximum stresses as indicated by these rosettes and the maximum stresses as indicated by the rosette used for the preliminary testing. Inasmuch as the length and width of the tire contact were nearly equal for a load of 1750 pounds, theoretically the longitudinal and transverse stresses should have been nearly equal. As can be seen from Table 4, the experimental data indicated large differences between the longitudinal and transverse stresses.

59. Slab DM-7. No dynamic or repetitive loadings tests were made on Slab DM-7. All tests were static loadings applied to the slab through single circular contact areas. The loads were applied at three locations on the slab, with a different size of contact area being used at each location. These static load tests were made to provide a means whereby the test results as reported herein for the repetitive loading model might be correlated with test results as obtained previously from small-scale static loading model tests (6).

60. For Slab DM-7, eleven Type AX-5 strain gage rosettes were arranged along two axes 45° apart at each load position, as shown in Figure 38. One of the axes was in the transverse direction of the slab and the rosette at the apex of the two axes was positioned over the intersection of two stressing wires. The load positions were located near the center and quarter-points of the longitudinal centerline of the slab. Spacing between individual rosettes was 4 inches. All rosettes were oriented to indicate radial and tangential strains.

61. The test set-up used for conducting the static loading tests is shown in Figure 39. The initial test was made at the center of the slab using a 3-inch diameter contact area. Subsequent tests were made at the quarter-point locations using 4-inch and 6-inch diameter contact areas. The loads were applied in 45-pound increments by jacking against a reaction beam.

Loading at each location was carried to complete failure at which point the loaded area punched through the slab. For loadings within the range of elastic behavior in the slab, strains at the center rosette were measured for each increment of load in an attempt to determine the load producing the initial cracking in the bottom surface of the slab. For loadings within the range of inelastic behavior in the slab, strain measurements were made for each increment of load only for the rosettes nearest the area where cracking due to excessive negative radial moment was expected to occur. At selected loadings, strain measurements were obtained for all eleven rosettes. These measured strains were converted to radial stresses and are presented in Figures 40 through 45. For the radial stress curves shown in these figures, the dashed portions of the curves indicate areas in which some degree of stress relief occurred. It was believed that this stress relief indicated the presence of cracking due to excessive negative radial moment, even though these cracks were not always detected by visual inspection of the slab surface.

Deflection Measurements

62. Static Loadings. Where static loading tests were conducted to determine the wheel load required to produce initial cracking in the bottom surface of the slab, deflection measurements generally were obtained in conjunction with the strain measurements. This provided alternate methods for determining the true cracking load. Static deflection measurements also were obtained for those slabs where volumetric displacement tests were made to determine the modulus of subgrade reaction. Typical load-deflection data for static loading tests are shown in Figure 46 for comparison with theoretical deflections based on elastic behavior of the slab and subgrade. Comparison of observed and theoretical maximum deflections per 100 pounds of wheel load are shown in Table 5 for five different test slabs. In this table, the indicated deflections per 100 pounds of wheel load are for loadings within the range of elastic behavior of the slab and subgrade. Examination of the data presented in Figure 46 and in Table 5 indicates relatively good

agreement between the model and the theory for deflections due to static loadings. Maximum total deflections as measured for the loads producing initial cracking in Slabs DM-1 through DM-5 are given in Table 6. Since deflections were not obtained at the center of the loaded area for Slabs DM-6 and DM-7, data on these two slabs could not be included.

63. Dynamic Loadings. During the repetitive loading tests, a continuous record of the slab deflection was made using the differential-transformer-type deflection gages. The recorded data was obtained in a form such that the permanent vertical displacement of the slab could be separated from the dynamic or transient deflection. By plotting the deflections at frequent intervals of coverages and by maintaining a close surveillance of the data as it was being automatically recorded, imminent failure of the slab could be noted and the development of this failure observed. Complete failure of the slab was presaged by an extremely rapid increase in the transient deflection. A typical deflection "history" showing the permanent, transient and total deflections for the repetitive loading tests prior to failure is given in Figure 47.

64. In addition to obtaining maximum deflections, the continuous recording of data also made it possible to construct the complete curve of deflection as related to the distance from the gage to the load wheel. During the testing of Slab DM-2, 40,000 coverages of the initial wheel load of 1200 pounds were applied without producing any noticable signs of distress in the slab. The shape of the dynamic deflection curve in the longitudinal direction is shown in Figure 48. In this figure, deflection curves determined at 1000, 5000, 10,000, and 40,000 coverages have been plotted to indicate the magnitude of change that occurred during application of this initial test loading. After completion of the 40,000 coverages at 1200 pounds, the wheel load was increased to 1850 pounds. This increased loading produced failure in the slab at 2211 coverages. Curves indicating the relative deflection per pound of wheel load are shown

in Figure 49 for: (1) at 40,000 coverages of the 1200-pound loading, and (2) at 2100 coverages of the 1850-pound loading. Inelastic behavior of the slab was indicated by the greater rate of deflection for the higher loading.

Slab Failures

65. Repetitive Loadings. In the repetitive loading tests, the wheel loads were determined on the basis of preliminary data relative to the flexural strength of the slab and the modulus of subgrade reaction, and with regard to the approximate number of coverages desired. After selection of the wheel load, the repetitive loadings were applied until a failure developed in the slab or until a specified number of coverages had been attained. When the test load did not produce a failure within the specified number of coverages, the wheel load was increased and the repetitive loadings were resumed. A summary of wheel loads and corresponding number of coverages applied to the slab subjected to repetitive loading tests is given in Table 7.

66. Once initial distress was observed to have developed in a test slab, the progression of this distress to a complete failure condition was extremely rapid under continued application of the wheel load. The initial distress appeared as circular cracking, 12 to 18 inches in diameter, in the top surface of the slab in the traffic area. As few as 5 to 10 additional coverages of the wheel load generally were sufficient to completely disintegrate the concrete for the full depth of the slab in the distressed area. Figure 50 shows a close-up view of the initial cracking as observed in the top surface of the test slabs. Under continued load application, this initial cracking rapidly developed into a condition similar to those shown in Figures 51, 52, and 53. At this point, the concrete within the distressed area was completely disintegrated. Figure 54 shows one of the failed areas with the disintegrated surface material removed. As can be

seen in this figure, the concrete below the exposed prestressing wires also had been completely broken up. There was, however, no indication in any of the test slabs of any yielding in the prestressing wires nor was there any evidence of bond failure between the wires and the concrete outside the disintegrated area.

67. In testing the first three slabs, the repetitive loadings were discontinued after development of the first failure. In the final three slabs, the repetitive loadings were continued until each slab had failed at three different locations. For those slabs where the repetitive loadings were continued after the first failure, the failed area was covered with a 30-inch square steel plate 1/4 inch thick. The steel plate served to bridge the failed area, thus preventing an enlargement of the failed area. A view of a steel plate in place on one of the test slabs is shown in Figure 55. After development of the second failed area, a second steel plate was placed on the slab surface so that the repetitive loadings could be continued to produce a third failure.

68. After completion of the repetitive loading tests, the slabs were removed from the subgrade and placed on edge so that the bottom surface of each slab could be inspected. All cracks in the bottom surface that could be detected visually were marked with ink. The resultant crack patterns for each test slab are shown in Figures 56 through 61. It can be noted from these figures that the cracking in the bottom surface of the slabs was confined almost entirely to the traffic area. Following the removal of the slabs from the subgrade, an imprint of the bottom surface crack patterns was observed on the polyethylene sheet placed between the slabs and the subgrade. Figure 62 shows a portion of the crack pattern for Slab DM-3 as it appeared on the polyethylene sheet. Apparently the imprint was formed by fine concrete dust abraded from the interfaces of the cracks as they opened and closed under the repeated passage of the wheel load.

69. Static Loadings. As described previously, static loading tests to failure were made only on Slab DM-7. In these tests, an attempt was made

to determine the loads producing the three phases of progressive failure as observed in previous small-scale model studies of prestressed pavement (6):

(1) initial tensile cracking in the bottom surface of the slab due to excessive positive moment,

(2) secondary circumferential tensile cracking in the top surface of the slab due to excessive negative radial moment,

(3) ultimate failure characterized by a punching-shear failure.

The initial test was made at the center of Slab DM-7 using a 3-inch diameter circular contact area as shown in Figure 39. The second and third tests were made approximately at the quarter-points using 4-inch and 6-inch diameter circular contact areas, respectively. A summary of the failure loads and corresponding failure stresses for the various sizes of contact areas is given in Table 8. For the 3-inch diameter contact area, the strain gage rosette under the center of the loading became inoperative after the load was increased above 700 pounds and no stress for failure due to excessive positive moment was obtained. For the second and third tests, the contact was recessed slightly over the center rosette to avoid damaging the strain gages at the higher loads.

70. No negative moment cracking was observed in the top surface of Slab DM-7 for either the 3-inch or the 4-inch diameter loadings. As pointed out previously in Paragraph 61, however, the radial strain measurements for these loadings indicated that some form of stress relief occurred in the top surface even though there were no visible cracks. Negative moment cracking did develop for the 6-inch diameter loading, as shown in Figure 64. Following completion of the static loading tests, Slab DM-7 was removed from the subgrade and an inspection made of the cracking in the bottom surface of the slab. A view of the bottom surface showing the failed areas and associated crack patterns is presented in Figure 63.

SECTION VI: ANALYSIS AND DISCUSSION OF TEST RESULTS

Strain Measurements

71. For all strain measurements, the orientation of the load contact area with respect to the strain gage rosettes was such that the measured strains were principal strains. Absolute determination of the principal strains, however, was possible only for the condition of elastic behavior of the slab. After development of initial cracking in the bottom surface of the slab, the gages may or may not have been indicating principal strains. Based on this limitation, the stresses computed from strains measured for loadings producing inelastic behavior should be considered as relative only. Even so, these data are considered as being sufficiently accurate to indicate the general pattern of behavior of prestressed pavements subjected to repetitive loadings.

72. Slab DM-1. For the static loading tests made on Slab DM-1, there were some points of difference noted between the stresses and strains determined experimentally and the corresponding stresses and strains determined theoretically. As stated previously in Paragraph 52, there was no apparent reason for the significant difference in maximum strains obtained from the two gages in the rosette directly under the wheel load (Figure 33). Although the maximum static loading of 1205 pounds was substantially greater than the theoretical first crack load of 750 pounds, the load-strain data presented in Figure 33 generally are linear throughout the entire load range. Thus, these maximum strains did not give a clear indication as to the load at which elastic behavior of the slab terminated. With regard to the distribution of radial stresses in Slab DM-1, the curves of experimental stress shown in Figure 34 indicate the point of zero stress to be 12 to 13 inches (1.4 ℓ) from the center of the wheel load. This is in contrast to a distance of 9 inches (1.0 ℓ) from the center of the wheel load for the point

of zero stress as determined theoretically. Otherwise, the general shapes of the experimental and the theoretical curves of radial stress are quite similar.

73. Experimental values of radial stress for dynamic loading conditions were obtained for Slab DM-1 as shown in Figure 35. These stresses were computed from strains measured after 2400 coverages of a 1240-pound wheel load. The radial stresses for static loading shown in Figure 35 for comparison with the dynamic loading stresses were obtained during the initial static loading tests made prior to any repetitive loadings. The cracking in the bottom of the slab at the time of the static loading tests was limited. As can be seen from Figure 35, the two stress curves bear little resemblance to each other. Considering that the slab failed at 2846 coverages, it was believed that the stresses for dynamic loading were affected significantly by the cracks present in the bottom surface of the slab (Figure 56). It was expected, however, that the maximum negative radial stress at this point in the life of the slab would be substantially greater than the indicated 200 pounds per square inch. Inasmuch as the radial stresses were based on strains measured outside the traffic area while all slab failures occurred within the traffic area, it is possible that the experimental data did not represent the maximum negative radial stress present in the slab. Although the magnitude of the maximum radial stress was not as great as anticipated, it was noted that the location of this stress was closer to the center of the wheel load than had been the case for the static loadings. Such behavior was in agreement with previous experience (6) and theoretical analyses (7).

74. Slab DM-4. Both radial and tangential stresses were computed from the strain data for static loadings on Slab DM-4, and are shown in Figure 36. As in Slab DM-1, there was an appreciable difference between the strains as indicated by the two gages in the rosette directly under the center of the load wheel. Thus, in Figure 36, the difference in radial and tangential stress under the center of the load is the result of the disagreement in measured strains. Based on an observed first crack load of 875 pounds, the

maximum positive radial stresses appear to be much too high to be considered as valid data. Additional strain measurements, after 2400 coverages of an 1800-pound wheel load, also were obtained for dynamic loading conditions on Slab DM-4. As stated previously in Paragraph 56, these strains gave highly unrealistic stress values and have not been included in this report.

75. Slab DM-5. Only maximum strains under the center of the load wheel were obtained from the initial series of static and dynamic loading tests on Slab DM-5. At the time these strains were obtained, the slab had been cracked to some degree on the bottom but had not been subjected to any repetitive loading. Since first the static and then the dynamic strains were obtained for any one load before progressing to the next higher load, the extent of the cracking for the static and dynamic loadings was practically the same. Load-stress curves based on these measured strains are shown in Figure 37 for comparison with theoretical stresses based on elastic behavior of the slab and subgrade. Examination of these curves indicates that, for elastic behavior (wheel loads of 430 and 749 pounds), the maximum stresses for dynamic loadings were less than half as great as the corresponding stresses obtained from static loadings. For loadings beyond the range of elastic behavior (wheel loads of 995 pounds or more), there was a tendency for the difference between the static and dynamic stresses to diminish. In all cases, however, the static stresses were greater than the corresponding dynamic stresses. The static stresses indicated a greater degree of linearity with load than did the dynamic stresses. The load-stress curve for static conditions generally was linear up to and including the 1494-pound wheel load, or well beyond the first crack load. In this load range, the experimental static stresses were approximately 30 percent greater than corresponding theoretical stresses. In the elastic range, the dynamic stresses were approximately 50 percent of the corresponding theoretical stresses. For inelastic behavior, the dynamic stresses increased with an increase in wheel load at a rate greater than the theoretical rate

of increase. Had the tire contact area remained constant for all loads, the theoretical load-stress curve in Figure 37 would have been linear. The small deviation from linearity was due to considering the change in contact area in computing the theoretical stresses. This small deviation also indicates the limited degree to which the stresses are influenced by such changes in tire contact area.

76. Maximum stresses computed from dynamic strain measurements made at various coverage levels throughout the life of Slab DM-5 are summarized in Table 4. Since the repetitive loading wheel load was 1750 pounds, all of the data presented in Table 4 are for inelastic behavior of the slab. While there was substantial disagreement between longtiudinal and transverse strain gages, relative to the magnitude of maximum stress, there was consistent agreement among all gages relative to the increase in stress with an increase in the number of coverages of the test load.

77. Slab DM-7. Two rows of strain gage rosettes were used for each of the three static loading tests on Slab DM-7. Previous experience with the small-scale static loading model (6) had indicated that the tensile cracking in the bottom surface of the slab could influence the top surface strain measurements if a radial crack occurred in close proximity to the line of gages. By using two rows of gages 45° apart, there was more assurance of obtaining valid data from at least one set of gages. Although both radial and tangential strains were measured, only the radial stresses were computed and considered for purposes of analysis. Curves of radial stress versus load for the three different sizes of load contact area are shown in Figures 40 through 45.

a. 3-inch Diameter Area. For the 3-inch diameter contact area, there was excellent agreement between radial stresses as indicated by the two rows of rosettes for loads up to and including 3569 pounds. For higher loads, it was believed that the transverse row of rosettes (Figure 40) provided the better data. Although no negative moment cracking was observed in the top surface of the slab, the radial stress curve for the 5073-pound

loading indicated that some measure of stress relief had been effected. The indicated failure stress of between 1000 and 1200 pounds per square inch was somewhat higher than the combined flexural strength and prestress of 986 pounds per square inch.

b. 4-inch Diameter Area. For the 4-inch diameter contact area, there was a substantial difference between radial stresses as indicated by the two rows of rosettes for loads exceeding the range of elastic behavior of the slab. For the higher loads, it was believed that the transverse row of rosettes (Figure 42) provided the better data. Although no negative moment cracking was observed in the top surface of the slab, the radial stress curve for the 5567-pound loading indicated that some measure of stress relief had been effected. The indicated failure stress of between 1050 and 1300 pounds per square inch was somewhat higher than the combined flexural strength and prestress of 986 pounds per square inch.

c. 6-inch Diameter Area. For the 6-inch diameter contact area, there was excellent agreement between radial stresses as indicated by the two rows of rosettes for loads up to and including 4071 pounds. Negative moment cracking occurred in the top surface of the slab at a load of 4494 pounds. As shown in Figure 64, this cracking extended slightly more than half way around the loaded area. Unfortunately, the cracking did not extend into the area in which the strain gages were located. Based on the radial stress versus load curves presented in Figure 44, it is indicated that the negative moment cracking occurred when the maximum negative radial stress was substantially less than the combined flexural strength and prestress of 986 pounds per square inch. The load-stress relationships given in Figure 44 for the higher loads are contradicted somewhat by the corresponding data given in Figure 45. In this latter figure, no stress relief was indicated prior to the 5575-pound loading. Similarly, the indicated failure stress of between 1020 and 1200 pounds per square inch was somewhat higher than the combined flexural strength and prestress of 986 pounds per square inch.

Deflection Measurements

78. Static Loadings. A comparison of measured and theoretical maximum deflections for static loadings within the range of elastic behavior of Slabs DM-1 through DM-5 is given in Table 5. As described previously in Paragraph 62, these data indicate relatively good agreement between the model and the theory. Ratios given in Figure 5 indicate that the measured deflections averaged 9.1 percent greater than the theoretical deflections. The curve of maximum measured deflection versus load for static loadings in the range of elastic behavior and beyond were used to determine the load and deflection at the formation of the initial tensile crack in the bottom surface of each slab. The curve of static load versus maximum deflection for Slab DM-3 shown in Figure 46 is representative of the data obtained for the static loading tests. As can be seen from the curve of Figure 46, the deflection per pound of wheel load for loadings in the elastic range was constant. When a deflection per pound of wheel load greater than the constant value observed for loadings in the elastic range was indicated, initial cracking was assumed to have occurred. After initial failure, the deflection per pound of wheel load increased gradually as the load in the range beyond that of elastic behavior increased. The experimental data presented for Slab DM-3 show that the change in deflection per pound of wheel load associated with the initial failure of a prestressed slab is not drastic. The maximum total deflections occurring at initial cracking are given in Table 6. These data indicate the maximum elastic deflections to be in relatively good agreement at approximately 0.02 inch for all five of the slabs listed.

79. Dynamic Loadings. The deflection data collected as the dynamic loads were being applied to Slabs DM-1 through DM-6 were similar in that the major portion of the increase in deflection that occurred with the increase in the number of coverages was attributable to a permanent displacement of the slab rather than to dynamic or "transient" deflection. Compaction of the subgrade permitted the permanent displacement of the slab. Failure of

the slabs was presaged by a rapid increase in the transient deflections. By monitoring the charts on which the deflections were being recorded during the repetitive loadings, the rapid increase in deflection could be observed and failure anticipated. Figure 47 illustrates the deflection "history" of Slab DM-5 during its repetitive loading life to 8600 coverages. At 8650 coverages, not shown on Figure 47, the transient deflections began to increase rapidly and by 8653 coverages the slab had failed completely.

80. The complete curves for transient deflection shown in Figures 48 and 49, illustrate another aspect of pavement behavior that can be observed in the model as a result of the continuous recording of data from the differential-transformer-type gages. It can be seen in these figures that the shape of the curve for transient deflection was not symmetrical about the deflection gage, but was influenced somewhat by the direction of travel of the load wheel with respect to the gage. The negative deflection of the slab was well-defined as the load wheel approached the gage. The portion of the curves which represents the deflection behind the wheel as the wheel moved away from the gage shows that not as much negative deflection developed behind the moving wheel as ahead of it, probably due, in part, to the fact that the area of the slab behind the wheel was in the process of rebounding from having been subjected to the full load. Also it can be seen in Figures 48 and 49 that the point of maximum deflection was recorded just after the load wheel passed over the gage. Apparently this was related to inertial forces within the slab and subgrade that resulted from the dynamic loading.

81. In Figure 48, the data presented are for a wheel load substantially less than that required to fail the slab. As a result, there was no increase in the maximum transient deflection with an increase in the number of coverages. Actually the deflection decreased somewhat after 1000 coverages and remained virtually unchanged thereafter. In Figure 49, the transient deflection has been presented in terms of deflection per pound of wheel load

in order to provide a direct comparison of the relative effects of the two wheel loads. A suggestion that some measure of structural deterioration was occurring in the slab under the 1800-pound wheel load was indicated by the increased negative deflection as the load wheel approached the gage. Inelastic behavior of the slab was indicated by the greater rate of deflection for the higher loading. Also it can be seen from the difference in the measured deflections behind the wheel that there was some additional lag in the rebound of the slab for the 1800-pound wheel load as compared to the 1200-pound wheel load.

Slab Failures

82. Repetitive Loadings. The repetitive loading tests for Slabs DM-1 through DM-6 produced failures in the top surface of the model slabs that closely resembled the failures produced during accelerated traffic testing of full-scale experimental prestressed pavements (3). Both the repetitive loading model and the full-scale tests indicated that, when subjected to repetitive loadings, prestressed pavements on a low-strength subgrade did not develop a well-defined circumferential cracking due to excessive negative radial moment. Once initial distress was observed to have developed in the surface of a model slab, the progression of this distress to a complete failure condition was extremely rapid under continued application of the wheel load. This rapid deterioration of the pavement to a completely failed condition also was experienced in the full-scale prestressed pavements following development of the initial cracking in the top surface of the slab.

83. The several variables associated with each model slab tested in this study (slab thickness, concrete flexural strength, modulus of subgrade reaction, wheel load and tire contact area) made it desirable to resolve the combined effects of these variables into some form whereby the relative performance of each individual slab might readily be compared. Accordingly, the load-carrying capacities of the slabs were analyzed using procedures

developed during previous small-scale static-loading model tests of prestressed slabs. In this method, the load that would be required to produce negative moment cracking under a single static application is determined. The load-moment relationships used in making this computation were the non-dimensional relationships presented in Reference No. 6. The equation for determining this failure load is as follows:

$$P_f = \frac{h^2 (R + R_p)}{6 \left[C \frac{M_o}{P_o} - \frac{M_r}{P_o} \right]} \quad \ldots\ldots\ldots\ldots \quad (6)$$

where h = thickness of the slab, inches,

R = flexural strength of the concrete, psi,

R_p = prestress, psi

C = radial moment correction factor,

M_o/P_o = moment coefficient under center of loaded area,

M_r/P_o = moment coefficient at point of negative moment cracking.

In using the above equation, values for C and M_r/P_o must be obtained from the appropriate curves given in Reference No. 6. Although values for M_o/P_o may be computed from equations given in Reference No. 15, a graphical solution is presented in Reference No. 6.

84. Tentative criteria for the design of prestressed airfield pavements have been predicated on defining failure for this type of pavement as the occurrence of negative moment cracking. Thus, to provide for the effect of load repetition, the design wheel load for a prestressed pavement must be less than the negative moment cracking load. The factor by which the negative moment cracking load is reduced for design purposes has been designated as the "design factor for repetitive loading." In evaluating the results of the model tests, repetitive loading design factors for each slab were determined

by dividing the negative moment cracking load, as determined from Equation 6, by the wheel load used for the repetitive loadings. In Test Slabs DM-4, DM-5, and DM-6, repetitive loading design factors were computed for each failure developed in these slabs. A summary of the design factors obtained from the model is given in Table 9. By plotting a curve of design factors versus coverages, as shown in Figure 65, the data from the model tests form the basis for predicting the traffic life of a prestressed pavement where other combinations of values for the design variables are involved. Since the failures experienced in the model were ultimate failures, the reader is cautioned that the relationship indicated in Figure 65 must be considered as being unconservative for design or evaluation purposes.

85. Static Loadings. As have been described previously herein, static loading tests were conducted on several of the test slabs prior to the initiation of the repetitive loading tests. While these static loading were not carried to ultimate failure, they were carried to a point well beyond the limits of elastic behavior in the slabs. This served to provide data for comparing the model and the theory with regard to the loads producing the initial tensile cracking in the bottom surface of the slabs. A summary of the observed and the theoretical first crack loads for Slabs DM-1 through DM-5 is presented in Table 10. Also shown in this table is a comparison of the theoretical cracking stress (based on the measured first crack load) and the sum of the flexural strength and the prestress. For all slabs where the wheel was used to apply the load, the measured first crack load was greater than that predicted by the theory. The difference ranged from 2.4% to 13.9% greater than the theory and averaged approximately 8%. Similarly, the theoretical cracking stress ranged from 1.9% to 12.3% greater than the sum of the flexural strength and the prestress, and the difference averaged approximately 7%.

86. For the static loading tests conducted on Slab DM-7, each size of contact area was loaded until an ultimate failure condition was produced in the slab. As discussed previously in Paragraph 69, during these tests an

attempt was made to determine the loads producing the initial tensile cracking in the bottom surface of the slab and the loads producing the negative moment cracking in the top surface of the slab. A summary of all failure loads as determined from the static loading tests on Slab DM-7 is given in Table 8.

87. The primary objective in conducting the static loading tests on Slab DM-7 was to determine the degree of correlation between the repetitive loading model and the smaller scale static loading model (6). A summary of test data as obtained from Slab DM-7 is given in Table 11 along with corresponding values predicted on the basis of the performance of the smaller model. Since negative moment cracking was observed only in the test using the 6-inch diameter contact area, much of the data presented in this table was based on values estimated from the stress relief indicated by the curves of radial stress shown in Figures 40 through 45. While admittedly the data presented in Table 11 are too meager to be considered conclusive, they do permit some comparisons of the statically loaded dynamic loading model (a concrete slab on a low strength clay subgrade) with the statically loaded static loading model (a Hydrocal slab on a natural rubber subgrade), including the following:

a. The radius of the negative moment cracking in the repetitive loading model was greater than that predicted by the static loading model.

b. The magnitude of the negative moment cracking loads in the repetitive loading model was greater than that predicted by the static loading model.

c. The repetitive loading model did not indicate any particular sensitivity to changes in the size of the load contact area except with respect to the punching shear failure load.

d. The difference between the punching shear failure load and the negative moment cracking load was substantially greater for the repetitive loading model than it was for the static loading model.

e. The mode of failure under static loading was the same for both models.

SECTION VII. CONCLUSIONS AND RECOMMENDATIONS

88. General Observations. In analyzing the results of the model tests performed to study the behavior of pre-tensioned prestressed rigid pavement supported by a low-strength subgrade and subjected to repetitive loadings by a rolling single wheel, as described herein, the following general observations were made:

a. Closer control over the concrete batching operations would reduce the variation in flexural strength observed for individual test slabs and thereby reduce the effect of flexural strength as a variable in the performance of the model.

b. The most uniform distribution of prestress was achieved by placing all longitudinal stressing wires in one plane at mid-depth in the slab and all transverse stressing wires alternately above and below the longitudinal wires.

c. Despite precautions taken during construction of the model, some moisture loss from the subgrade was experienced. This loss resulted in a gradual increase in the modulus of subgrade reaction during the test series, and required that k be considered as a variable in analyzing the performance of the model.

d. Plate bearing tests generally proved to be more consistent in determining the modulus of subgrade reaction than did tests based on the total volumetric displacement of the subgrade for static loadings on the slab.

e. Performance of the pavement-subgrade separation gages indicated that the slabs remained in contact with the subgrade throughout the repetitive loading tests.

f. Performance of the subgrade reactive pressure gages proved to be too erratic to provide any usable data. This later was shown to be due to a design deficiency in the gage.

g. By the use of protective coveringa, the SR-4 strain gages could be placed within the traffic area and maintained in an operating condition throughout several thousand coverages of the wheel load.

h. Determination of true principal stresses from the measured strains was restricted by the fact that such determinations were possible only in those areas of a slab where the behavior of the slab was essentially elastic. Stresses computed from measured strains obtained for conditions of inelastic behavior (wherein the direction of the principal strain was not known) must be considered approximate only.

i. Measured strains from static loading more nearly agreed with the theoretical strains than did measured strains obtained from dynamic loadings.

j. The magnitude of strain in the top surface of the prestressed slabs increased with an increase in the number of applications of the repetitive loading.

k. Maximum strains and deflections produced by the rolling wheel load were considerably less than corresponding strains and deflections produced by a static application of the same load.

l. For static loadings within the range of elastic behavior, measured deflections averaged approximately eight percent higher than corresponding theoretical deflections.

m. For the rolling dynamic loadings, the shape of the deflection curve was influenced somewhat by the direction of travel of the load wheel.

n. No abrupt increase in pavement deflection was observed in conjunction with the development of the initial tensile cracking in the bottom surface of the slab.

o. For the repetitive traffic loadings, the major portion of the increase in deflection that occurred with an increase in the number of load applications was attributable to the permanent vertical displacement of the slab which compaction of the subgrade permitted.

p. A rapid increase in the transient deflection during the repetitive loading tests presaged the impending failure of the slab.

q. Once initial structural distress became visible in the top surface of a slab, the progression of this distress to a condition of complete failure was brought about by only a few additional passes of the load wheel.

r. For prestressed slabs, excessive radial stresses in the top surface were relieved without the formation of visible cracking.

s. For loadings beyond the range of elastic behavior, an increase in wheel load resulted in the point of maximum negative radial stress moving toward the center of the load contact area.

t. The magnitude of the negative moment cracking load for static loading tests in the repetitive loading model was greater than that predicted by the static loading model tests.

u. The radius of the negative moment crack for static loading tests in the repetitive loading model was greater than that predicted by the static loading model tests.

v. For static loading tests carried to ultimate failure, the mode of progressive failure in the repetitive loading model was similar to that observed in previous small-scale static loading model studies.

w. For repetitive loading tests, tensile cracking in the bottom surface of the slab was contained almost entirely within the traffic area.

89. Specific Conclusions. Results of the series of model tests described herein are considered adequate to warrant the following conclusions:

a. The repetitive loading model provided a reliable simulation of the behavior of full-scale prestressed pavements subjected to moving loads. Failures induced in the model slabs closely resembled failures induced in full-scale accelerated-traffic tests of prestressed pavements supported on a low-strength subgrade.

b. The degree of agreement between the repetitive loading model and full-scale experimental prestressed pavements is sufficient to permit

application of the relationships developed from the repetitive loading model to the design and evaluation of prestressed airfield pavements. In view of the abruptness with which the failures have been observed to develop in such pavements, the designer is cautioned that the specific relationships presented herein must be considered as being unconservative.

c. The model provided a means of obtaining experimental strain and deflection data for comparison with generally accepted theories based on purely elastic structural behavior. Good agreement between the model and the theoretical analyses of Westergaard was obtained for static loadings within the range of elastic behavior of the slab.

d. The repetitive loading model test results indicated that a load is less severe when applied dynamically than when applied statically.

e. The effect of repetitive loadings on prestressed rigid pavements can be defined by the use of a "design factor" relating the design wheel load to the static load producing failure from negative moment cracking.

f. The repetitive loading model appears sufficiently versatile to be used for investigating the effects of other variables such as subgrade strength and magnitude of prestress.

90. Recommendations. Inasmuch as the tests described herein did not simulate the entire range of conditions encountered in the design and evaluation of full-scale prestressed rigid pavement, it is recommended that sufficient additional repetitive loading model tests be performed for the aggregate test results to be applicable to all conditions. It is recommended that the additional repetitive loading model tests include:

a. Tests to study the behavior of rigid pavement, prestressed equally longitudinally and transversely, on a high-strength subgrade.

b. Tests to study the behavior of rigid pavement, prestressed equally longitudinally and transversely, on an intermediate-strength subgrade, should the data obtained using the low-strength subgrade and the

high-strength subgrade not provide sufficient information.

c. Tests to study the behavior of rigid pavement having the prestress in the longitudinal direction different than the prestress in the transverse direction.

REFERENCES

1. "Theoretical and Practical Aspects of Prestressed Concrete for Highway Pavements," Thomas Cholnoky, Highway Research Board Bulletin 179, 1958.

2. "Experimental Prestressed Concrete Highway Project in Pittsburgh," Ben Moreell, et al., Proceedings, Highway Research Board, 1958.

3. "Development of a Procedure for the Design of Prestressed Airfield Pavements," James P. Sale, et al., Proceedings, Highway Research Board, 1961.

4. "Design and Construction Report, Prestressed Concrete Test Tracks P1 and P2, Sharonville, Ohio," Carl F. Renz, et al., Ohio River Division Laboratories Technical Report No. 4-14, November 1960.

5. "Small-Scale Model Studies of Prestressed Rigid Pavements for Military Airfields, Part I, Development of the Model and Results of Exploratory Tests," Paul F. Carlton, et al., Ohio River Division Laboratories Technical Report No. 4-13, May 1962.

6. "Small-Scale Model Studies of Prestressed Rigid Pavements for Military Airfields, Part II, Single-Wheel Loadings on Pre-Tensioned and Post-Tensioned Slabs," Paul F. Carlton, et al., Ohio River Division Laboratories Technical Report No. 4-25, September 1962.

7. "Experimental Theoretical Study of a Prestressed Slab on an Elastic Support Beyond the Limits of Elasticity," Franco Levi, Annales de L'Institut Technique du Batiment et des Travaux Publics, June 1953.

REFERENCES (Cont'd)

8. "Design of Prestressed Concrete Runways," Pierre D. Cot, et al., Revue Generale des Routes et des Aerodromes," No. 292, May 1956.

9. "Prestressed Concrete Taxiway No. 1, Naval Air Station, Lemoore, California," Carl F. Renz, Ohio River Division Laboratories, Memorandum Report, August 1960.

10. "Prestressed Concrete Taxiway, Biggs Air Force Base, Texas, U.S.A.," J. P. McIntyre, et al., Proceedings, Fourth Congress of the Federation Internationale de la Precontrainte, May 1962.

11. "Review of French and British Procedures in the Design of Prestressed Pavements," Phillip L. Melville, Highway Research Board Bulletin 179, 1958.

12. "Prestressed Concrete Airfield Pavements," Frank M. Mellinger, Proceedings, The World Conference on Prestressed Concrete, August 1957.

13. "Experience With Prestressed Concrete Airfield Pavements in the United States," Carl F. Renz, et al., Journal of the Prestressed Concrete Institute, Volume 6, No. 1, March 1961.

14. "Summary of Prestressed Concrete Pavement Practices," Frank M. Mellinger, Journal of the Air Transport Division, ASCE, Volume 87, No. AT2, August 1961.

15. "New Formulas for Stresses in Concrete Pavements of Airfields," H. M. Westergaard, Transactions, ASCE, Volume 113, 1948.

REFERENCES (Cont'd)

16. "Deflections, Moments and Reactive Pressures for Concrete Pavements," Gerald Pickett, et al., Kansas State College Bulletin No. 65, October 1951.

17. "Load-Carrying Capacity of Concrete Pavements," G. G. Meyerhof, Journal of the Soil Mechanics and Foundations Division, ASCE, Volume 88, No. SM3, June 1962.

Table 1

Concrete Flexural Strength as Determined from Control Beams

Slab No.	Flexural Strength, psi
DM-1	872
DM-2	970
DM-3	900
DM-4	890
DM-5	930
DM-6	950
DM-7	820

Table 2

Concrete Flexural Strength as Determined from "After-Traffic" Beams

Slab No.	Position of Stressing Wires	Beam Direction and Orientation	Average Slab Thickness, in.	Failure Stress, psi		Prestress, psi	Flexural Strength, psi
				As Tested	Average		
DM-1	Longitudinal Wires Above Transverse Wires	Longitudinal Normal Reverse	0.941	 1280 (13) 949 (9)	1115	266	849
DM-2	Longitudinal Wires Below Transverse Wires	Longitudinal Normal Reverse	0.996	 991 (8) 1326 (8)	1159	251	908
DM-3	Longitudinal Wires Below Transverse Wires	Longitudinal Normal Reverse	1.017	 851 (8) 1290 (8)	1071	246	825
		Transverse Normal Reverse	1.017	 1194 (10) 980 (10)	1087	246	841
DM-4	Longitudinal Wires Below Transverse Wires	Longitudinal Normal Reverse	1.002	 967 (8) 1236 (8)	1102	250	852
		Transverse Normal Reverse	1.002	 1185 (11) 978 (11)	1081	250	831

Table 2 (Cont'd)

Concrete Flexural Strength as Determined from "After-Traffic" Beams

Slab No.	Position of Stressing Wires	Beam Direction and Orientation	Average Slab Thickness, in.	Failure Stress, psi		Prestress, psi	Flexural Strength, psi
				As Tested	Average		
DM-5	Longitudinal Wires Between Transverse Wires	Longitudinal Normal Reverse	1.028	984 (16) 1046 (16)	1015	243	772
DM-6	Longitudinal Wires Between Transverse Wires	Longitudinal Normal Reverse	1.008	1072 (16) 1116 (16)	1094	248	846
DM-7	Longitudinal Wires Between Transverse Wires	Longitudinal Normal Reverse	1.001	963 (16) 1008 (7)	986	250	736

Notes: All Beams were Approximately 3.8" Wide by 30" Long.

Values in parenthesis indicate number of observations on which average is based.

Table 3

Results of Pull-Out Tests for Prestressing Wire and Concrete

Concrete Age, days	Embedment Length, in.	Pull-Out Load, lb.		Maximum Wire Stress, psi
		Total	Per Linear Inch	
Wires Cleaned With Acetone				
7	6	385	64	44,040
7	10	575	58	65,775
14	7	540	77	61,770
14	8	410	51	46,900
Wires Etched With Dilute Hydrochloric Acid				
7	8	1050	131	120,110
7	18	1470	82	168,160
10	6	665	111	76,070
10	10	1070	107	122,400
14	12	725	60	82,930
14	18	1350	75	154,430

Note: All Beams were 1" x 1" in Cross-Section.

Table 4

Maximum Stresses in Slab DM-5 at Various Coverage Levels for a 1750-Pound Wheel Load

Number of Coverages	Maximum Stress, psi			
	Rosette No. 1		Rosette No. 3	
	Transverse	Longitudinal	Transverse	Longitudinal
400	2541	1652	2873	1340
800	2535	1628	2916	1550
1400	2563	1544	2859	1490
2000	2549	1698	2936	1429
3600	2366	1617	2796	1401
8000	2699	1542	3051	1550
10,000	2765	1814	3283	1701

Table 5

Comparison of Measured and Theoretical Maximum Deflections for Static Loadings Within the Range of Elastic Behavior

Slab No.	Modulus of Subgrade Reaction, lb./in.^{3}	Average Slab Thickness, inch	Maximum Deflection per 100 pounds of Wheel Load		Ratio of Measured to Theoretical
			Measured, inch	Theoretical, inch	
DM-1	47	0.941	0.00350	0.00304	1.151
DM-2	53	0.996	0.00312	0.00262	1.191
DM-3	66	1.017	0.00242	0.00228	1.061
DM-4	68	1.002	0.00234	0.00230	1.017
DM-5	70	1.028	0.00226	0.00218	1.037

Note: Modulus of subgrade reaction values are for the times at which the deflection tests were made.

Table 6

Summary of Maximum Total Deflections at First Crack Failure Loads

Slab No.	Modulus of Subgrade Reaction, $lb/in.^3$	Average Slab Thickness, inch	First Crack Failure Load, lb.	Total Deflection, inch
DM-1	47	0.941	715	0.0250
DM-2	53	0.996	800	0.0250
DM-3	66	1.017	835	0.0202
DM-4	68	1.002	875	0.0205
DM-5	70	1.028	820	0.0185

Table 7

Summary of Repetitive Loadings Applied to Prestressed Slabs

Slab No.	Wheel Load, lb.	Coverages		
		1st Failure	2nd Failure	3rd Failure
DM-1	1240	2846	----	----
DM-2*	1850	2211	----	----
DM-3	1896	6157	----	----
DM-4	1800	1881	1923	2445
DM-5	1750	8653	11,818	12,434
DM-6	2392	480	592	683

* Slab DM-2 had been subjected previously to 40,000 coverages of a 1200-pound wheel load without any failure resulting.

Table 8

Summary of Static Failure Loads on Slab DM-7

Contact Area Diameter, in.	Positive Moment Cracking		Negative Moment Cracking		Punching Shear Failure Load, lb.
	Failure Load, lb.	Failure Stress, psi	Failure Load, lb.	Failure Stress, psi	
3	935	----	----	----	5567
4	972	1088	----	----	6356
6	1121	1024	4494	----	7951

Table 9

Summary of Repetitive Loading Design Factors

Slab No.	Modulus of Subgrade Reaction, lb./in.3	Average Slab Thickness at Failed Area in.	Radius of Relative Stiffness, in.	Flexural Strength + Prestress psi	Wheel Load, lb.	Computed Failure Load, lb.	Coverages at Failure	Design Factor
DM-1	47	0.922	8.98	1120	1240	2539	2846	2.05
DM-2	65	0.970	8.61	1166	1850	3073	2211	1.66
DM-3	67	1.031	8.94	1067	1896	3151	6157	1.66
DM-4	68	0.993	8.66	1104	1800	3054	1881	1.70
	68	1.017	8.82	1098	1800	3170	1923	1.76
	68	1.003	8.73	1101	1800	3046	2445	1.69
DM-5	70	1.010	8.71	1020	1750	2910	8653	1.66
	70	1.027	8.82	1015	1750	2969	11,818	1.70
	70	1.051	8.97	1010	1750	3084	12,434	1.76
DM-6	71	0.994	8.57	1098	2392	3161	480	1.32
	71	1.028	8.79	1089	2392	3324	592	1.39
	71	0.998	8.60	1097	2392	3189	683	1.33

Table 10

Summary of First Crack Failure Loads and Stresses for Static Loading

Slab No.	Average Slab Thickness, in.	Modulus of Subgrade Reaction at First Crack, lb./in.^{3}	Radius of Relative Stiffness, in.	First Crack Load, lb.		First Crack Stress, psi	
				Measured	Theoretical	Flexural Strength + Prestress	Theoretical (Based on measured first crack load)
DM-1	0.941	47	9.12	715	666	1115	1189
DM-2	0.996	53	9.24	800	781	1159	1181
DM-3	1.017	66	8.88	835	764	1071	1158
DM-4	1.002	68	8.72	875	768	1102	1237
DM-5*	1.028	70	8.82	820	827	1015	1006

* 3-inch square contact area, all others with wheel load.

Table 11

Comparison of Dynamic Loading Model and Static Loading Model as Indicated by Static Loading Tests on Slab DM-7 ***

Contact Area Radius a, inch	a/ℓ ***	Strain Gage Row	Distance to Maximum Negative Radial Stress, inch		Negative Moment Cracking Load, lb.		Measured Punching Shear Failure Load, lb.
			Measured in Slab DM-7	Predicted from Static Loading Model	Measured in Slab DM-7	Predicted from Static Loading Model	
1.5	0.181	Transverse	12.0*	6.5	4500*	2725	5567
1.5	0.181	Diagonal	----	6.5	----	2725	5567
2.0	0.241	Transverse	10.2*	7.4	5320*	3090	6356
2.0	0.241	Diagonal	12.0*	7.4	4820*	3090	6356
3.0	0.362	Transverse	12.8*	9.5	4320*	3400	7951
3.0	0.362	Diagonal	9.5*	9.5	5330*	3400	7951
3.0	0.362	-----	13.2	9.5	4494	3400	7951

* Estimated values based on partial relief of radial stress as indicated by strain measurements.

** Dynamic loading model - concrete slab on low-strength clay subgrade; static loading model - Hydrocal slab on natural rubber subgrade.

*** ℓ, radius of relative stiffness.

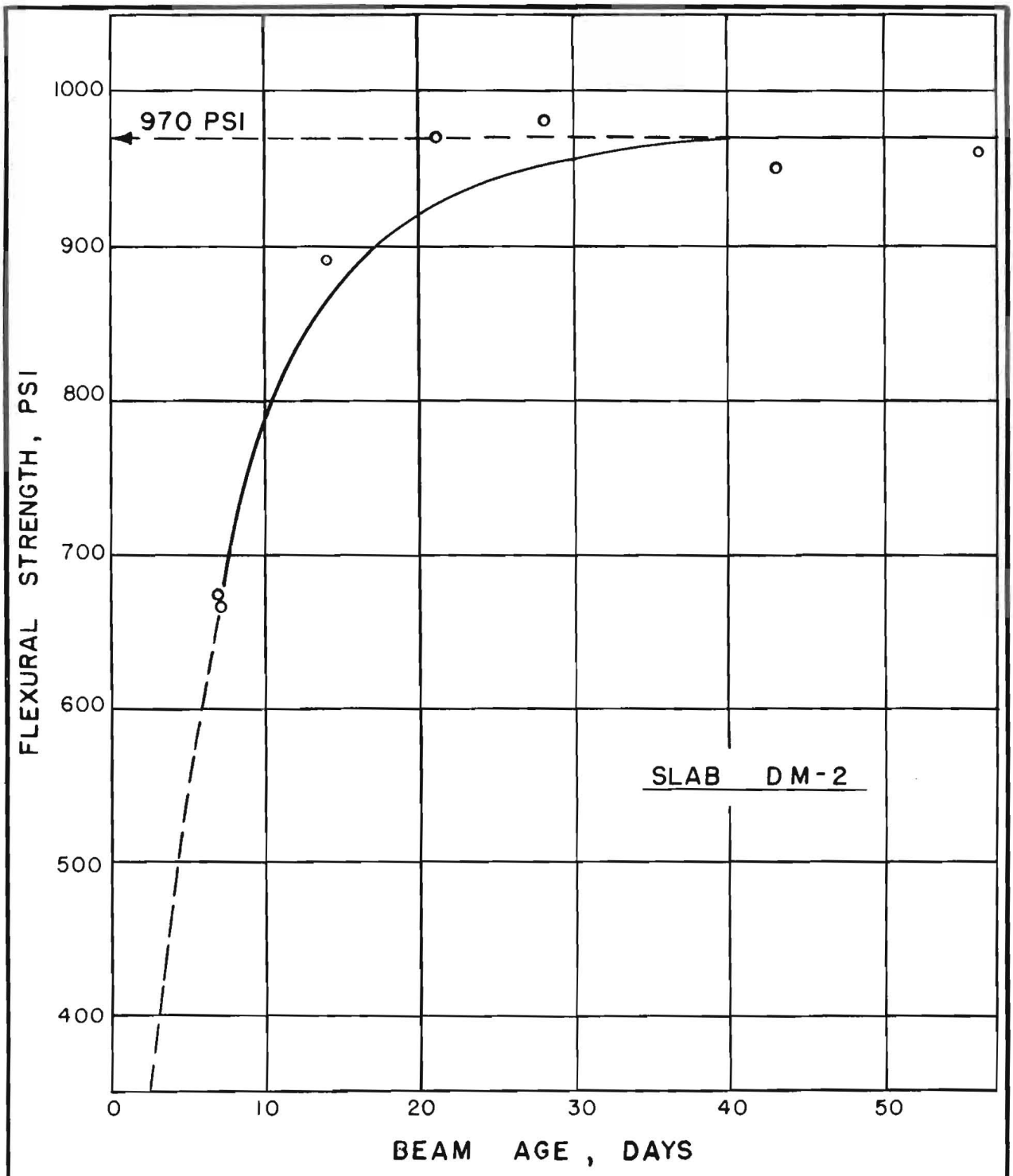

TYPICAL CURVE OF FLEXURAL STRENGTH GAIN VERSUS TIME FOR MODEL SLABS

FIGURE 1

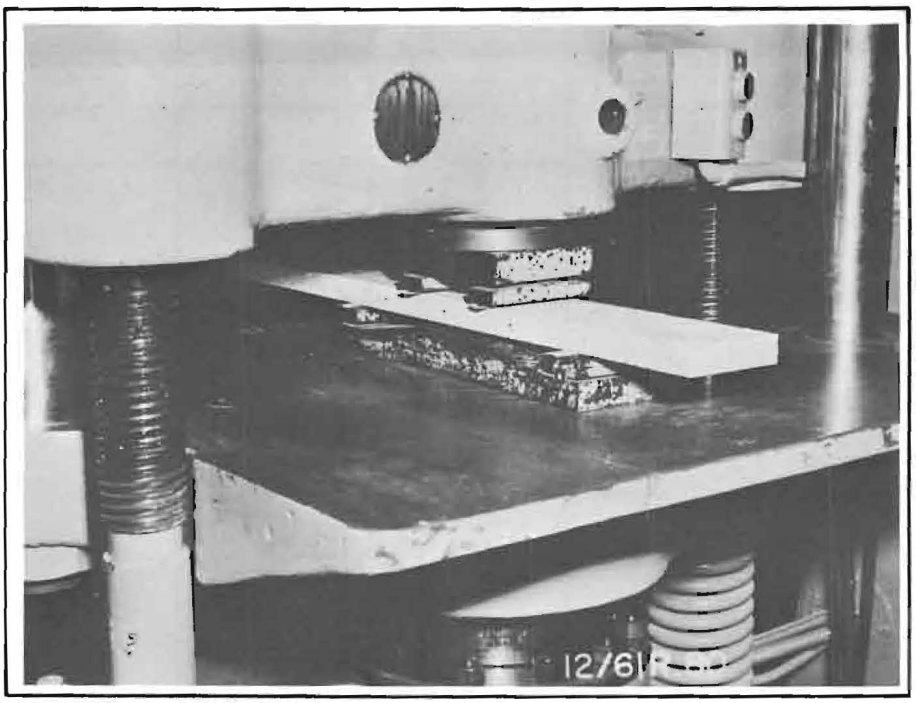

Figure 2. Set-up used for determining slab strength (flexural strength plus prestress) after completion of traffic tests. 1" × 4" × 30" beams were sawed from untrafficked areas of slabs and subjected to third-point loading.

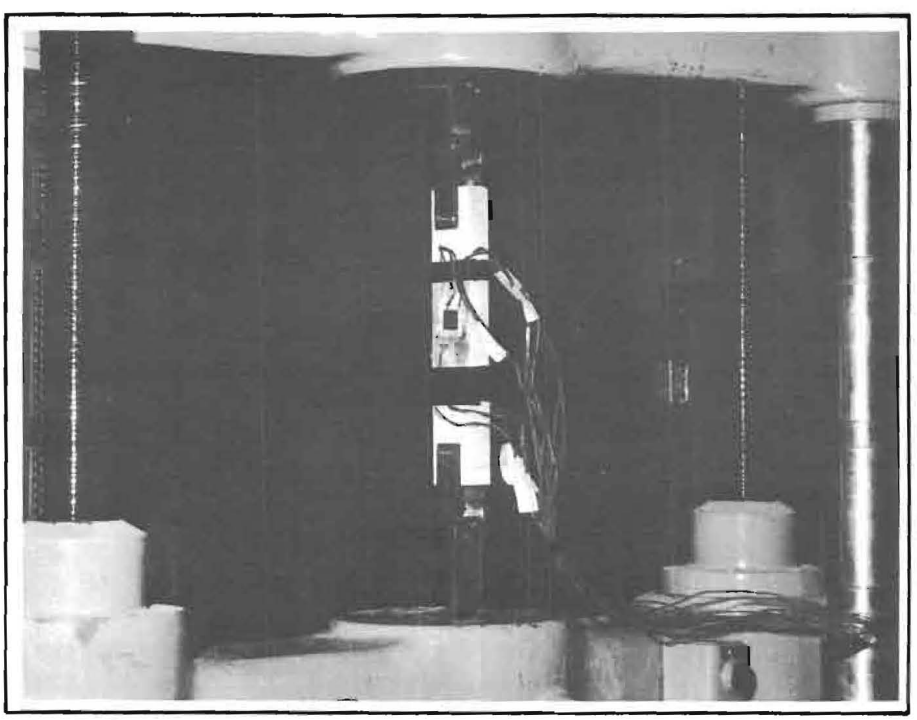

Figure 3. Set-up used for determining modulus of elasticity and Poisson's ratio for concrete used in the model slabs. Strains were measured by Type AX-5, SR-4 electrical strain gages.

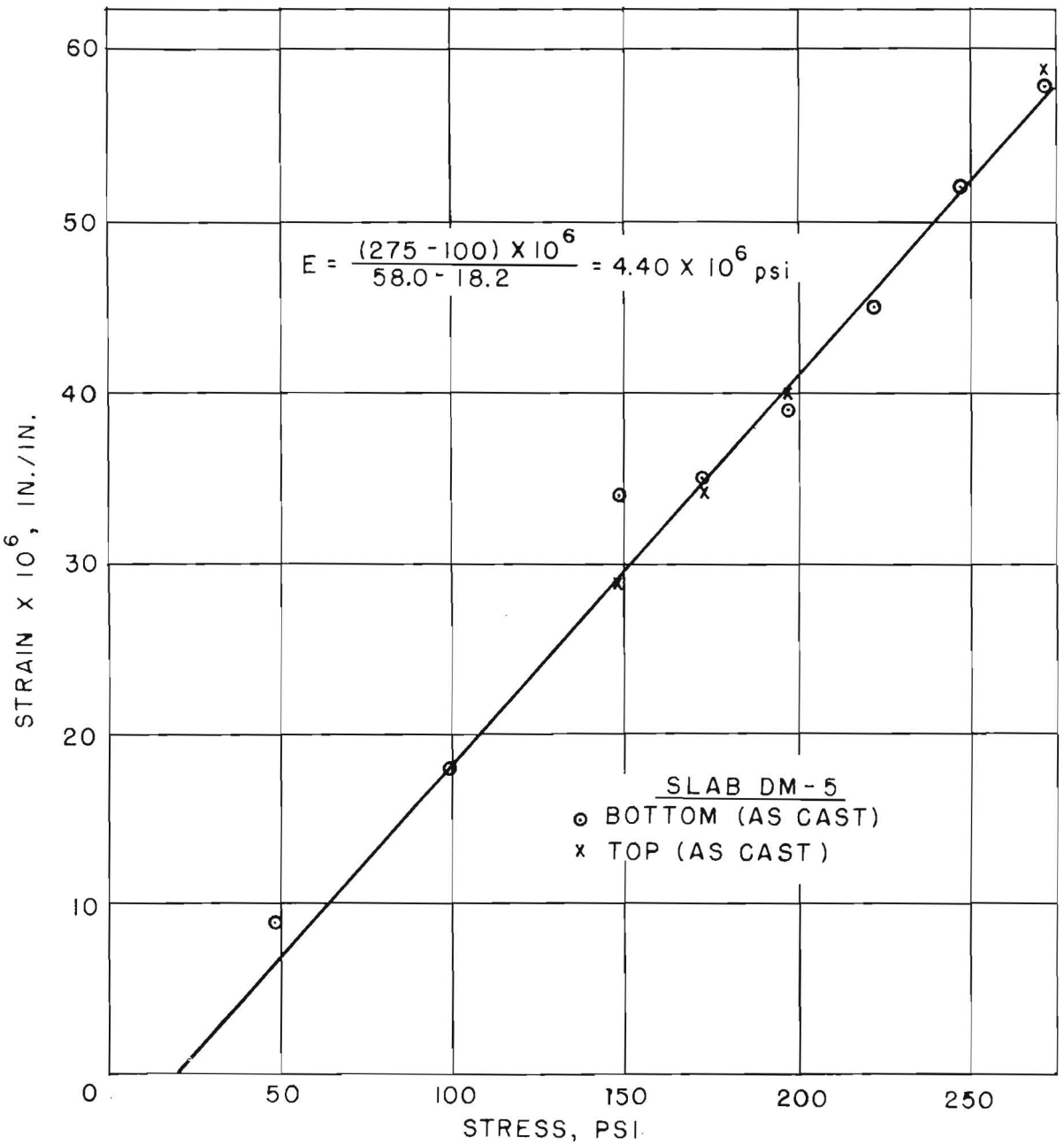

STRESS-STRAIN CURVE FOR MODULUS OF ELASTICITY TEST ON CONCRETE

FIGURE 4

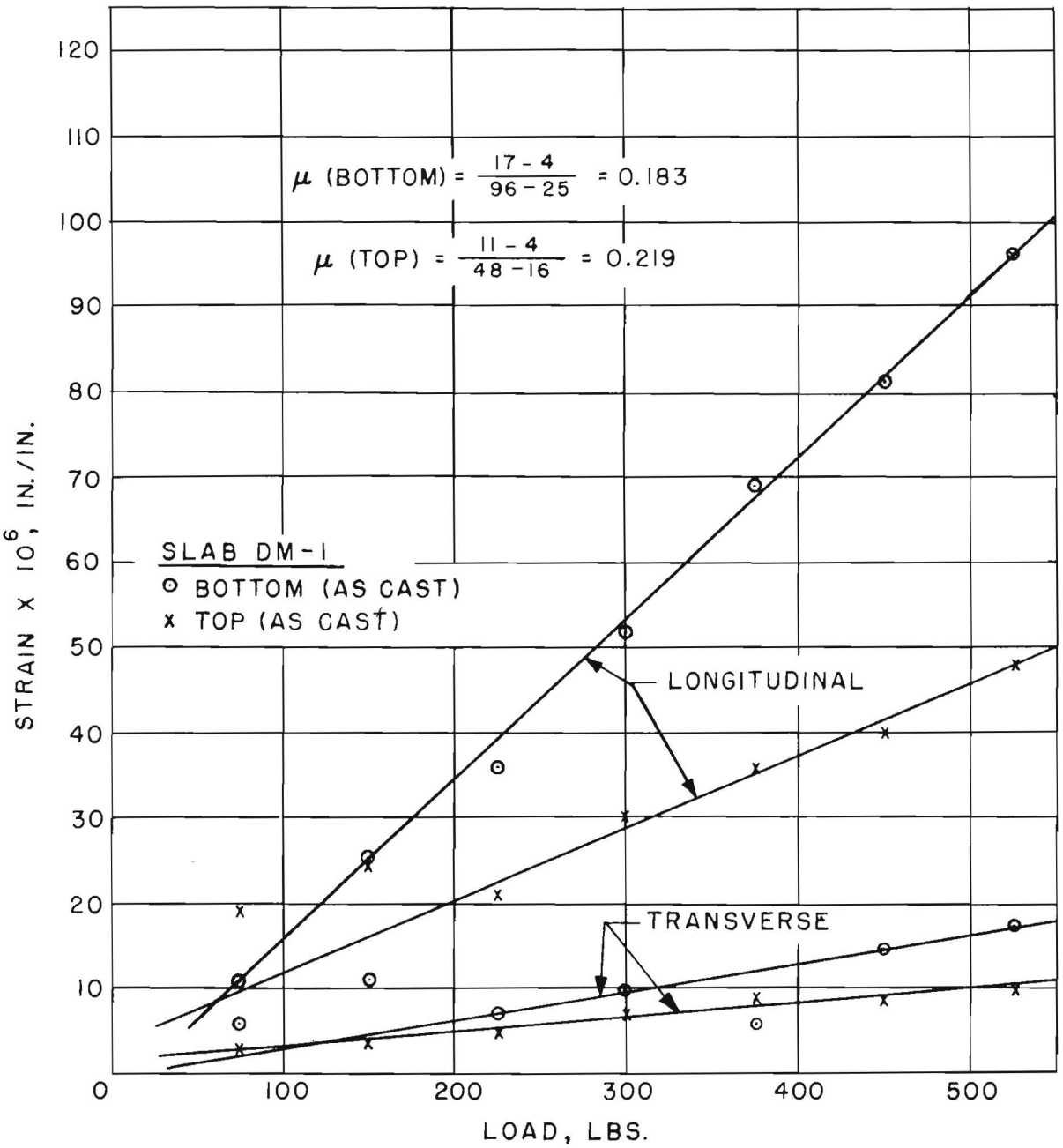

LOAD-STRAIN CURVE FOR POISSON'S RATIO TEST ON CONCRETE

FIGURE 5

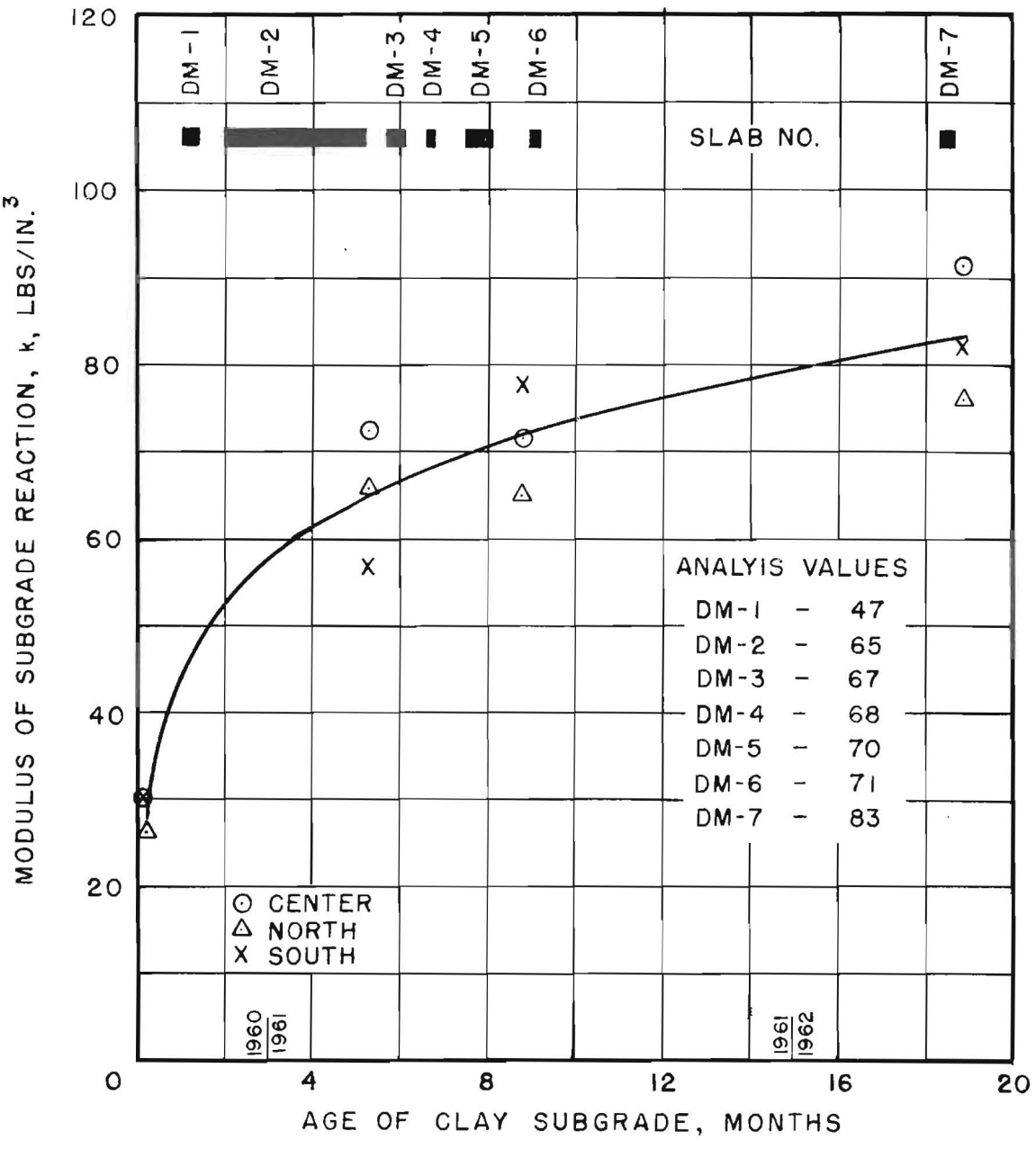

MODULUS OF SUBGRADE REACTION FOR LOW STRENGTH CLAY SUBGRADE

(30-INCH DIAM. PLATE BEARING TESTS)

FIGURE 6

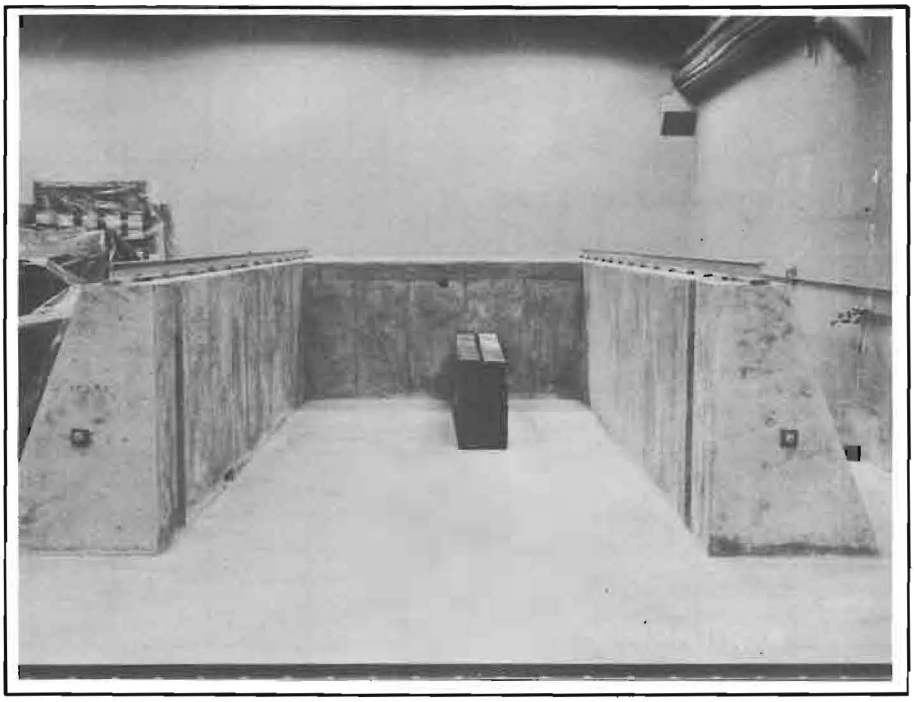

Figure 7. Completed enclosure for containing the subgrade. The 6-inch by 6-inch timbers were used to form a removable wall at the open end in the foreground.

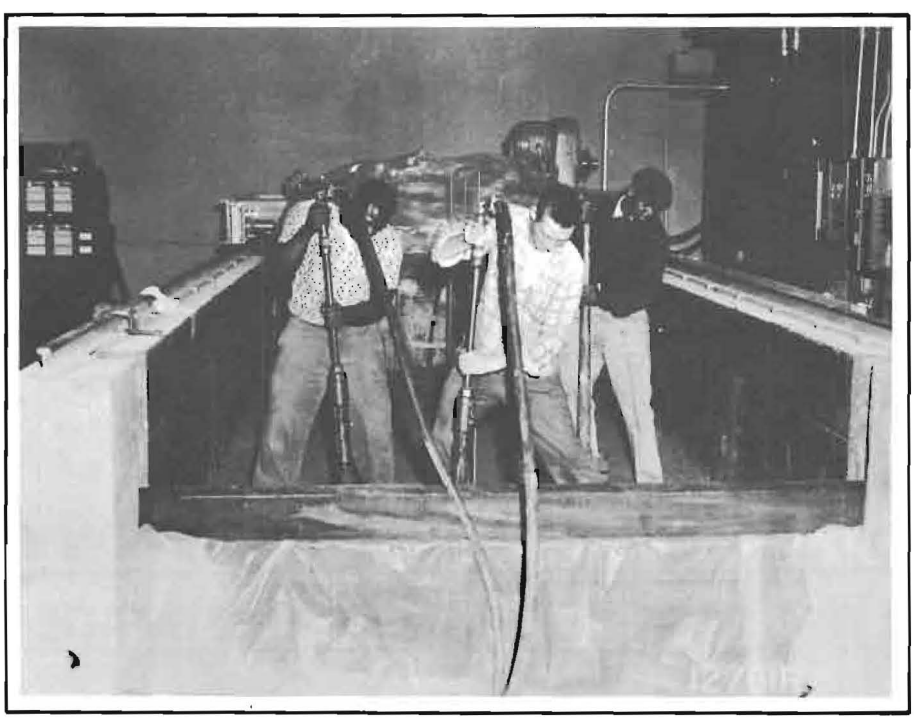

Figure 8. Compaction of the clay subgrade using pneumatic tampers.

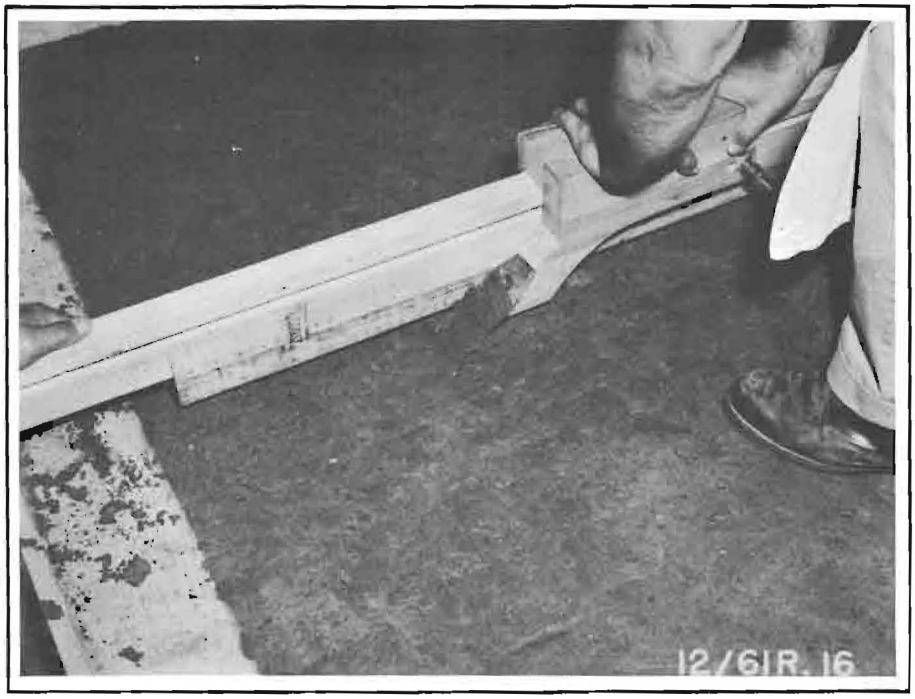

Figure 9. Subgrade planer devised for leveling the subgrade surface to provide uniform support for the test slabs.

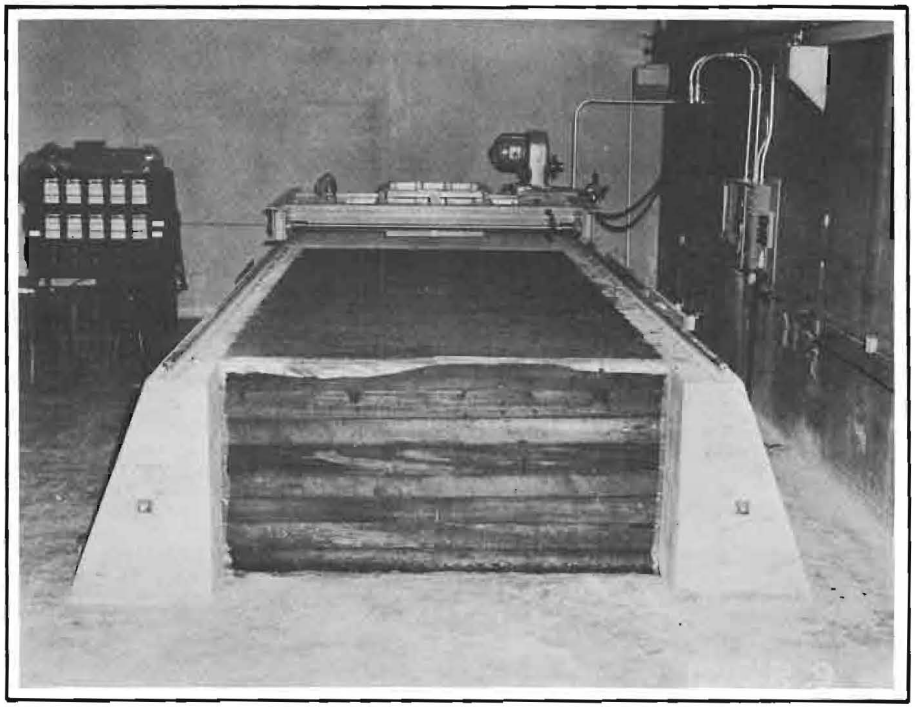

Figure 10. Completed low-strength subgrade covered by a polyethylene sheet to prevent loss of moisture. Electrically-operated loading device shown in the background.

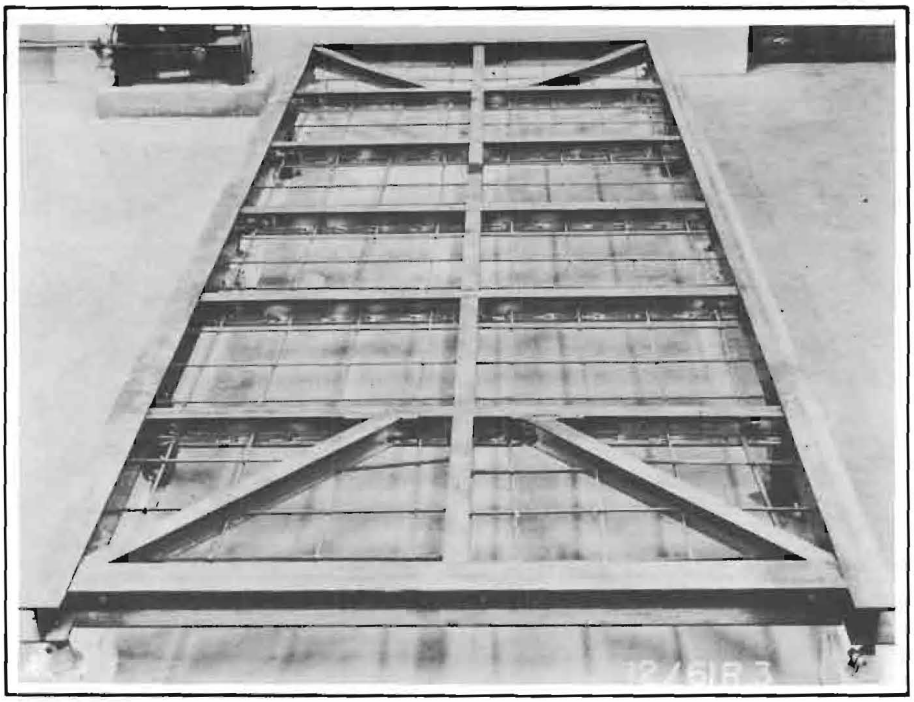

Figure 11. Steel framework for the combined casting bed and stressing frame used in constructing the model prestressed slabs.

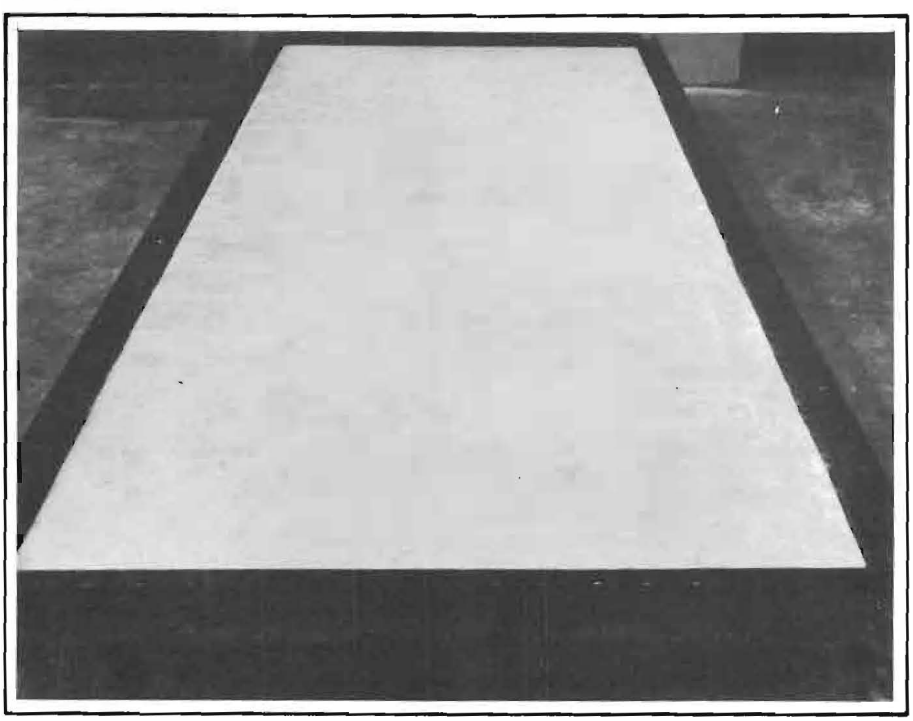

Figure 12. Completed casting bed and stressing frame with the side forms bolted in place.

Figure 13. Dipping stressing wires in dilute hydrochloric acid to etch the surface of the wire and improve the bond between the wire and the concrete.

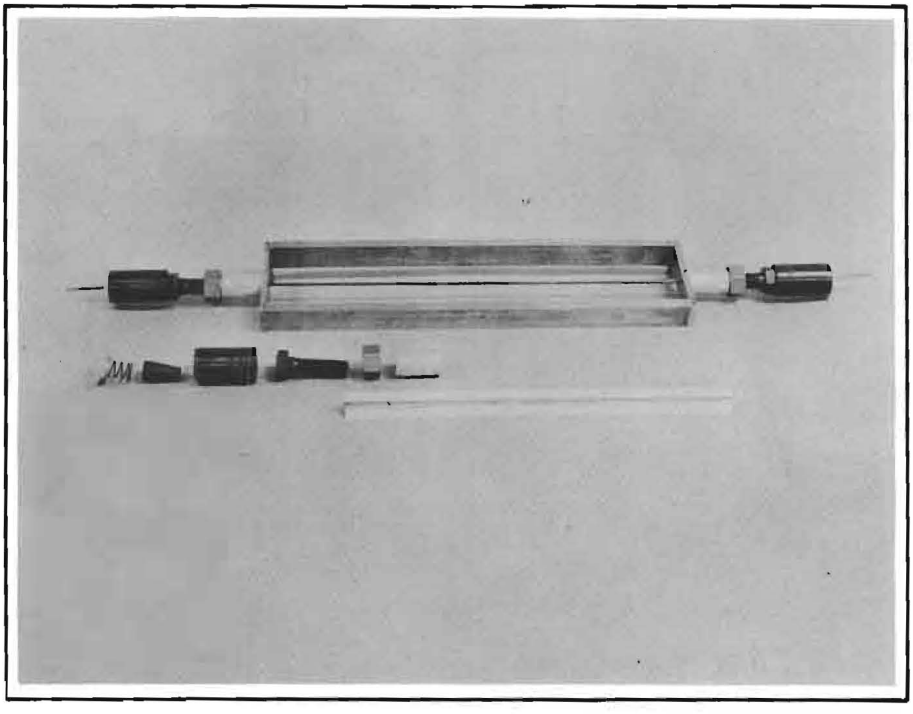

Figure 14. Arrangement used for anchoring the stressing wires to eliminate prestress losses due to slippage or "take-up" in the strand chuck.

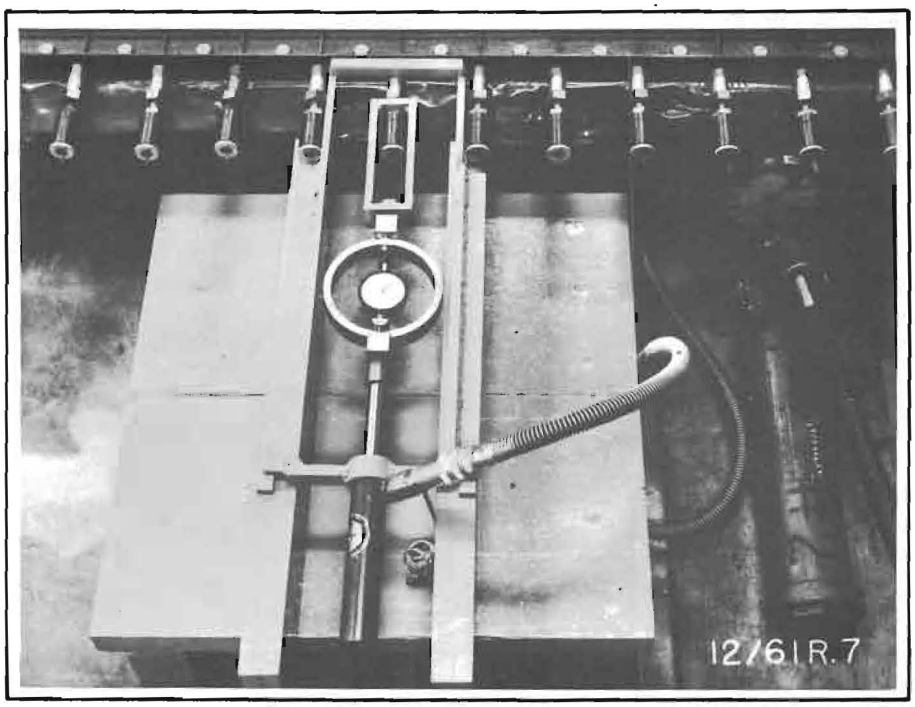

Figure 15. Arrangement used, including hydraulic jack, ram, and proving ring, for tensioning the stressing wires.

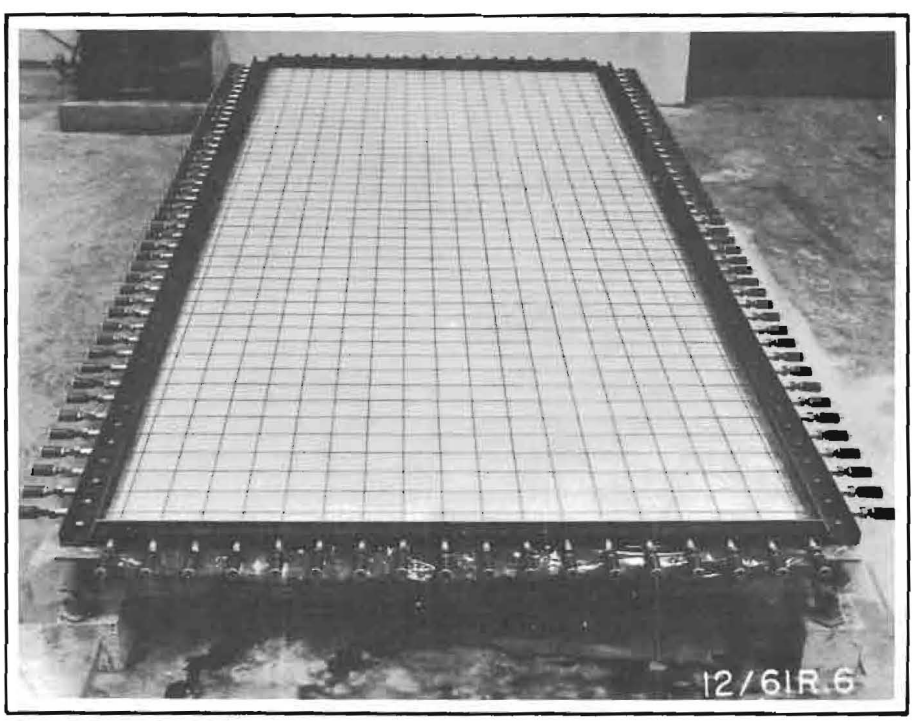

Figure 16. Completed installation of stressing wires spaced 4 inches center to center longitudinally and transversely. A polyethylene sheet was used to prevent the model slab from bonding to the casting bed.

Figure 17. Plate-type vibrator being used to consolidate the concrete during construction of the test slabs.

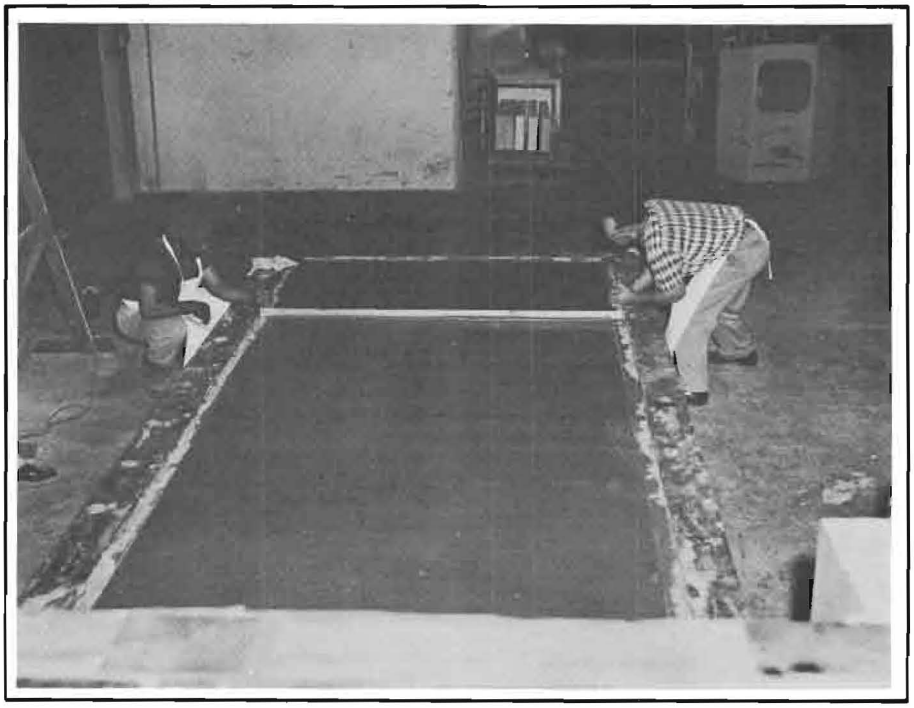

Figure 18. Strike-off procedure used in finishing the test slabs. Final finish was made by hand using a steel trowel.

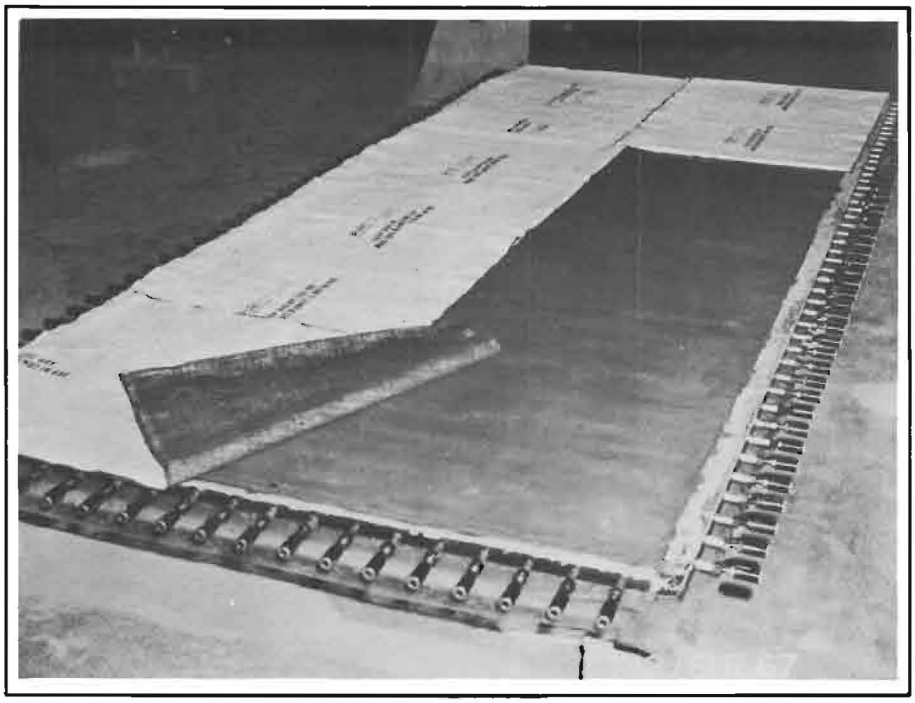

Figure 19. Plastic-backed burlap used in curing the model slabs. Burlap was soaked in water prior to placement on the slab, and then covered with a polyethylene sheet for the 7-day curing period.

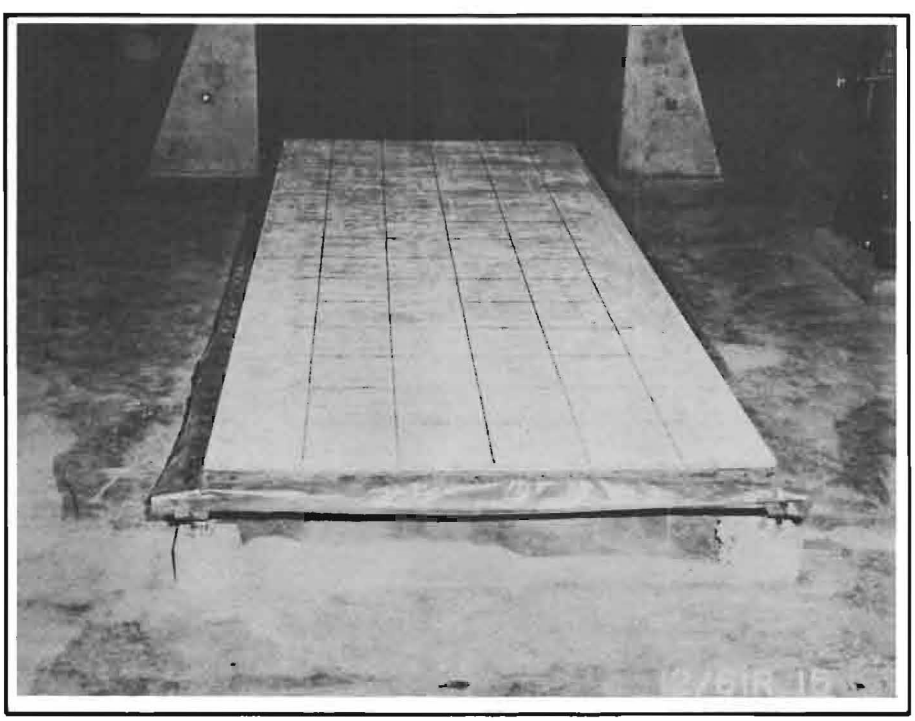

Figure 20. Completed test slab after removal of side forms. Grid lines were used to facilitate recording crack development during traffic tests.

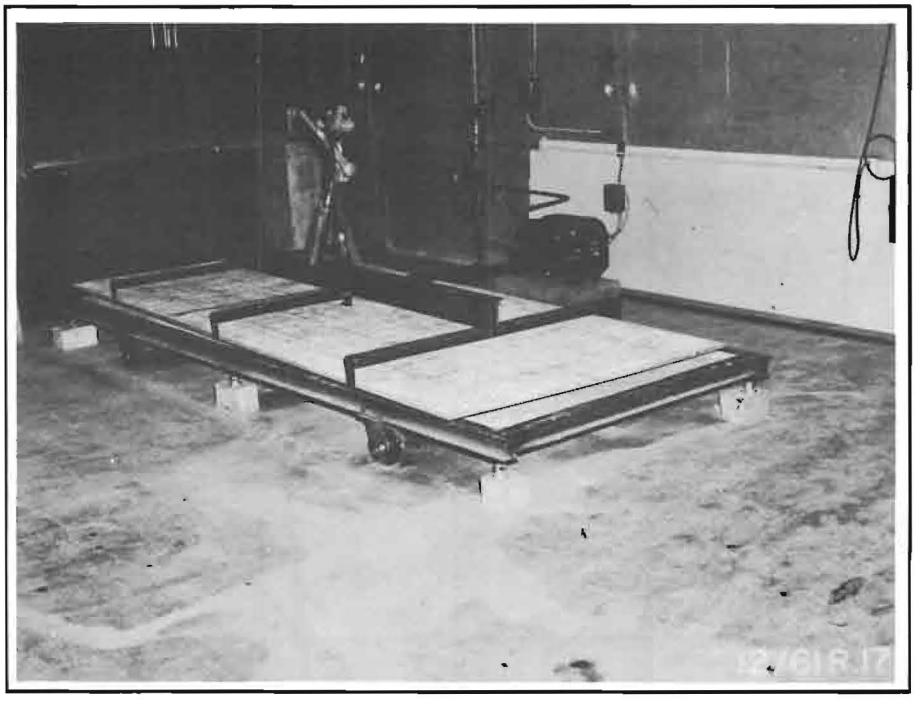

Figure 21. Method used in transferring the prestressed slabs from the casting bed to the subgrade.

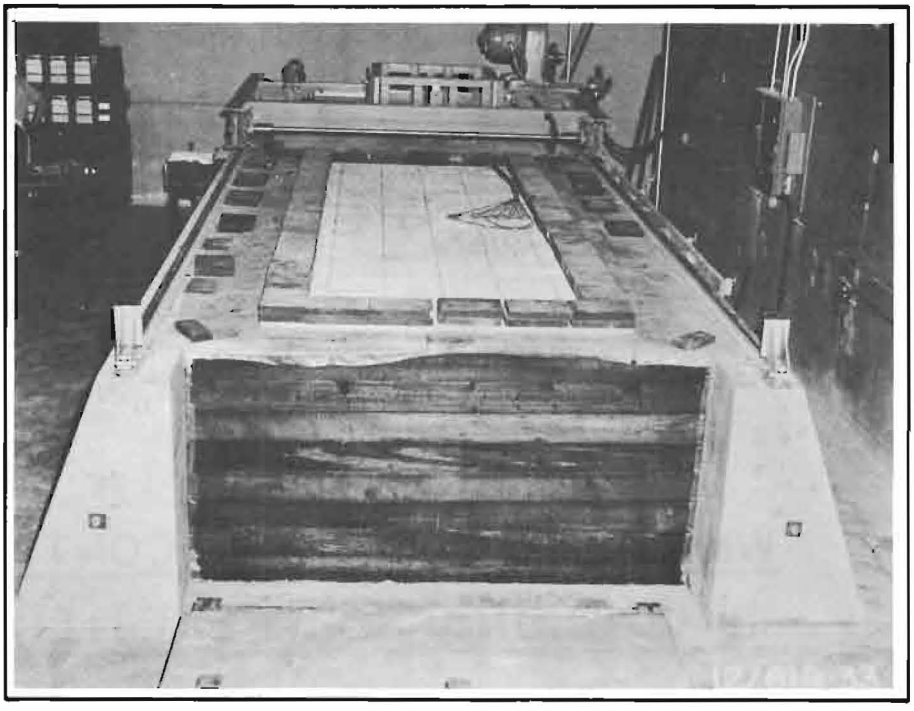

Figure 22. General view of the model showing a slab in place ready for testing. Steel blocks around the slab edges were used to insure that the slab remained in contact with the subgrade.

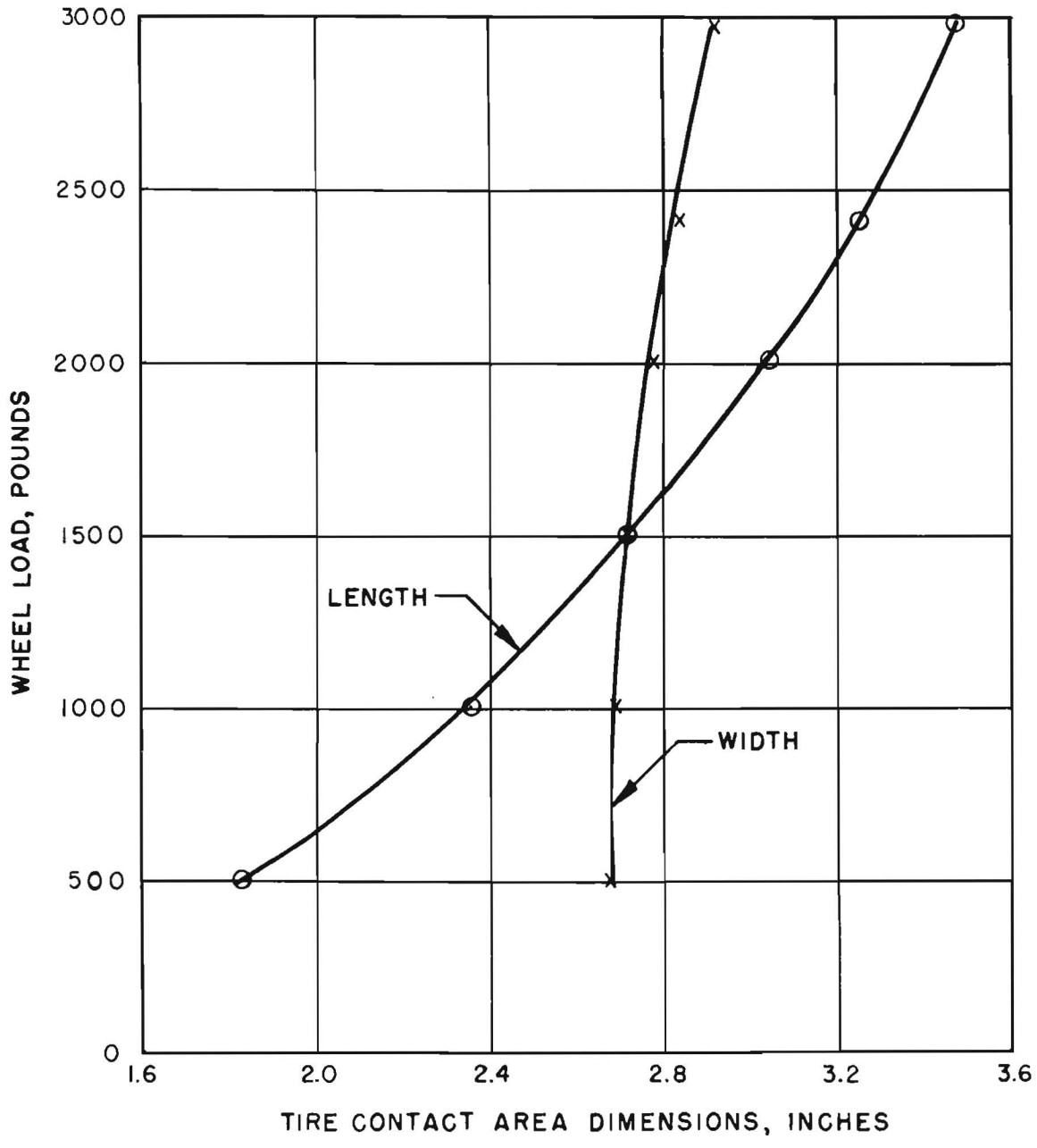

WHEEL LOAD VS TIRE CONTACT DIMENSIONS FOR REPETITIVE LOADING MODEL

FIGURE 23

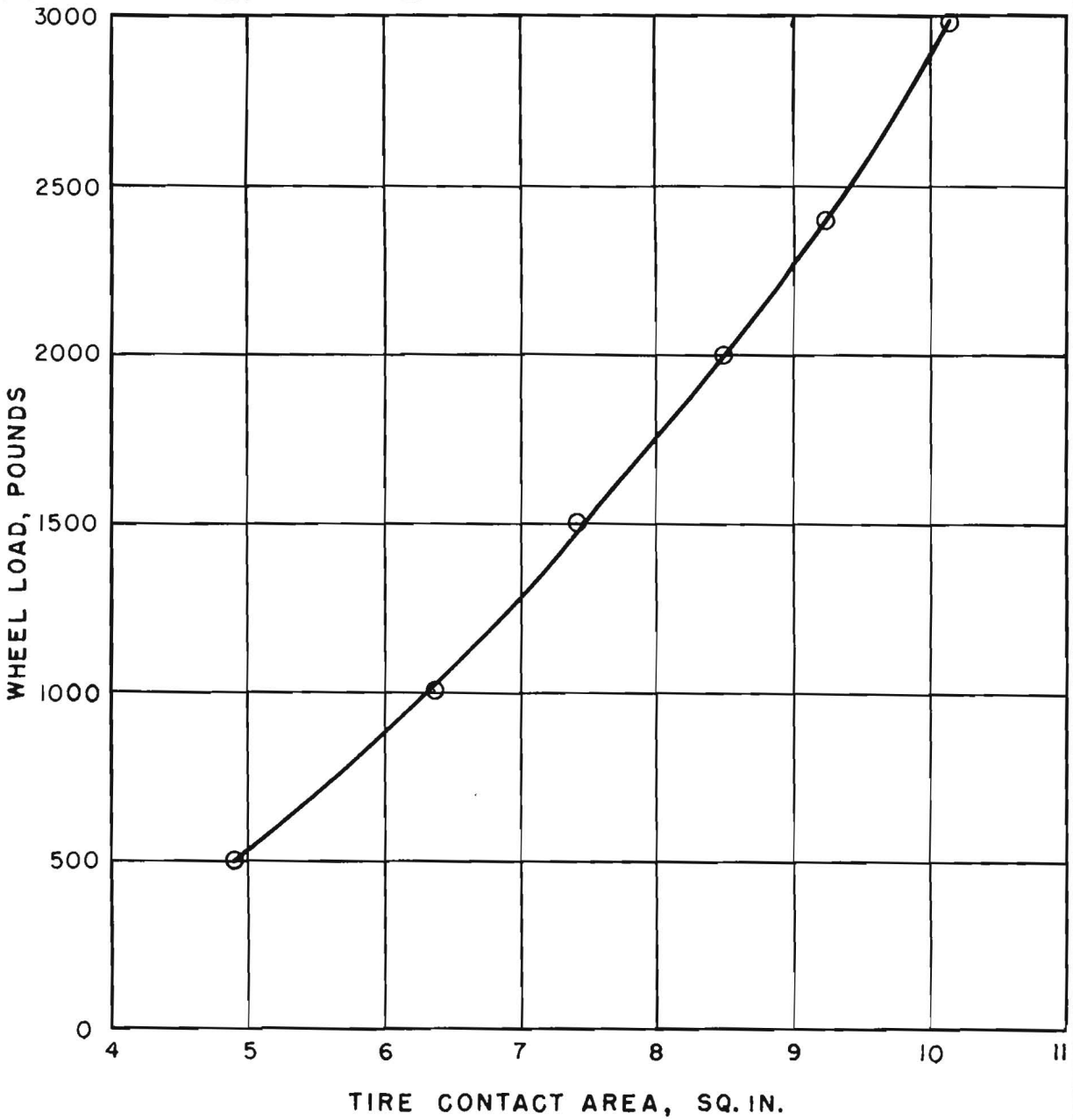

WHEEL LOAD VS TIRE CONTACT AREA FOR REPETITIVE LOADING MODEL

FIGURE 24

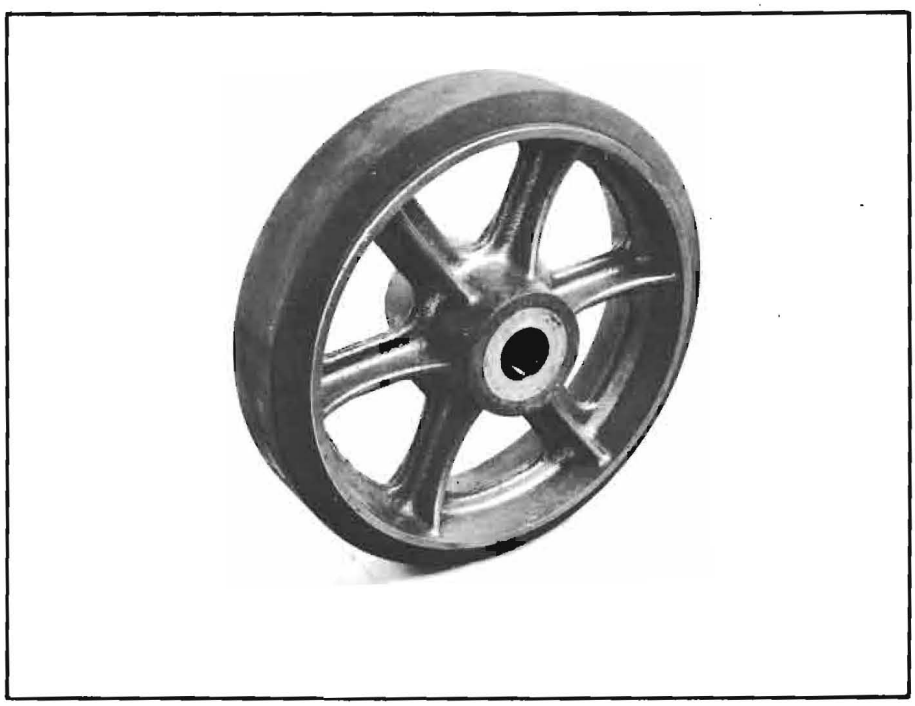

Figure 25. Load wheel used in the repetitive loading model.

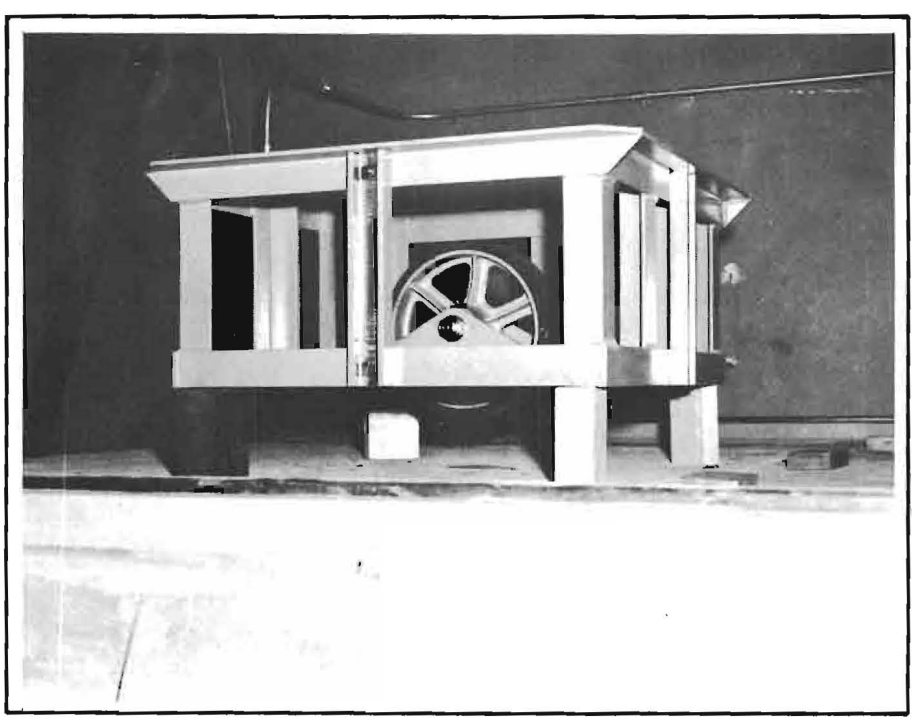

Figure 26. View showing the load box removed from the stabilizing frame. Steel blocks stacked inside the load box were used to provide the desired wheel load.

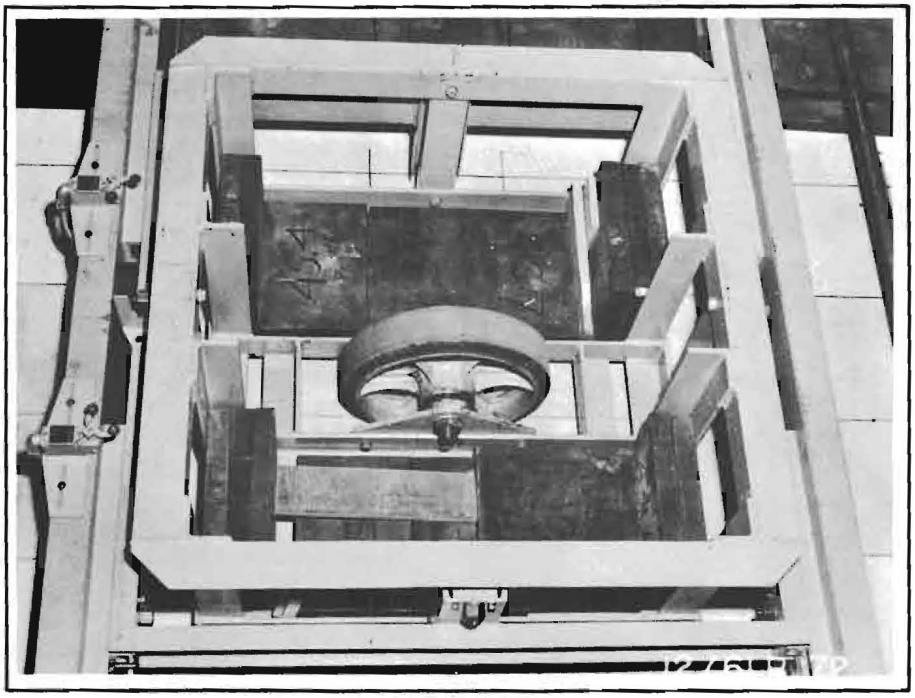

Figure 27. View showing the load box in place within the stabilizing frame. Limit switches to control the transverse motion of the load box and load wheel are shown on the left.

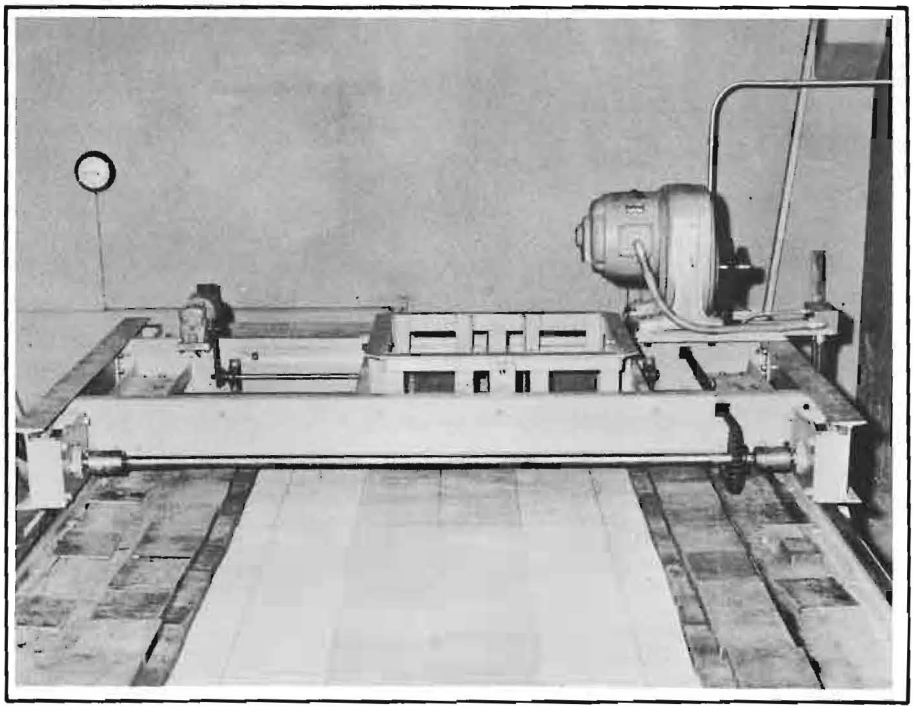

Figure 28. Over-all view of the load rig. Longitudinal motion and braking is provided by the large motor on the right. Transverse motion is provided by the small motor on the left.

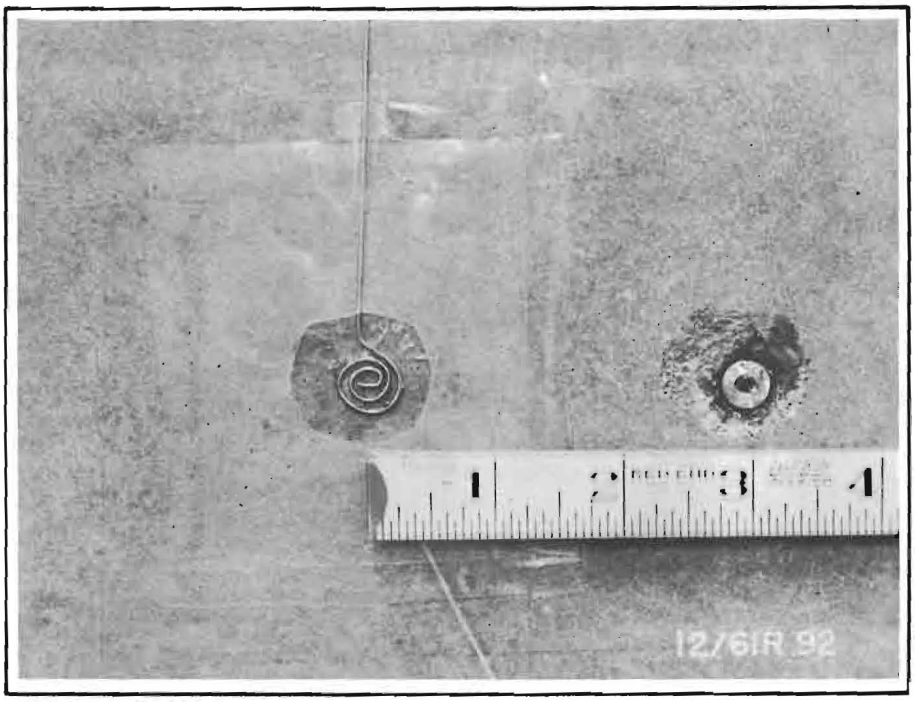

Figure 29. Close-up view of the wire coil portion of the pavement-subgrade separation gage, on the left; and the threaded brass fitting for attaching the deflection gage reference rods, on the right.

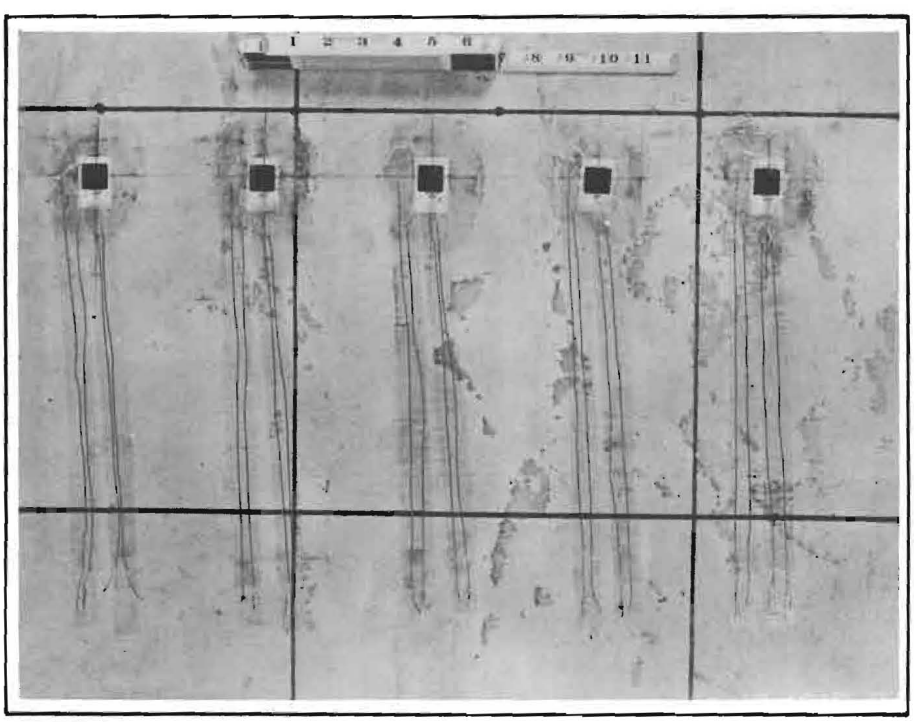

Figure 30. Type AX-5, SR-4 strain gage rosettes cemented to the top surface of a test slab. For traffic testing, the gages were protected with a 1/4-inch thick layer of foam rubber covered by a piece of brass shim stock.

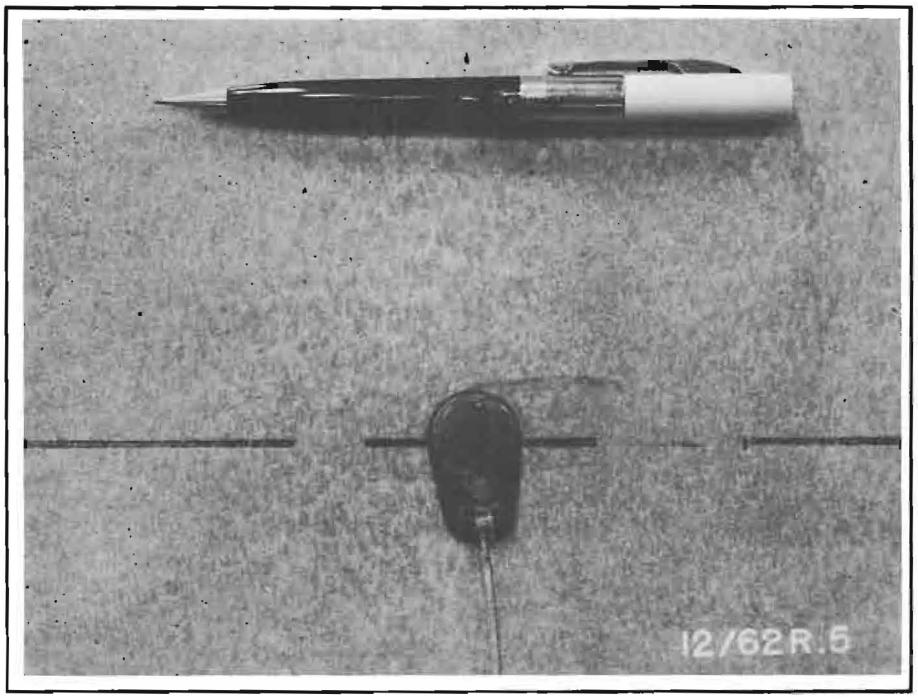

Figure 31. Filpip pressure gage mounted on the bottom side of Slab DM-7.

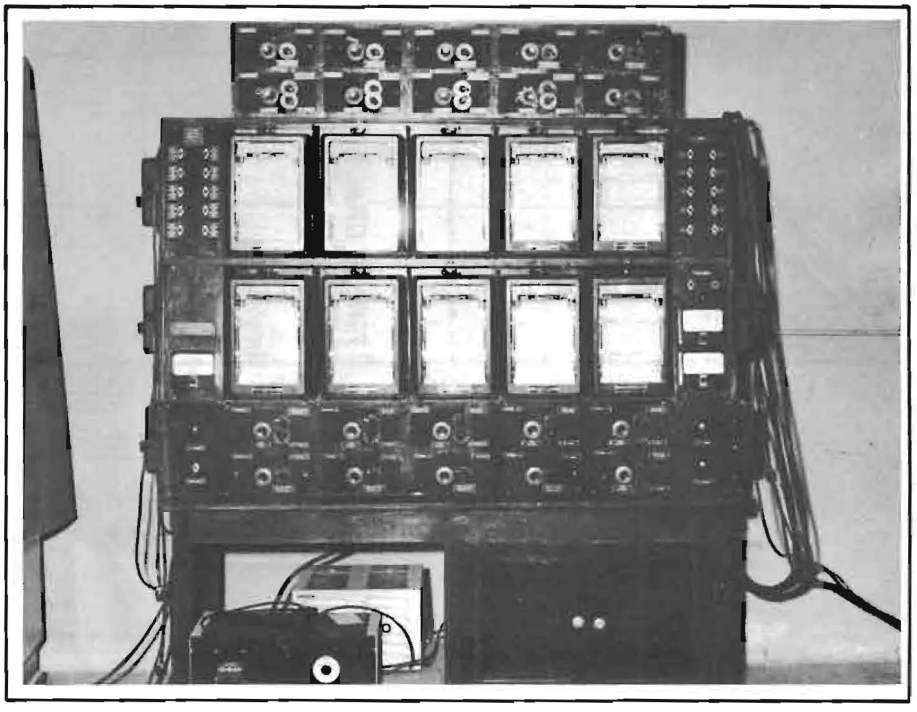

Figure 32. Instrument panel of strip-chart recorders and amplifying circuits used to record deflection, strain and pressure measurements.

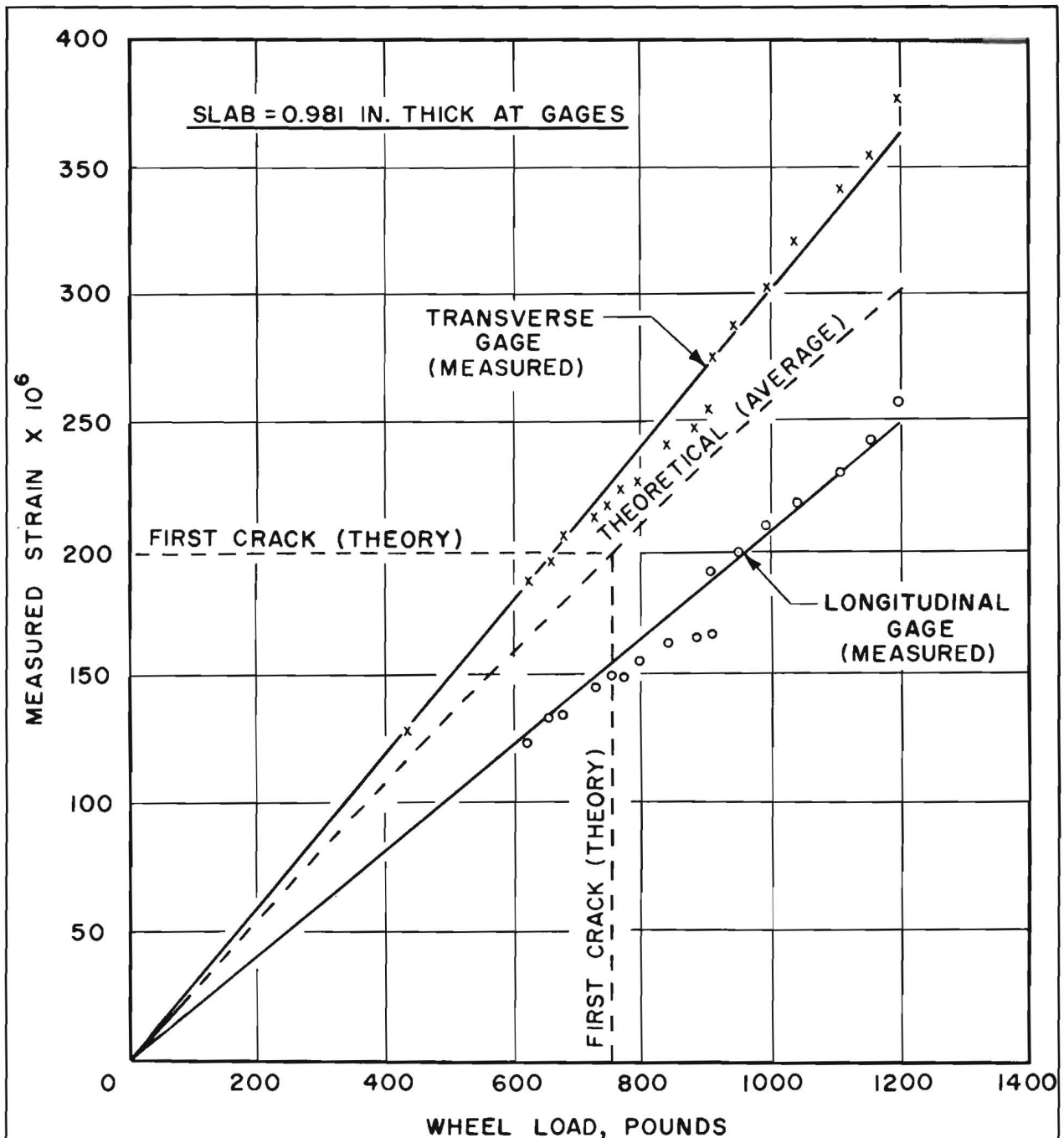

STATIC STRAIN AT CENTER

OF TIRE CONTACT AREA

SLAB DM-1

FIGURE 33

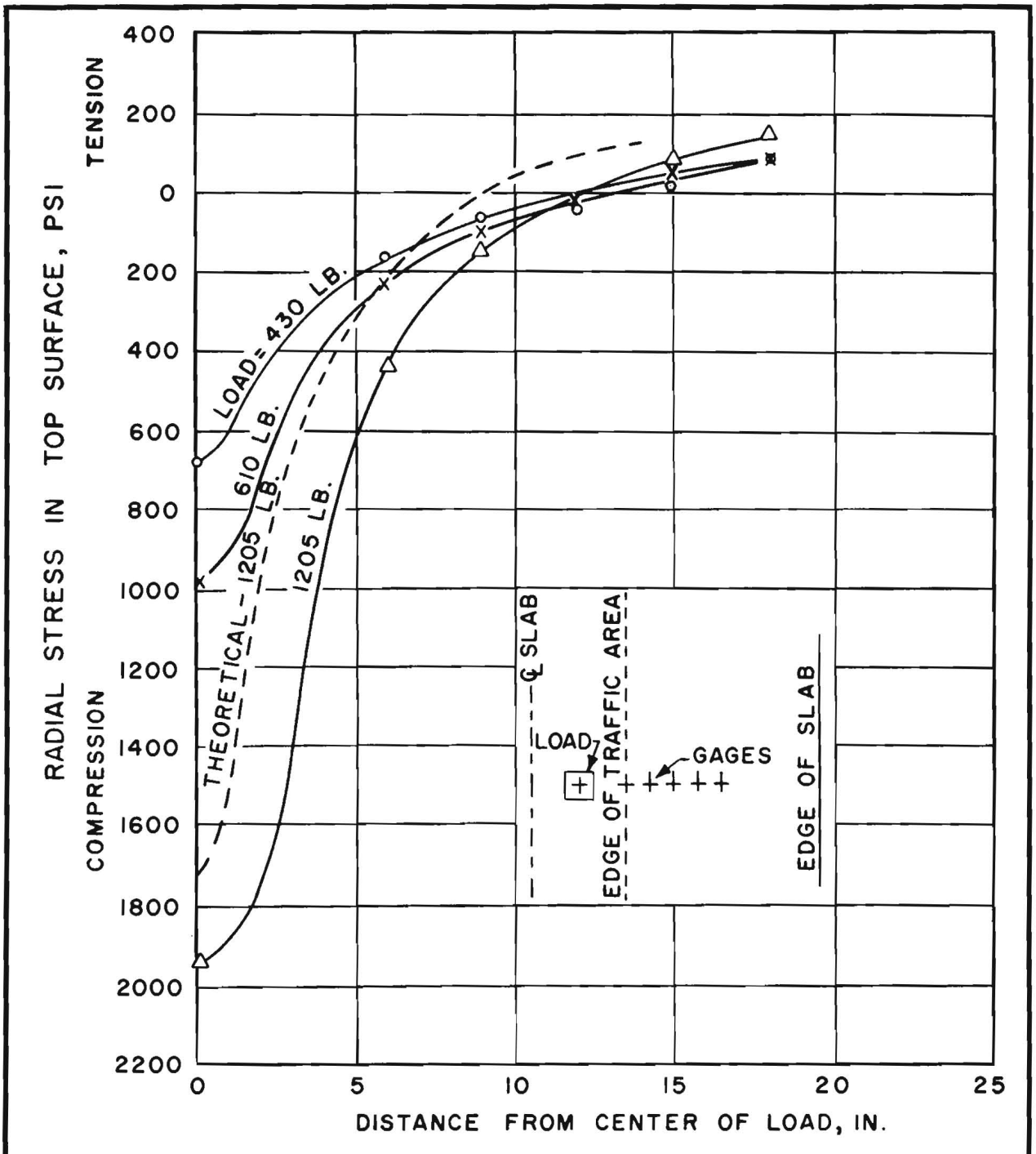

RADIAL STRESSES FOR STATIC LOADING ON SLAB DM-1

FIGURE 34

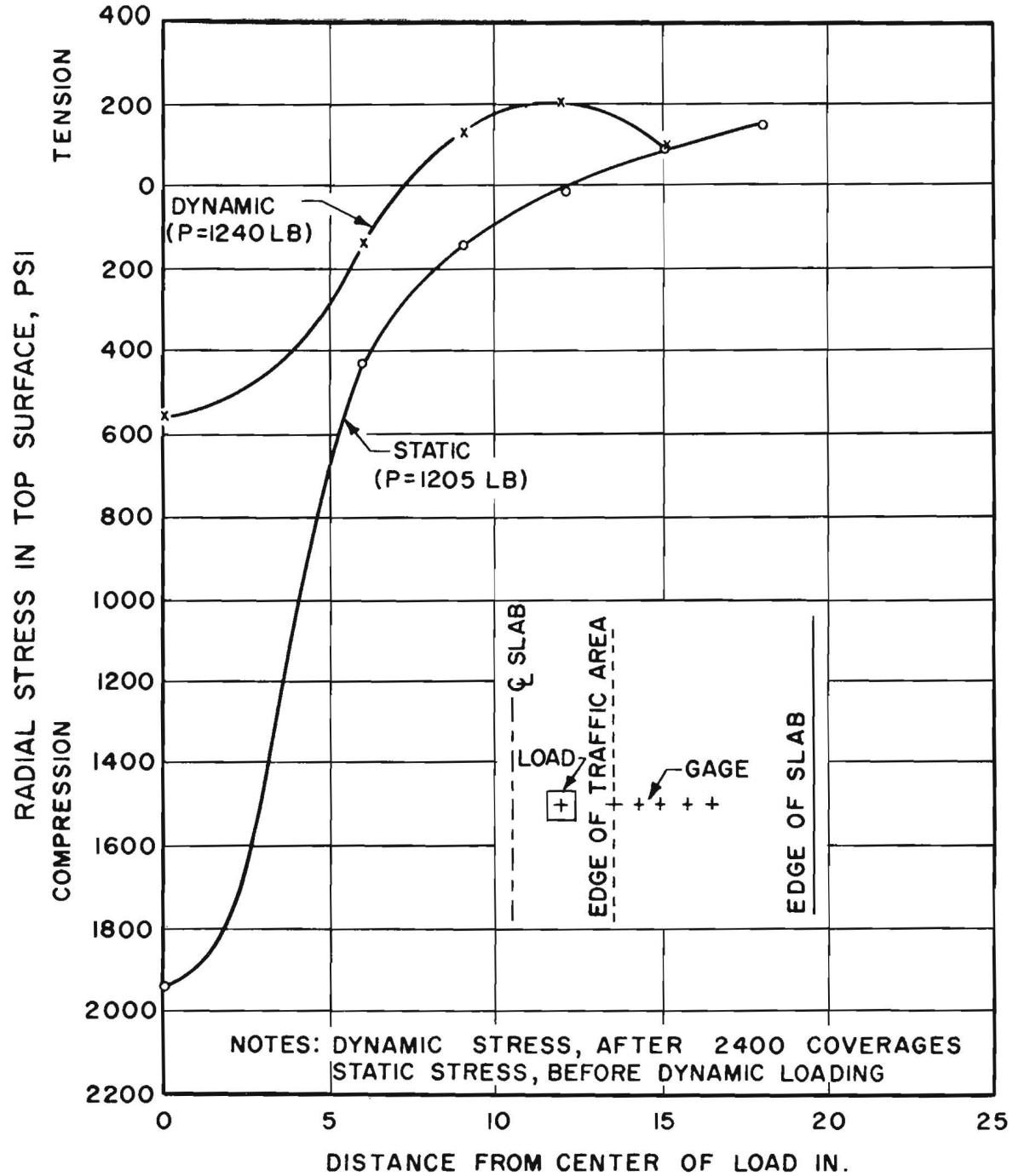

RADICAL STRESSES FOR STATIC AND DYNAMIC LOADINGS ON SLAB DM-1

FIGURE 35

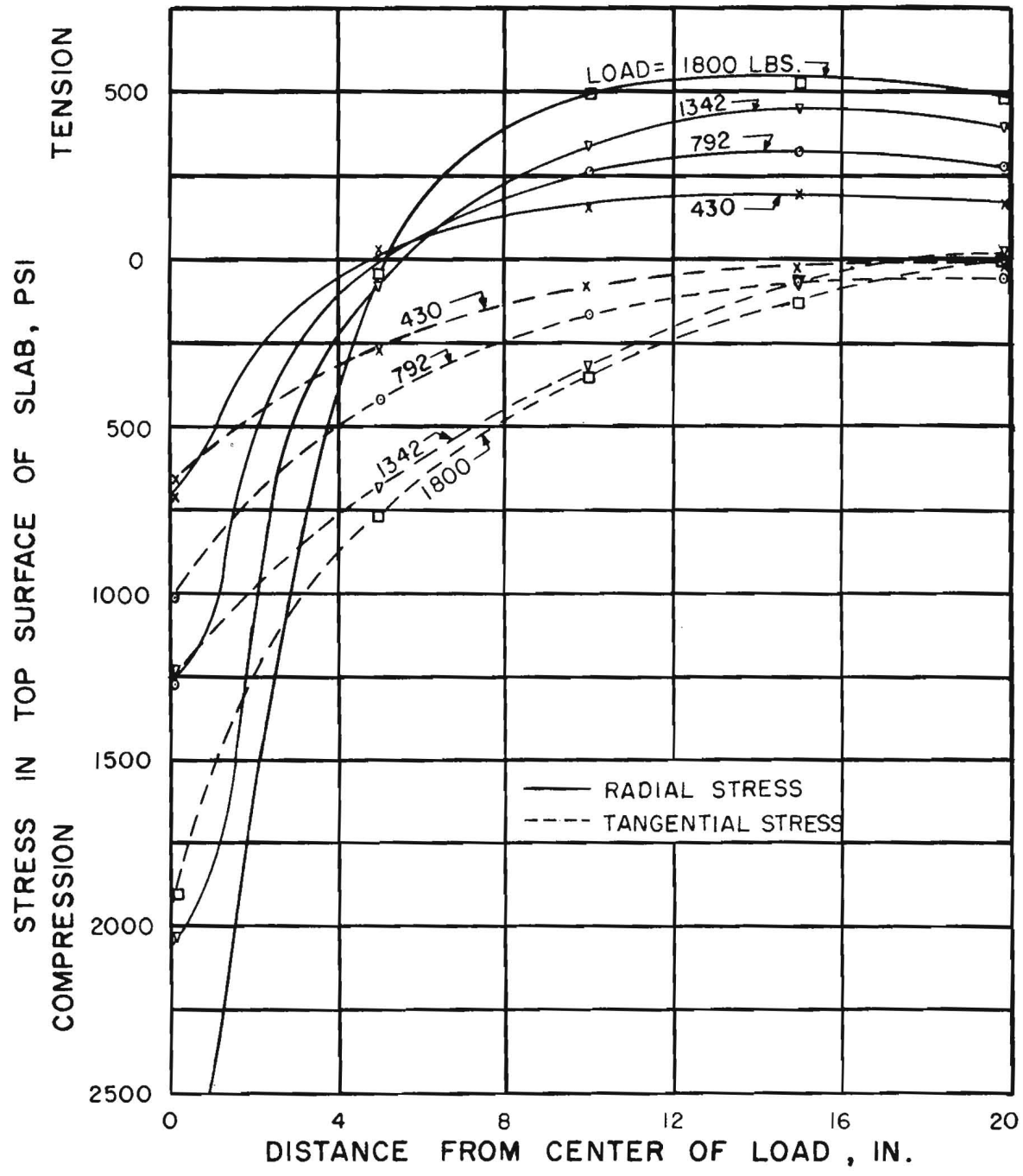

RADIAL AND TANGENTIAL STRESSES

FOR STATIC LOADINGS ON SLAB DM-4

FIGURE 36

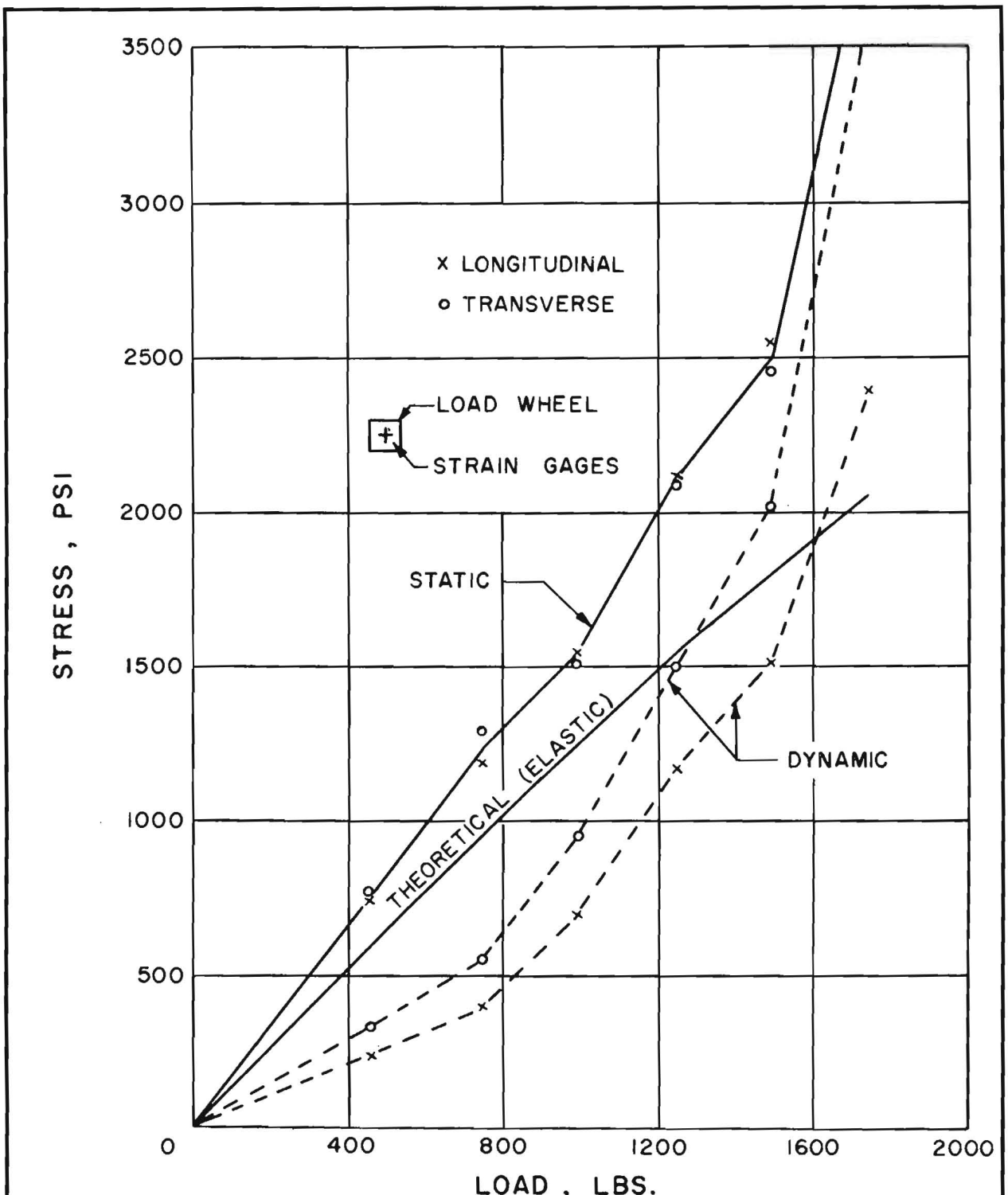

MAXIMUM STRESSES FOR STATIC AND DYNAMIC LOADINGS ON SLAB DM-5

FIGURE 37

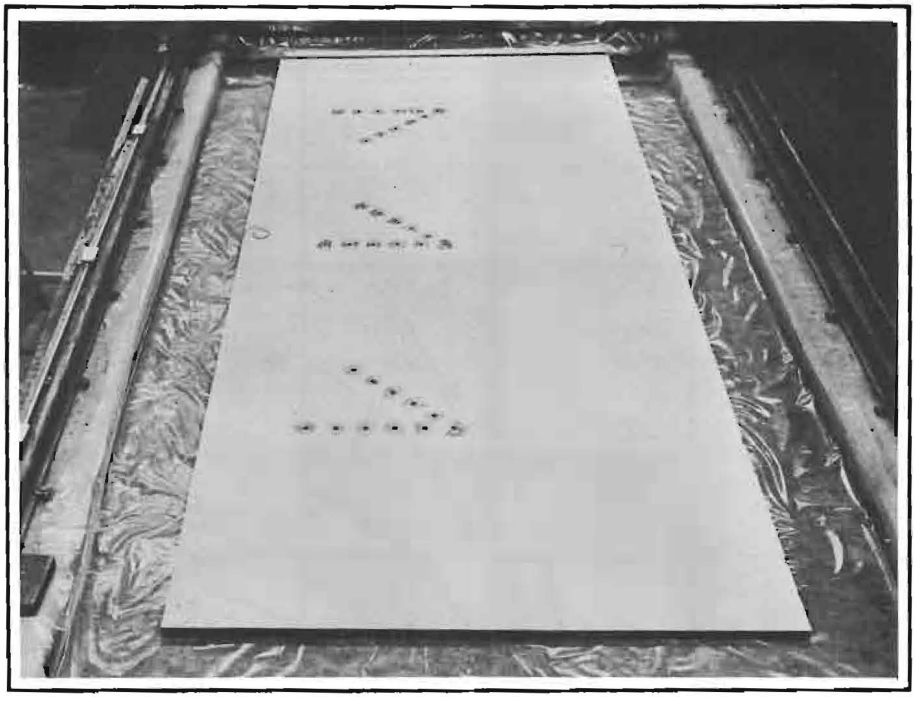

Figure 38. Arrangement of Type AX-5, SR-4 strain gage rosettes for static loading tests on Slab DM-7.

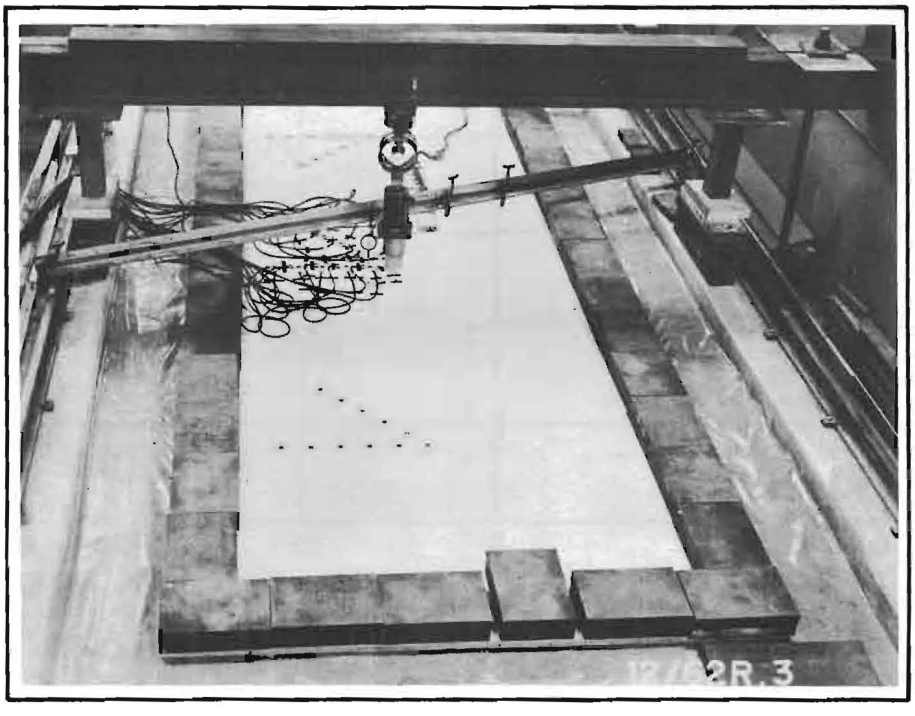

Figure 39. General view of test set-up used for static loading tests on Slab DM-7. The loads were applied by jacking against the reaction beam.

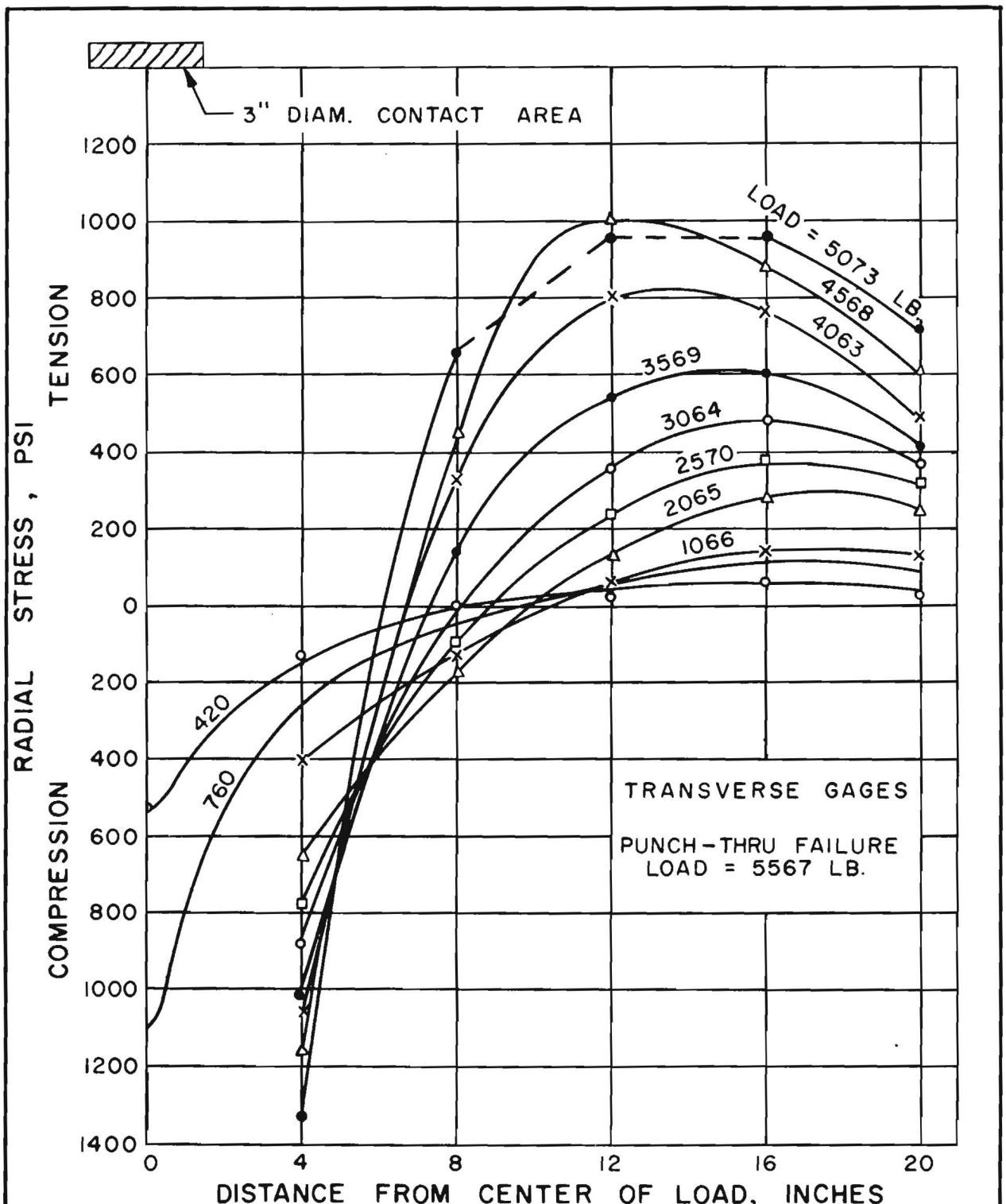

RADIAL STRESSES FOR STATIC LOADING ON SLAB DM-7

FIGURE 40

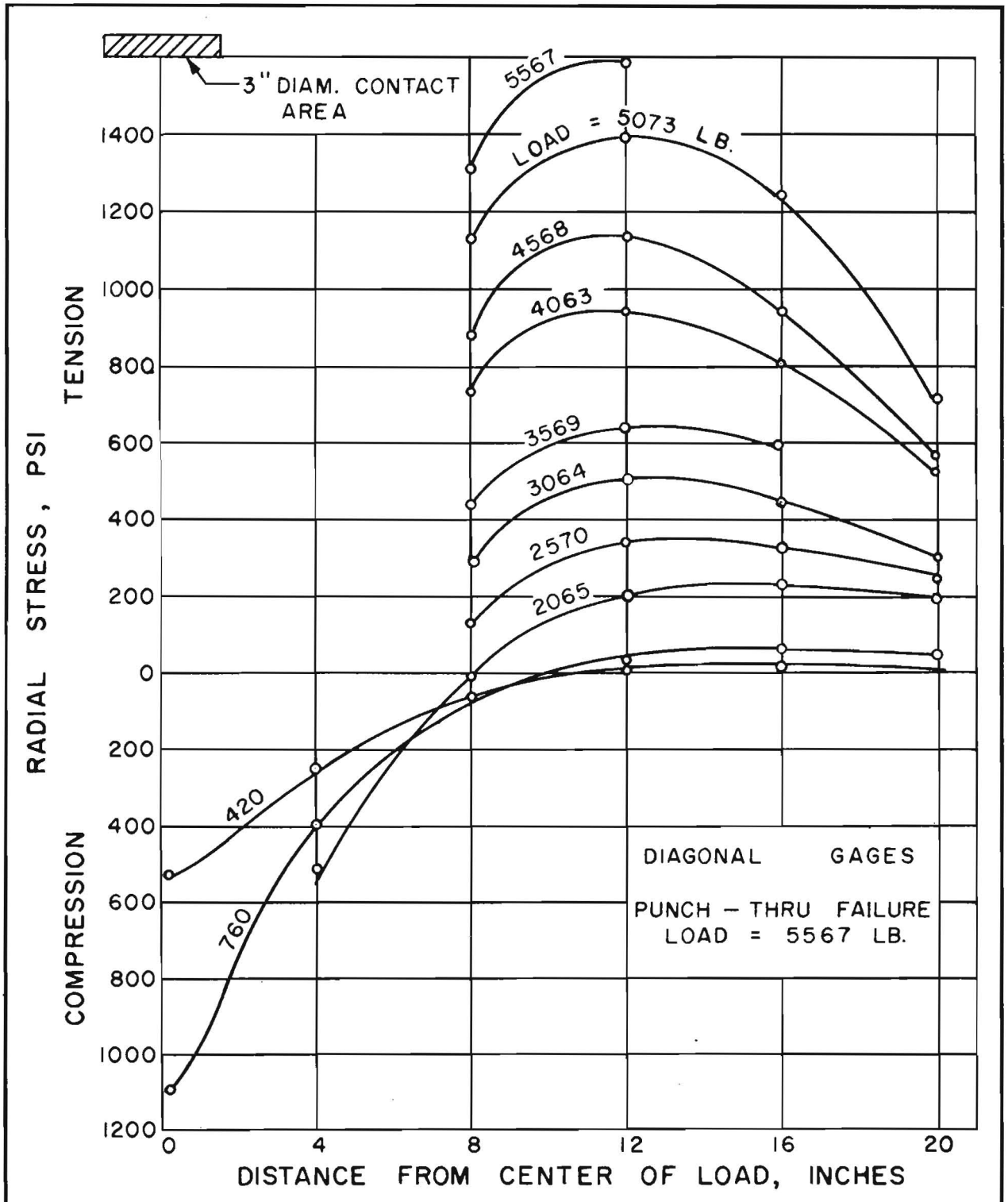

RADIAL STRESSES FOR STATIC LOADING ON SLAB DM-7

FIGURE 41

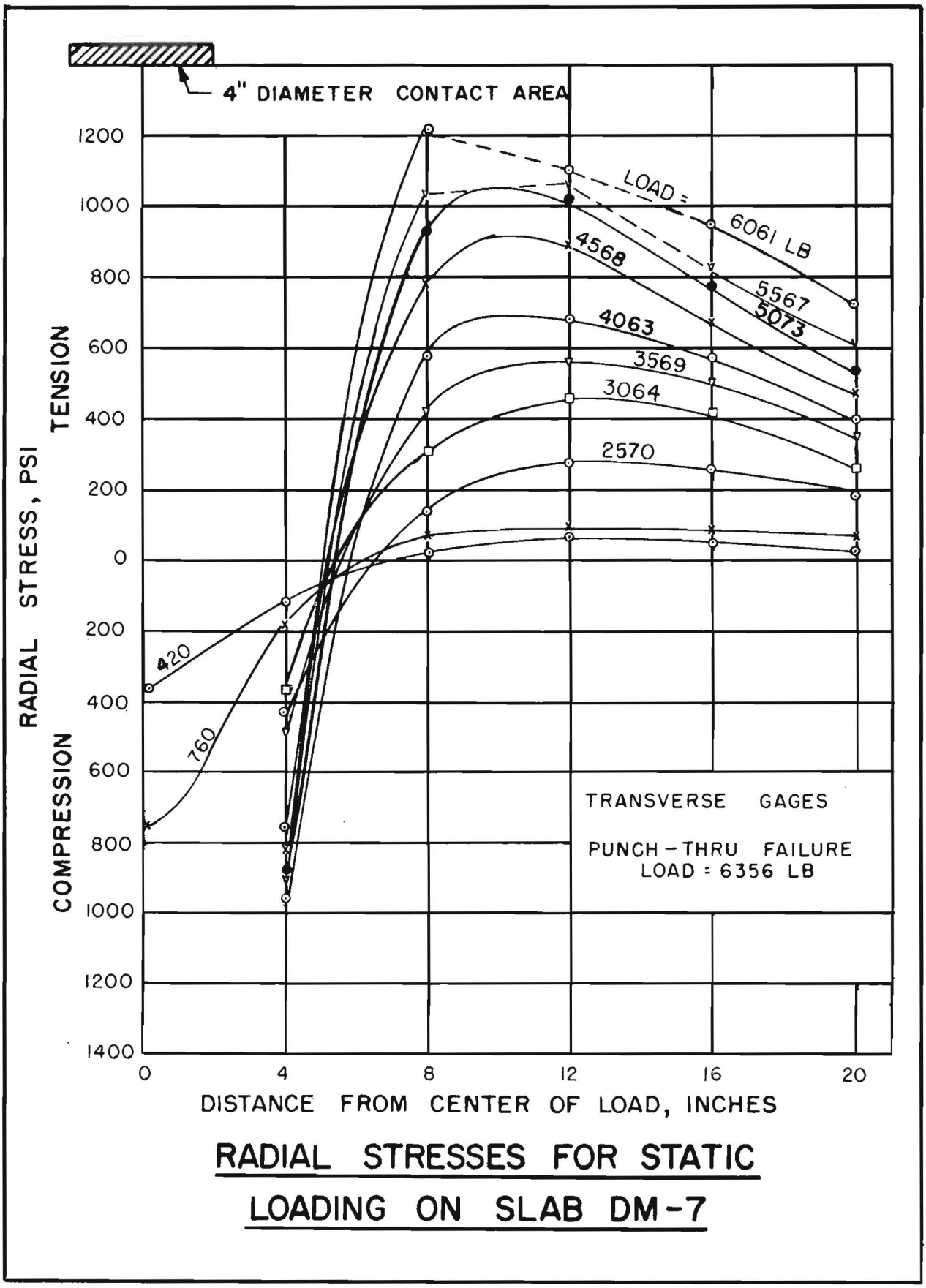

RADIAL STRESSES FOR STATIC LOADING ON SLAB DM-7

FIGURE 42

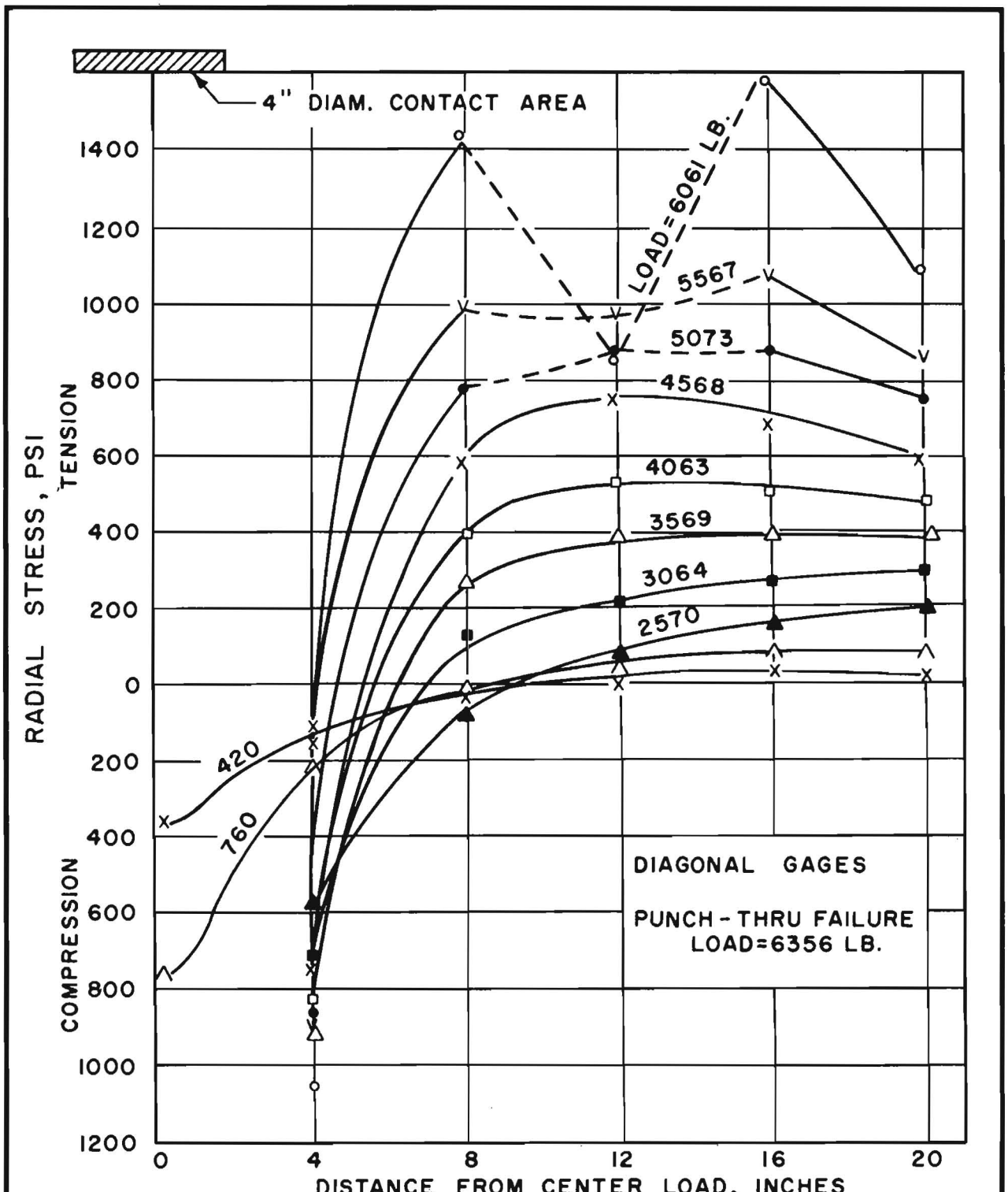

RADIAL STRESSES FOR STATIC LOADING ON SLAB DM-7

FIGURE 43

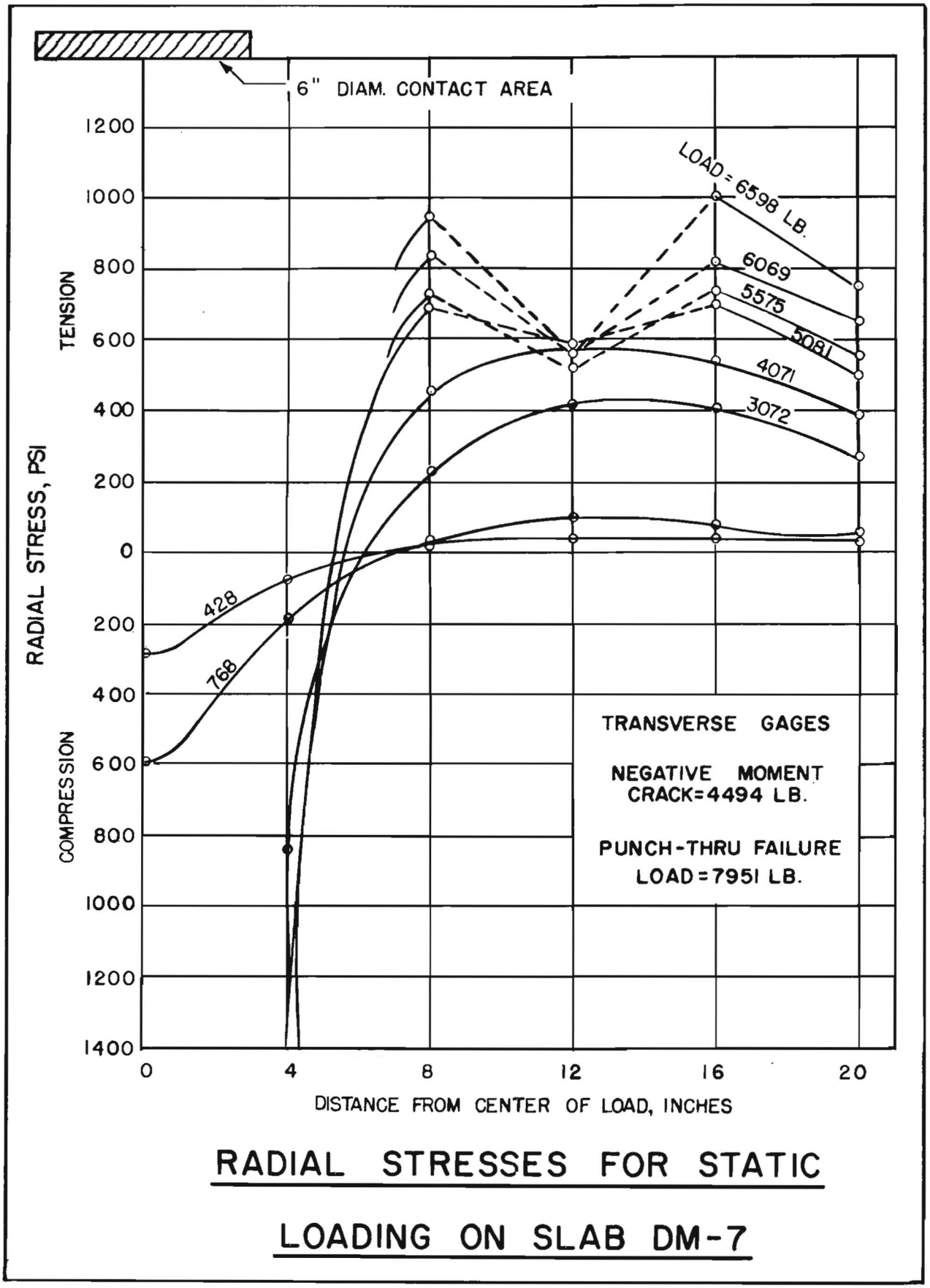

RADIAL STRESSES FOR STATIC LOADING ON SLAB DM-7

FIGURE 44

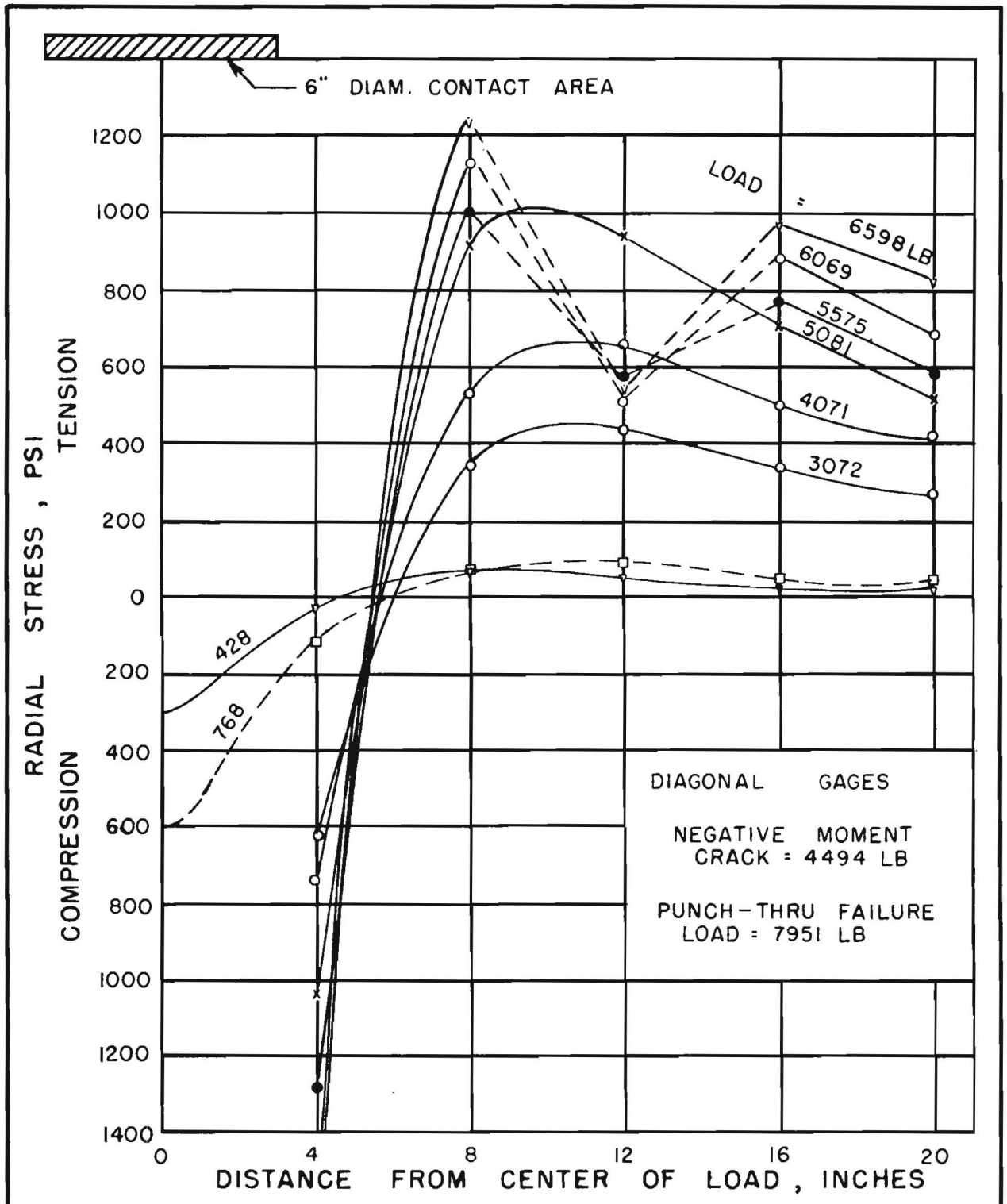

RADIAL STRESSES FOR STATIC LOADING ON SLAB DM-7

FIGURE 45

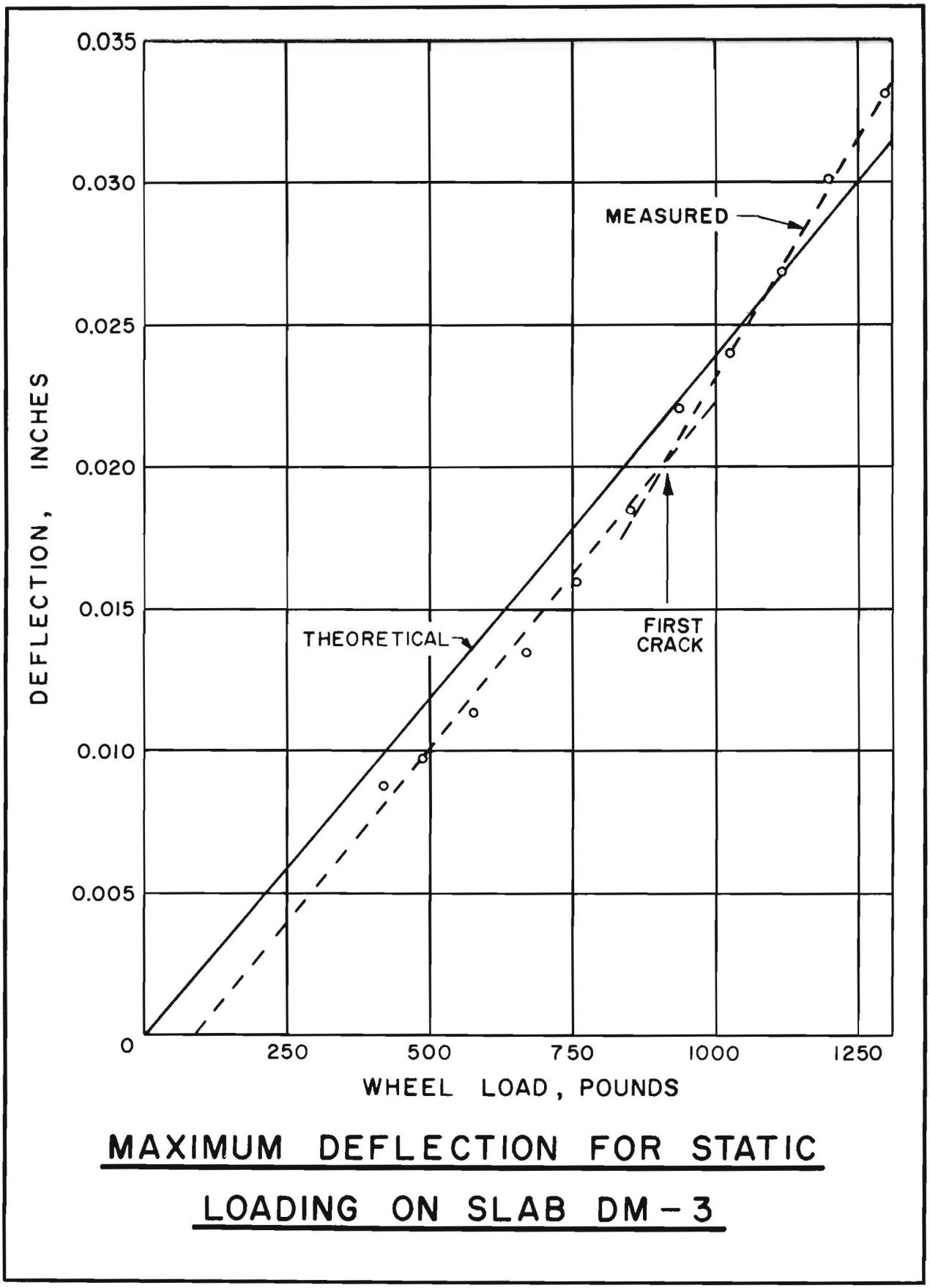

MAXIMUM DEFLECTION FOR STATIC LOADING ON SLAB DM-3

FIGURE 46

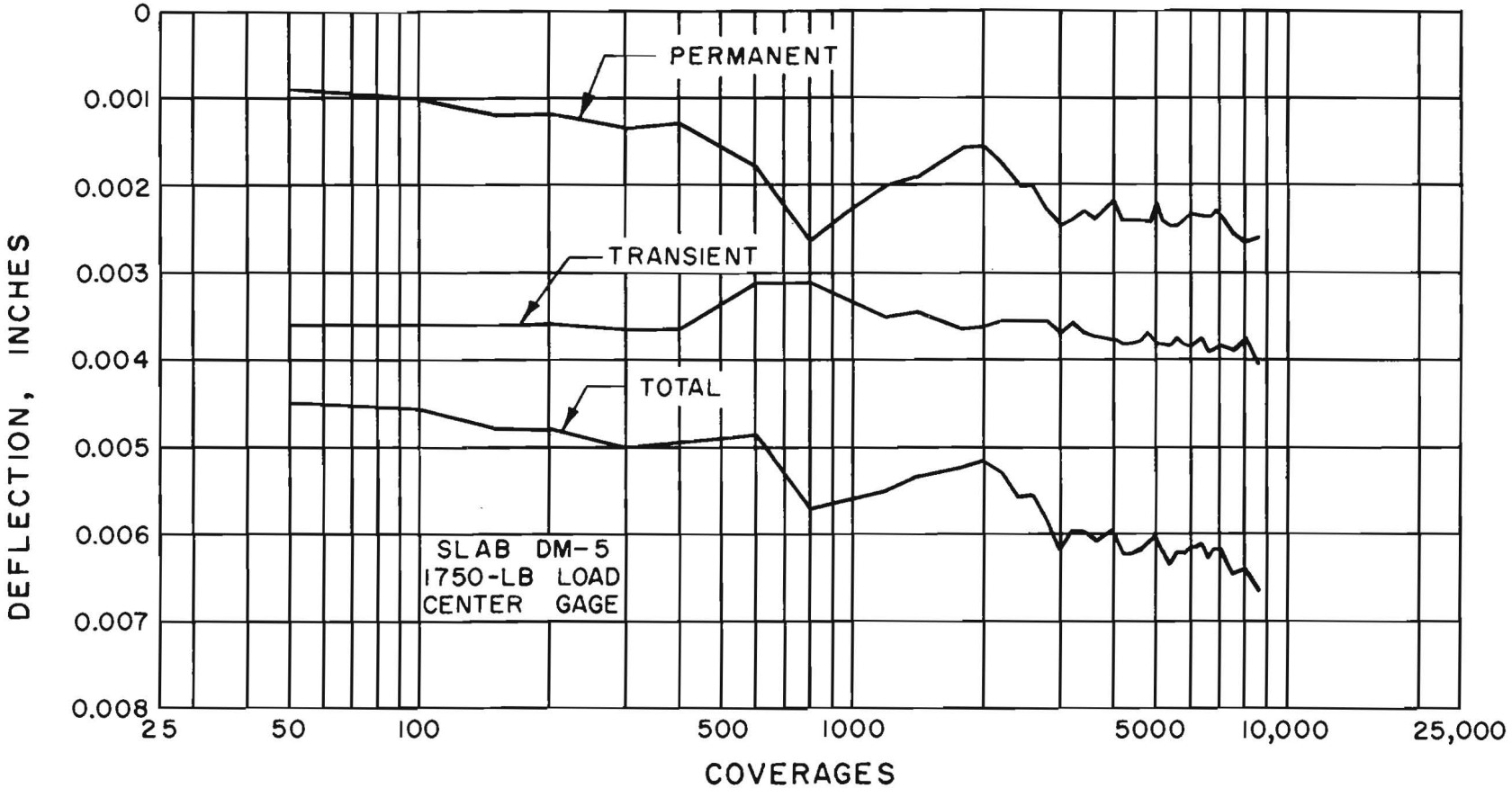

TYPICAL DEFLECTION VS COVERAGES DATA FOR REPETITIVE LOADING MODEL TESTS ON PRESTRESSED SLABS

FIGURE 47

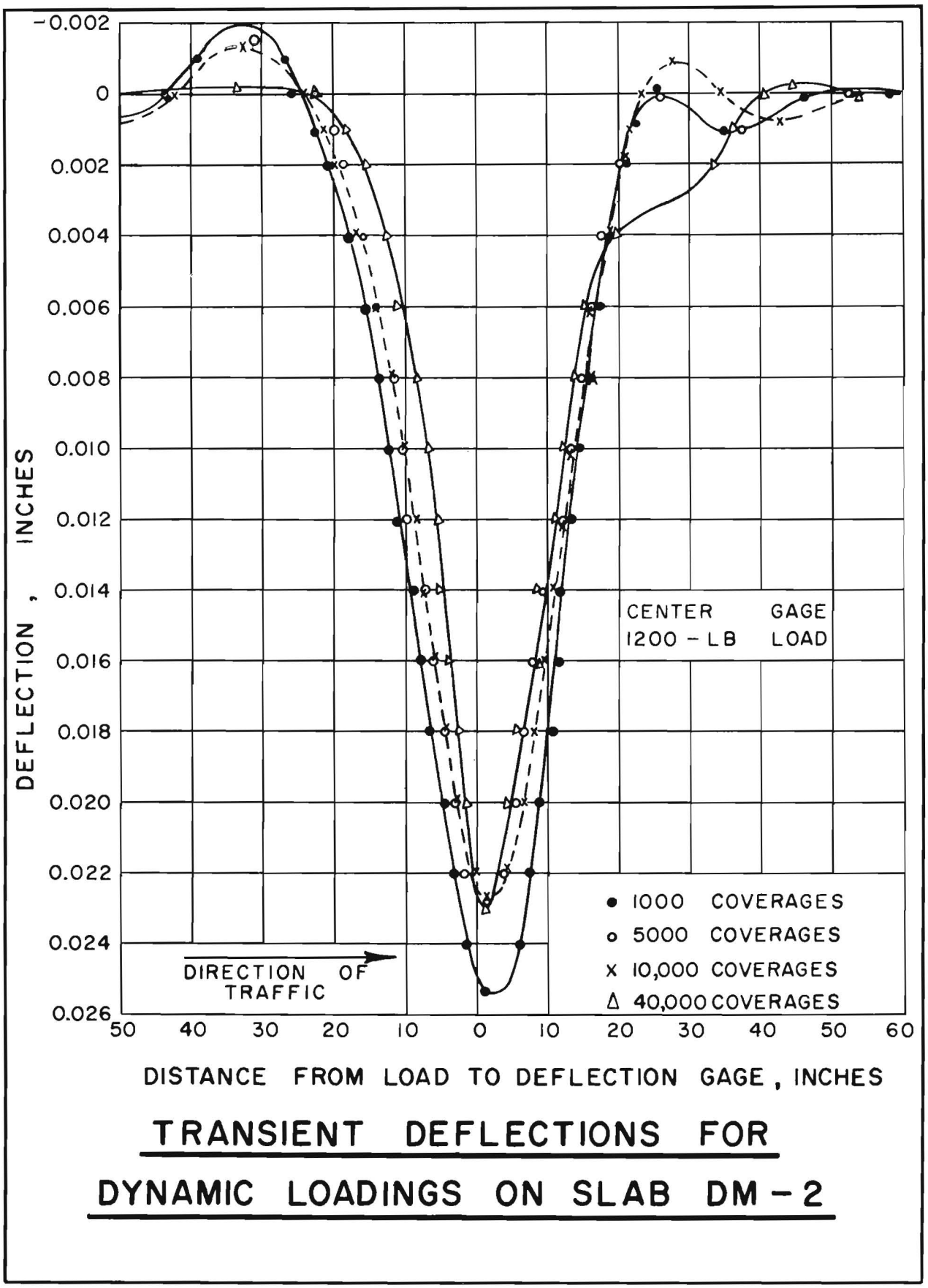

TRANSIENT DEFLECTIONS FOR DYNAMIC LOADINGS ON SLAB DM-2

FIGURE 48

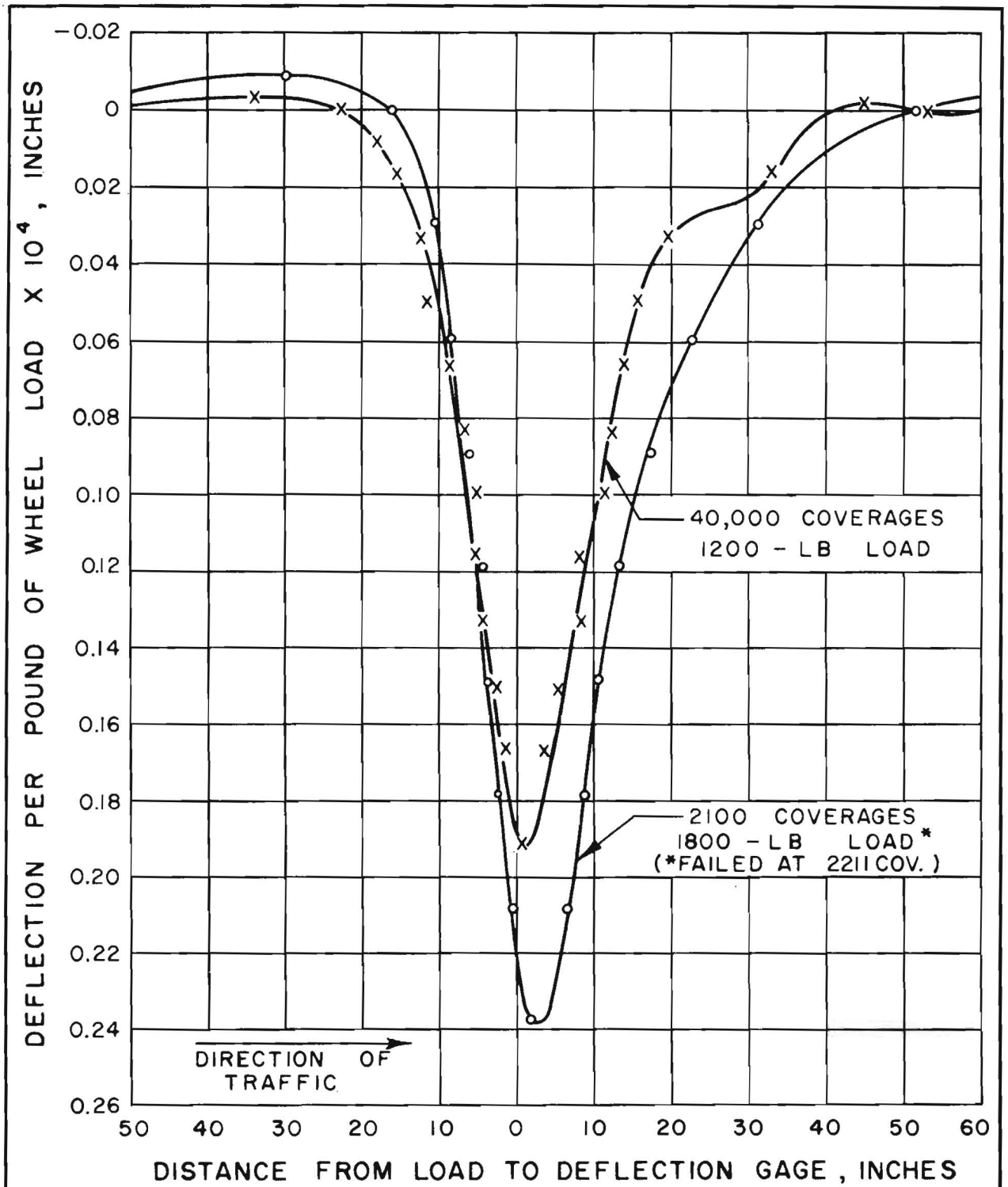

TRANSIENT DEFLECTIONS FOR DYNAMIC LOADINGS ON SLAB DM-2

FIGURE 49

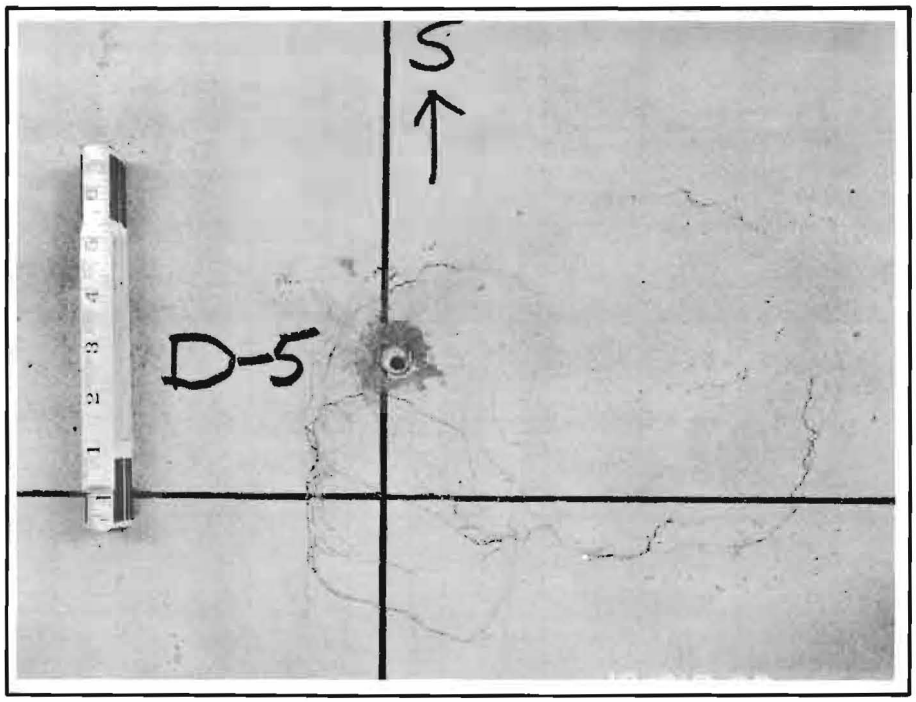

Figure 50. Initial cracking in the top surface of Slab DM-6.

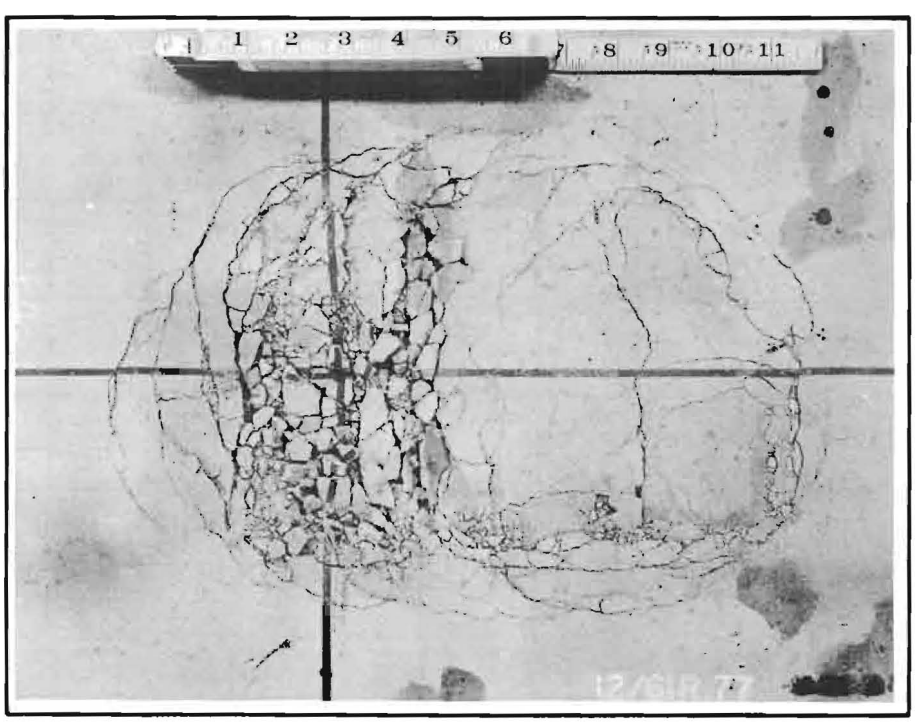

Figure 51. Initial failure in the top surface of Slab DM-3, showing disintegration of the concrete.

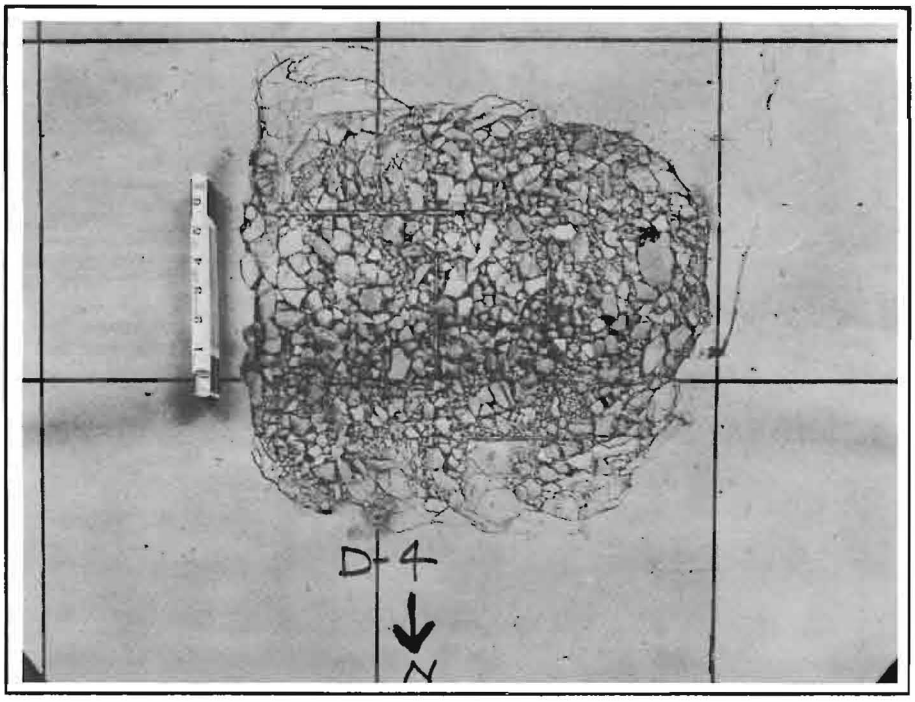

Figure 52. Second failed area in the top surface of Slab DM-6, showing exposed prestressing wires.

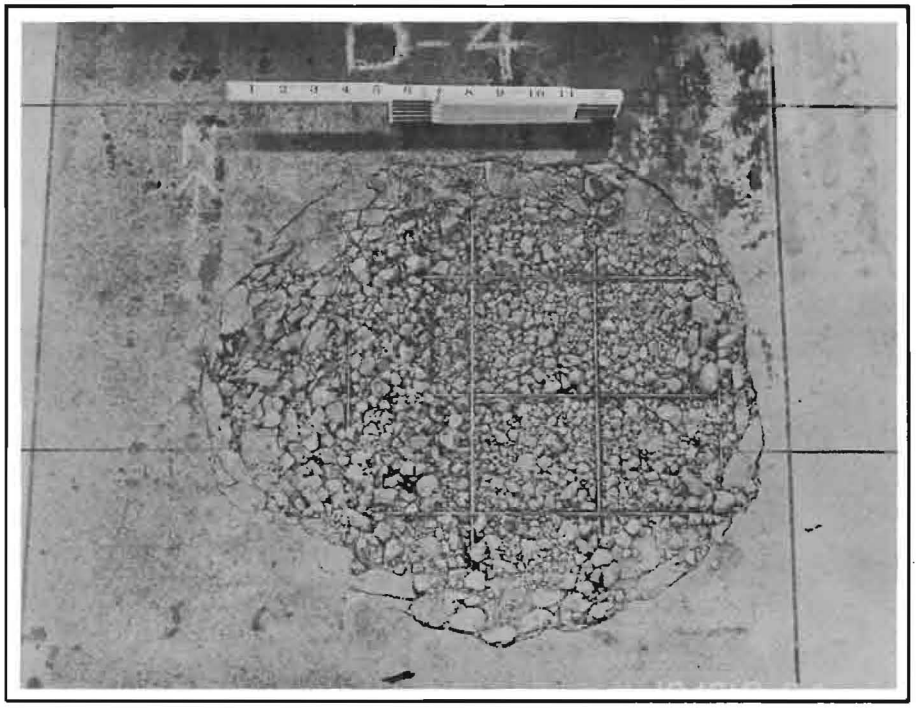

Figure 53. Initial failure in the top surface of Slab DM-5, showing exposed prestressing wires and completely disintegrated concrete.

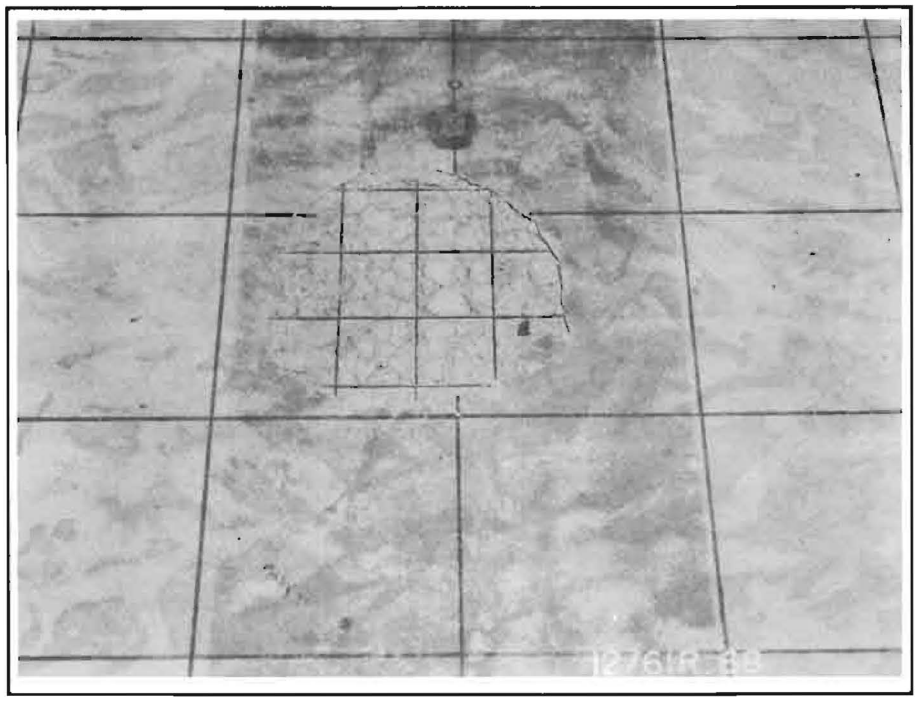

Figure 54. Failure in Slab DM-1 after removal of the disintegrated surface material to expose the prestressing wires and shattered concrete in the lower portion of the slab.

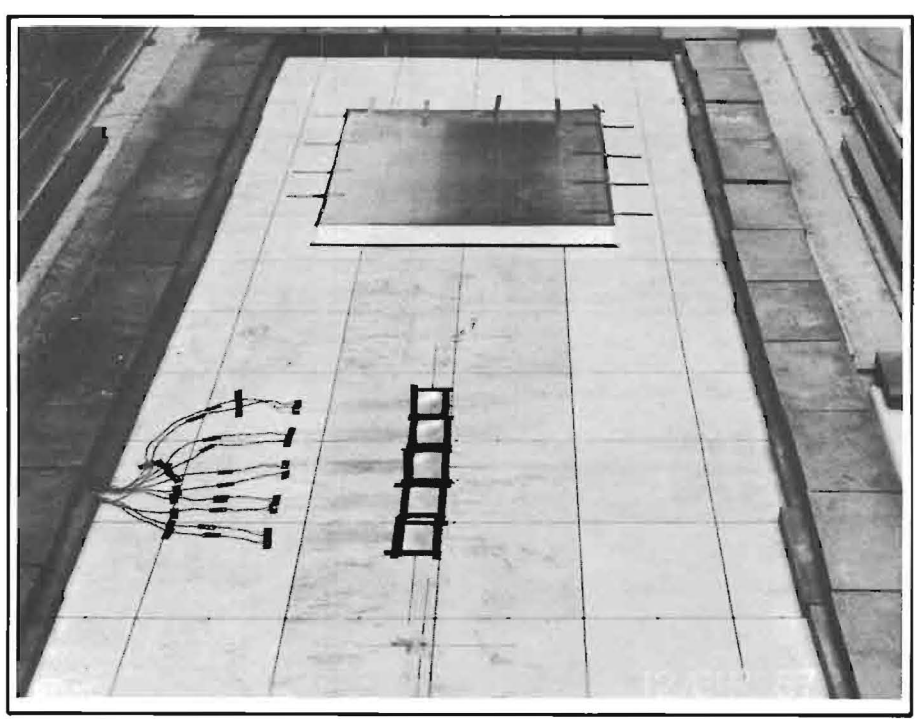

Figure 55. View showing use of a steel plate to bridge a failed area and permit continued testing. SR-4 gages with protective coverings are shown along the centerline of the traffic area.

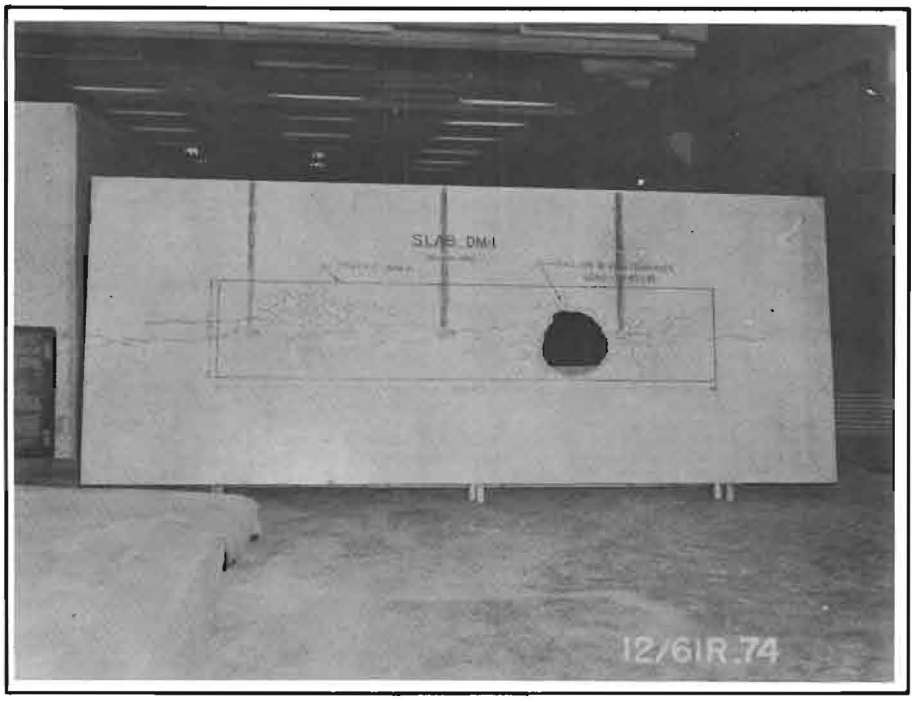

Figure 56. Crack pattern in the bottom side of Slab DM-1 after 2846 coverages of a 1240-pound wheel load.

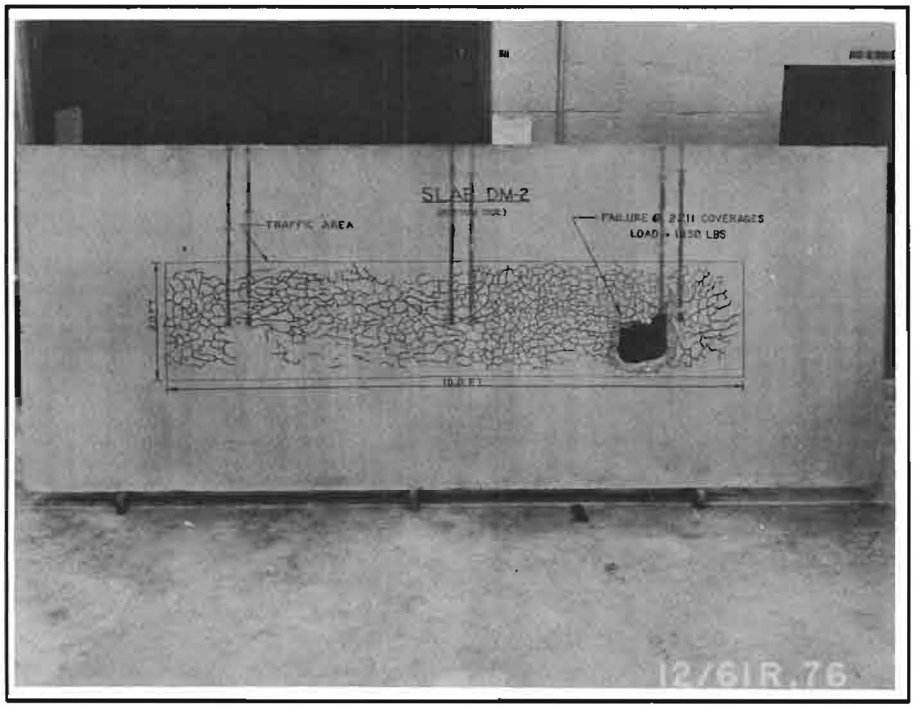

Figure 57. Crack pattern in the bottom side of Slab DM-2 after 40,000 coverages of a 1200-pound wheel load and 2211 coverages of an 1850-pound wheel load.

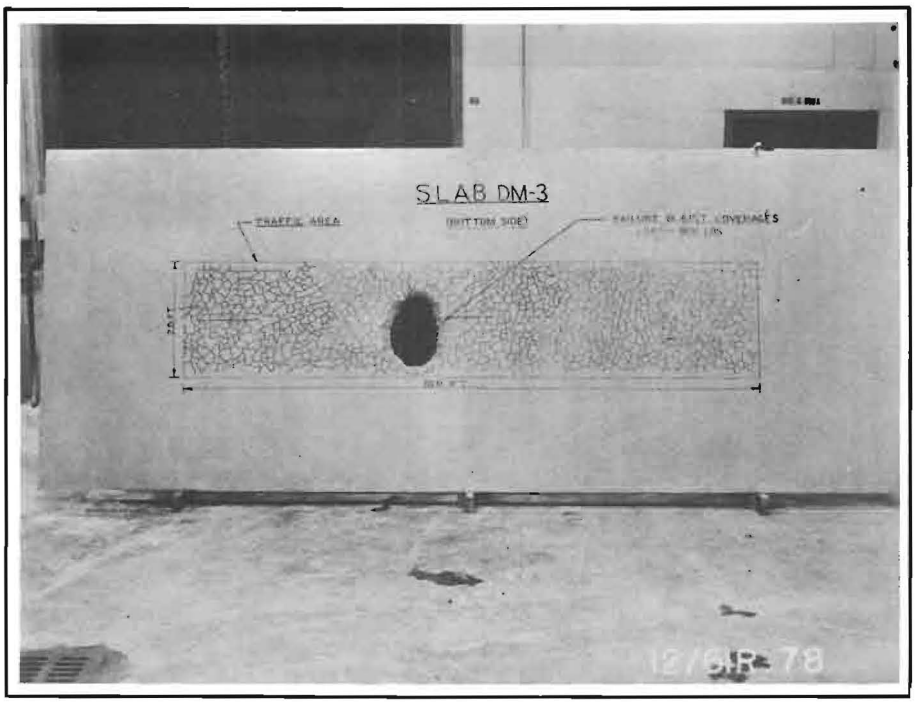

Figure 58. Crack pattern in the bottom side of Slab DM-3 after 6157 coverages of an 1896-pound wheel load.

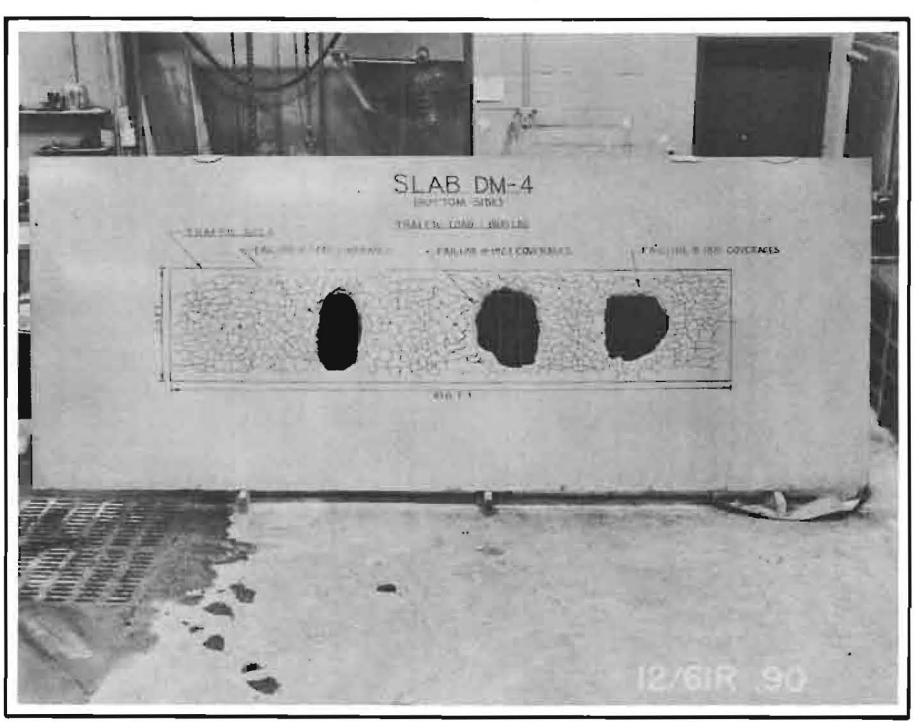

Figure 59. Crack pattern in the bottom side of Slab DM-4 after 2445 coverages of an 1800-pound wheel load. Earlier failures occurred at 1881 and at 1923 coverages.

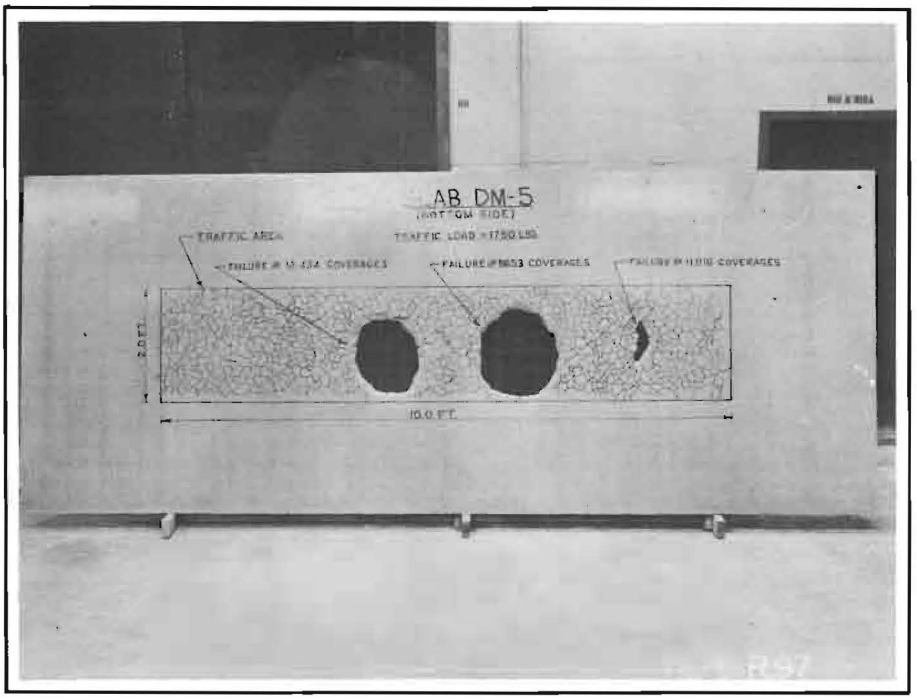

Figure 60. Crack pattern in the bottom side of Slab DM-5 after 12,434 coverages of a 1750-pound wheel load. Earlier failures occurred at 8653 and at 11,818 coverages.

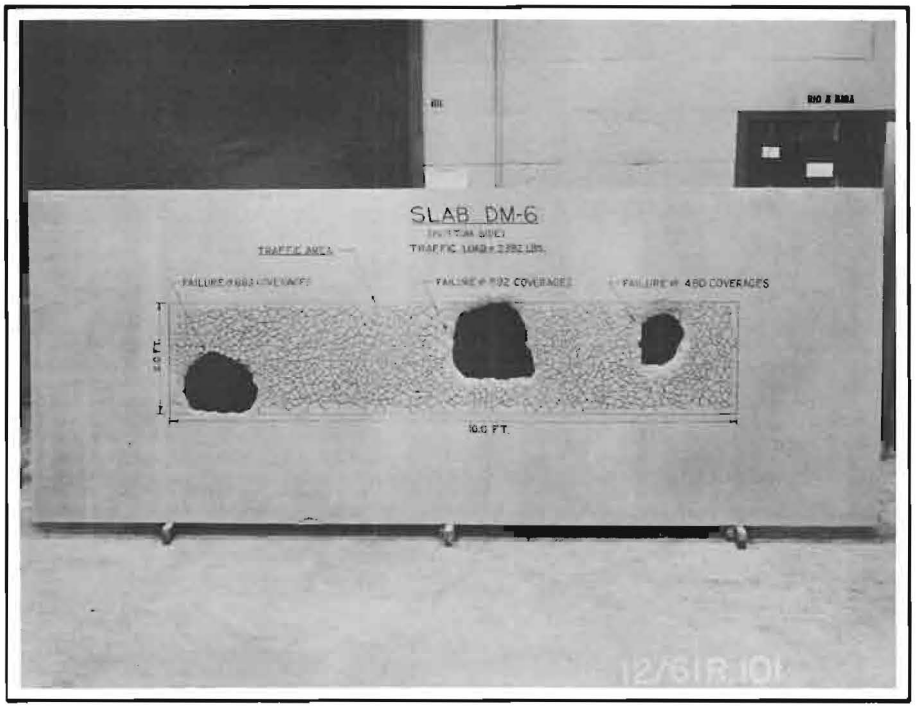

Figure 61. Crack pattern in the bottom side of Slab DM-6 after 683 coverages of a 2392-pound wheel load. Earlier failures occurred at 480 and at 592 coverages.

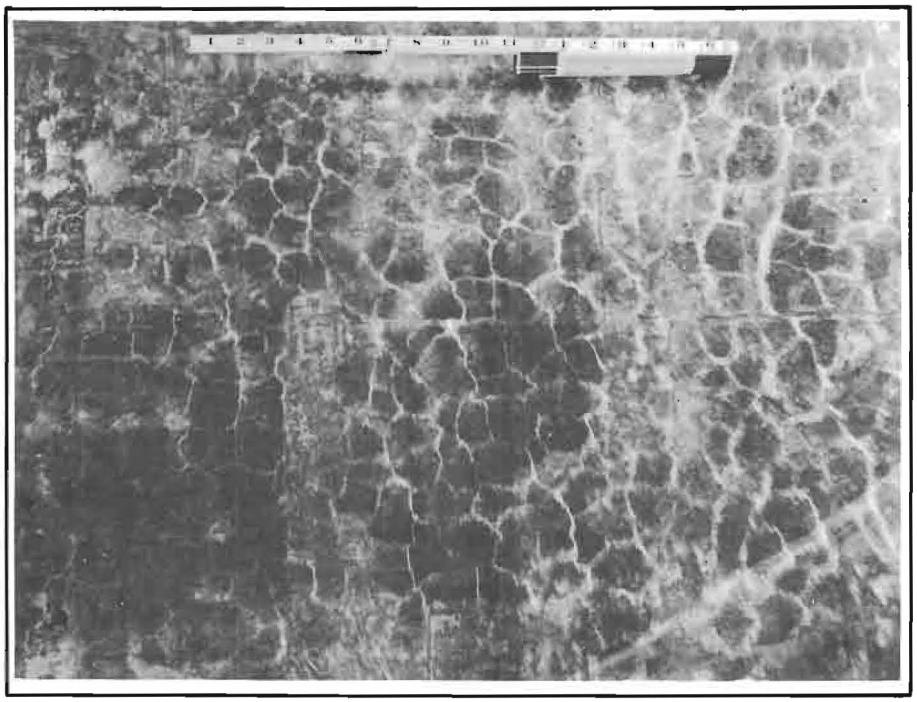

Figure 62. Imprint of the crack pattern developed in the bottom side of Slab DM-3 on the polyethylene sheet placed between the slab and the clay subgrade.

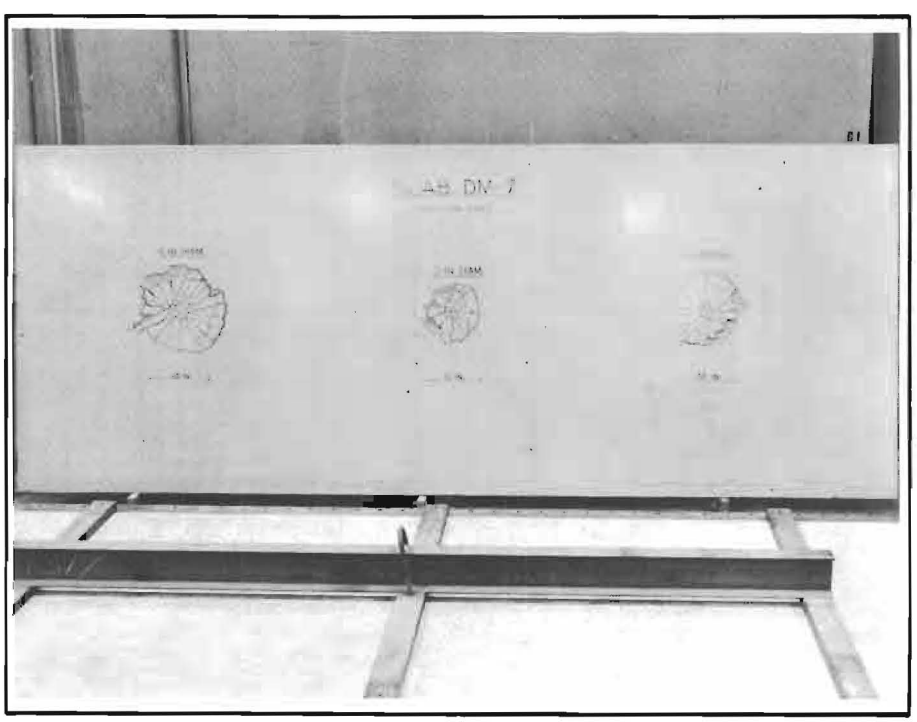

Figure 63. Crack pattern in the bottom side of Slab DM-7 after completion of the static loading tests using a 3-inch, a 4-inch and a 6-inch diameter circular contact area.

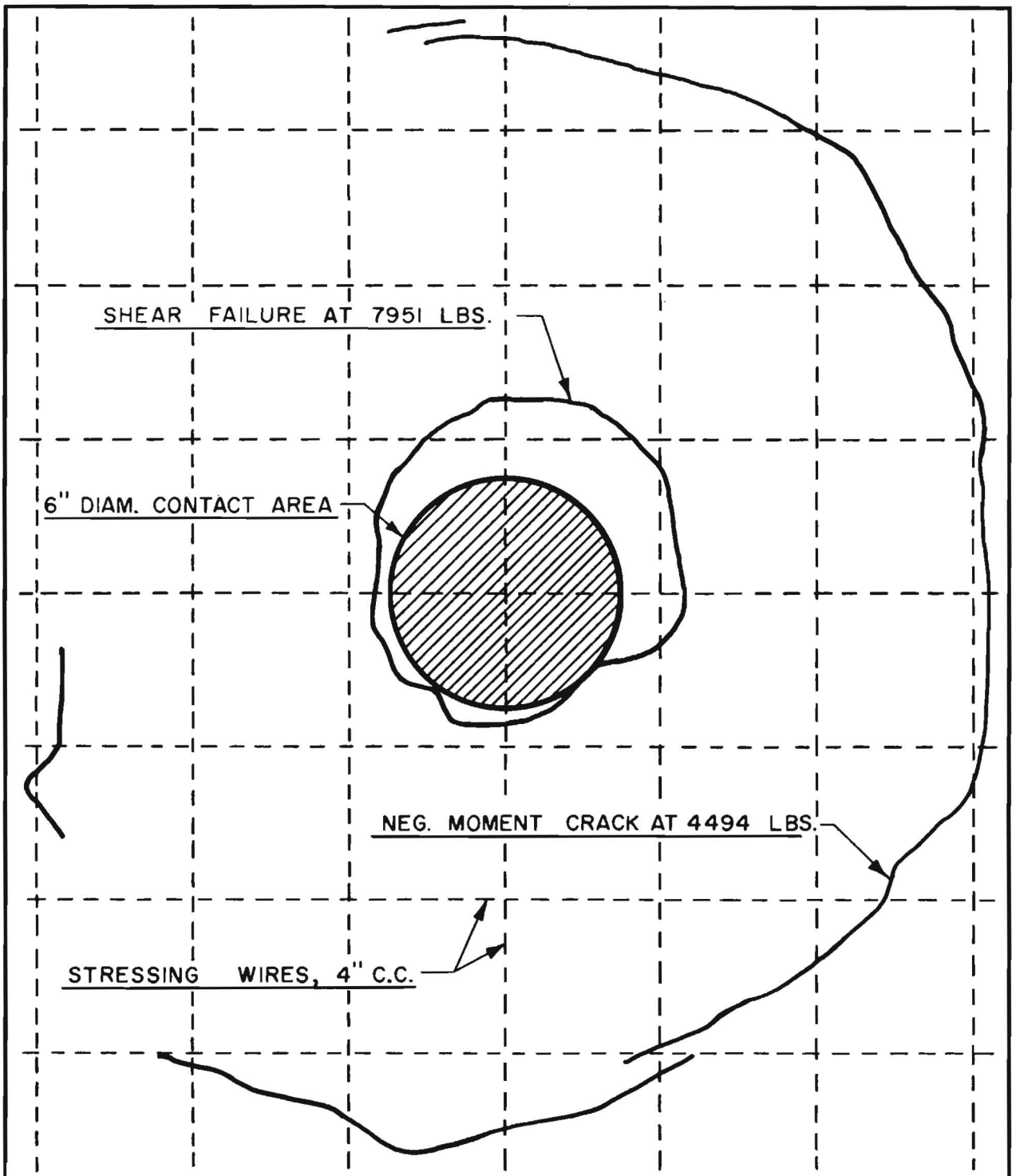

CRACKING IN TOP SURFACE OF SLAB DM-7

FIGURE 64

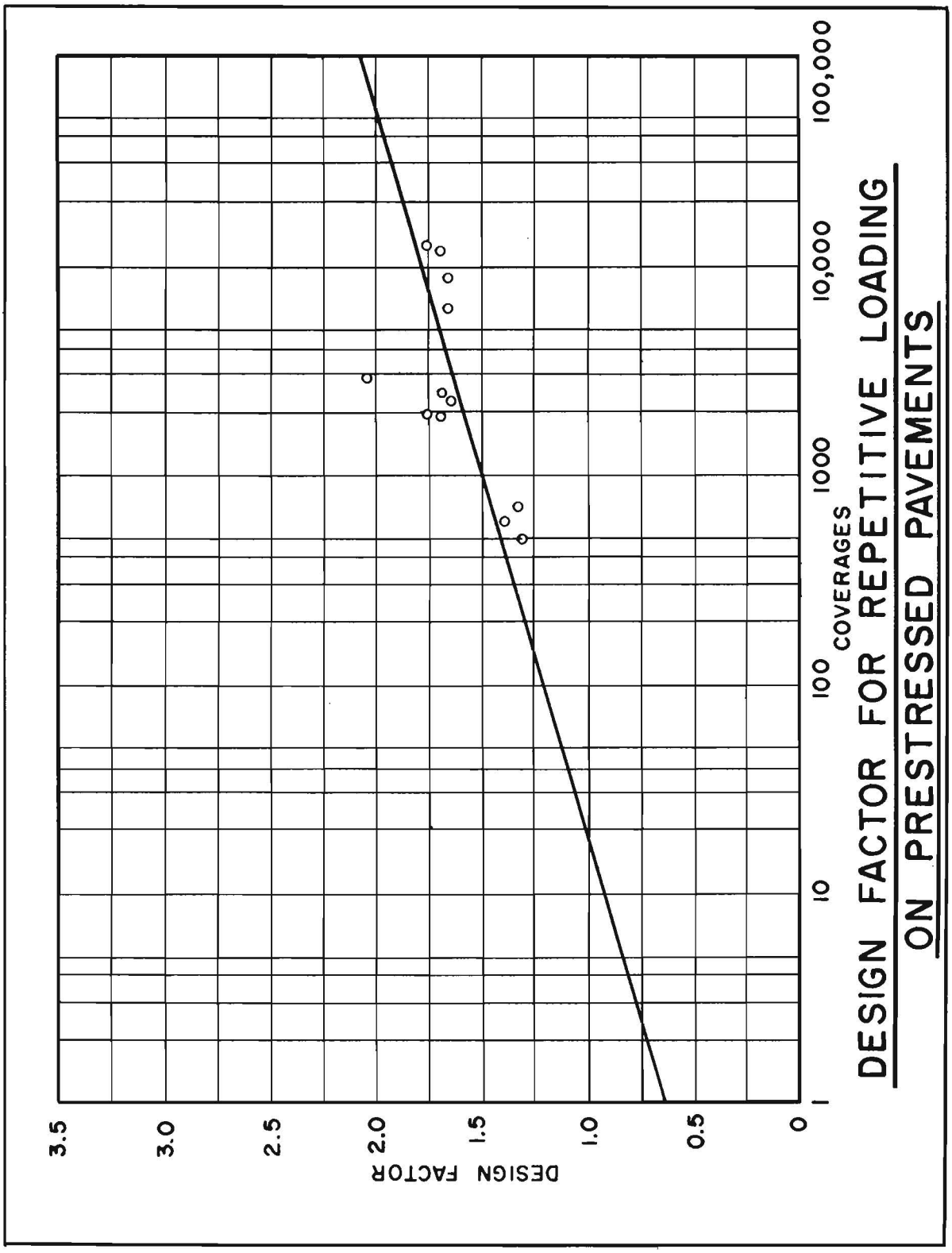
DESIGN FACTOR FOR REPETITIVE LOADING
ON PRESTRESSED PAVEMENTS
DESIGN FACTOR
3.5
3.0
2.5
2.0
1.5
1.0
0.5
0
1
10
100
1000
10,000
100,000
COVERAGES

FIGURE 65